공 학 박 사 학 위 논 문

Redesigning gut bacterial oxidoreductases for biosynthesis of functional soy phytoestrogens in the whole-cell biotransformation system

장내 미생물 유래 산화환원효소의 재설계 및 전세포 생산 시스템 구축을 통한 기능성 대두 파이토에스트로겐의 생산 연구

2018 년 8 월

서울대학교 대학원

공과대학 화학생물공학부

이 평 강

Redesigning gut bacterial oxidoreductases for biosynthesis of functional soy phytoestrogens in the whole-cell biotransformation system

A Thesis
Submitted to the Faculty of Seoul National University
by

Pyung-Gang Lee

In Partial Fulfillment of the Requirements
For the Degree of Doctor of Philosophy

Advisor: Professor Byung-Gee Kim, Ph. D.

August, 2018

School of Chemical and Biological Engineering
Seoul National University

Abstract

Redesigning gut bacterial oxidoreductases for biosynthesis of functional soy phytoestrogens in the whole-cell biotransformation system

Pyung-Gang Lee

School of Chemical and Biological Engineering

Seoul National University

Soy isoflavones are naturally occurring phytochemicals, which are biotransformed into functional derivatives through oxidative and reductive metabolic pathways of diverse microorganisms. Such representative derivatives, equols and *ortho*-dihydroxy isoflavones (ODIs), have attracted great attention for their versatile health benefits since they were found from soybean fermented foods and human intestinal fluids. Recently, scientists in food technology, nutrition, and microbiology began to understand their correct biosynthetic pathways and nutraceutical values, and have attempted to produce the valuable bioactive compounds using microbial fermentation and enzyme/whole-cell-based biotransformation. Furthermore, artificial design of microbial catalysts and/or protein engineering of oxidoreductases

were also conducted to enhance production efficiency and regioselectivity of products.

In this thesis, reductive metabolite equols and oxidative derivative ODIs were selected as production targets and efficient biosynthetic strategies were introduced. Primarily, recombinant *E. coli* strain retaining equol production capability was constructed and engineered for synthesis of equol and its derivatives. Because the reductive pathway is highly dependent on intracellular reductive potential comprised of NAD(P)H, whole-cell biotransformation was recognized as efficient and low-cost bioprocess. On the other hand, regioselective ODI production was investigated with engineered tyrosinase. Since the biocatalysis depends on monooxygenase activity of tyrosinase, inhibition of second oxidation step (or pigmentation) of tyrosinase should be immediately supplemented in the reaction buffer.

For microbial productions of equols using the recombinant *E. coli* strain, four key enzymes in equol production pathway, daidzein reductase (DZNR), dihydrodaidzein racemase (DDRC), dihydrodaidzein reductase (DHDR) and tetrahydrodaidzein reductase (THDR) were manipulated. Then, rate-determining enzymes have been identified for the biotransformation with low and high initial substrate loads, respectively. Hydrophilic polymer supplementation, reaction compartmentalization and computationally designed enzyme engineering were also introduced to achieve g/L level production of equol derivatives. As a result, equol derivatives could be produced with fine yields, 1.9 (for equol) and 1.3 g/L (for 5-hydroxy-equol), showing remarkable productivities. The biotransformation system

also takes advantage of aerobic manipulation, a favorable fermentation process for industrial-scale production.

While, to achieve the massive production of ODIs, mono-oxygenase activity of a bacterial tyrosinase has been exploited. Because the wild-type tyrosinase has poor regioselectivity and catalytic activity, circular permutation (CP) and site-directed mutagenesis were performed. In results, a CP variant with enhanced polyphenol hydroxylation activity was demonstrated for 1.5 g/L of 3'-hydroxygenistein production, and several mutants with some amino acid substitutions were verified to produce 6 or 8-hydroxyformononetin with increased regioselectivity.

In short, this study explored efficient biosynthetic methods of functional isoflavone derivatives, equols and ODIs using artificially reconstructed enzymes or microbial catalysts. It would provide useful catalytic platforms to produce various bioactive isoflavone derivatives.

Keywords: equol, *ortho*-dihydroxyisoflavone, whole-cell biotransformation, protein engineering, hydrophilic polymer, tyrosinase

Student number: 2013-20986

Contents

List of Tables

List of Figures

Chapter 1.

Introduction

1.1 Microbially modified isoflavone derivatives

Soybean is a representative legume containing fair amount of isoflavone ranging from 0.1 to 0.3 % of its total weight, which are mainly consisted of daidzein, genistein and glycitein predominantly as malonyl-, acetyl-, β-glucoside conjugates (Wang and Murphy 1994). Unlike flavones, isoflavones are phytoestrogens, and their derivatives sometimes become selective estrogen receptor modulators (SERMs) due to their preferential binding properties to human estrogen receptors (ERs) and activator function, especially for ERβ (Hwang et al. 2006; Kuiper et al. 1998; Setchell 2001). The estrogenic characters of isoflavones are practically associated with relieving post-menopausal symptoms, so that more than 75 mg/d dietary isoflavone (or 15 mg/d genistein) intake has been nutraceutically recommended for alleviating osteoporosis, hot-flash, and low-density lipoprotein (LDL) cholesterol level (Uesugi et al. 2002; Wei et al. 2012; Williamson-Hughes et al. 2006). Recently, it was revealed that the biological estrogenic effects of isoflavone could not be simply explained by the intake of isoflavone itself, but its metabolism of host intestinal microflora plays an important role for the individual effects (Setchell et al. 2002). In this section, equol and *ortho*-dihydroxyisoflavone (ODI) will be exclusively introduced for their origin, activity and biosynthesis.

1.1.1 Equols

Equol is one of the representative microbial isoflavone metabolite which belongs to isoflavan class that lacks the ketone group on isoflavone C-ring. Equol is abundantly

found in Asian soybean fermented products such as stinky tofu, *etc* (Jou et al. 2013), however, its major origin was known as a metabolic product by gut microflora (Tsangalis et al. 2005; Wang et al. 2007; Wang et al. 2005a). Therefore, plant isoflavones digested by mammalian hosts are actually transformed into equol by host commensal gut bacteria, then equol is finally absorbed into the hosts with moderate estrogenic activity.

Biosynthesized equols have predominantly S-configuration at the chiral center C3 (Wang et al. 2005a). Because (*S*)-equol binds selectively to estrogen receptor ERβ over α, it can escape general adverse effects prompted by ERα activation (Setchell et al. 2005). It has been clinically verified for various biological activities on menopausal disorders, cardiovascular risk, osteoporosis, anti-breast/prostate cancer, anti-oxidative, and anti-skin aging with significant higher efficiency, compared to its isoflavone origin (Itsumi et al. 2016; Jackson et al. 2011; Lephart 2016; Setchell et al. 2005). Due to the versatile and potent activities, (*S*)-equol has been developed as a dietary supplement for postmenopausal women, and racemic equols have been used as additives for anti-aging cosmeceuticals. Its market has been expanding in USA and Japan, substituting for the market of traditional hormone supplement and cosmetic ingredients.

On the other hand, 5-hydroxy-equol, a kind of equol derivative derived from genistein, has lower ER binding affinity than equol, but it is the most potent antioxidant among other isoflavone derivatives and its anticancer activity against hematocellular carcinoma has been recently proved (Arora et al. 1998; Gao et al. 2018; Lee et al. 2017). It is also suggested that other equol derivatives are present,

but practical applications and synthetic methods have not been extensively investigated yet (Rufer et al. 2006).

1.1.2 *Ortho*-dihydroxyisoflavones (ODIs)

Whereas equol has been known in recent times, *ortho*-dihydroxyisoflavone (ODI) is a well-known bioactive isoflavone derivative isolated from traditional soy fermented foods. In addition, ODIs are oxidative metabolites, but equols are reductive products (**Fig. 1.1**). Fermented soy pastes such as Doenjang (from Korea), Miso (from Japan), and Tempeh (from Indonesia) contain a variety of isoflavone derivatives subjected to oxido-reductions, but their hydroxylation modifications were the best studied (GYöRGY et al. 1964; Hirota et al. 2004; Park et al. 2008). The hydroxylation is mainly performed by several microorganisms during fermentation, and the hydroxylated isoflavones can function as beneficial components for human health with superior bioactivity to original isoflavones without fermentation. For example, ODIs in the soy foods were reported to show anti-inflammatory, anti-cancer and anti-oxidant activities through various biological mechanisms (Lee et al. 2011). Because they share the catechol functional group in the polyphenol backbone, their radical-scavenging efficacy is common property with some variations according to the position of hydroxyl groups on the aromatic rings (Park et al. 2008). Moreover, 6-ODI and 8-ODI have been validated to show preventive effects on adipogenesis (anti-diabetic effect) and atopic dermatitis symptoms (skin anti-inflammatory effect), respectively (Kim et al. 2014; Seo et al. 2013b). In a recent study, 8-ODI has been

also validated to show preventive effect on atherosclerosis via attenuating adhesion of THP-1 monocytes to human vein endothelial cells (Lee et al. 2018a). Therefore, it could be generally said that *ortho*-dihydroxylation of isoflavones endows enhancement and novel functions in the biological activities that could not be found in the original isoflavones.

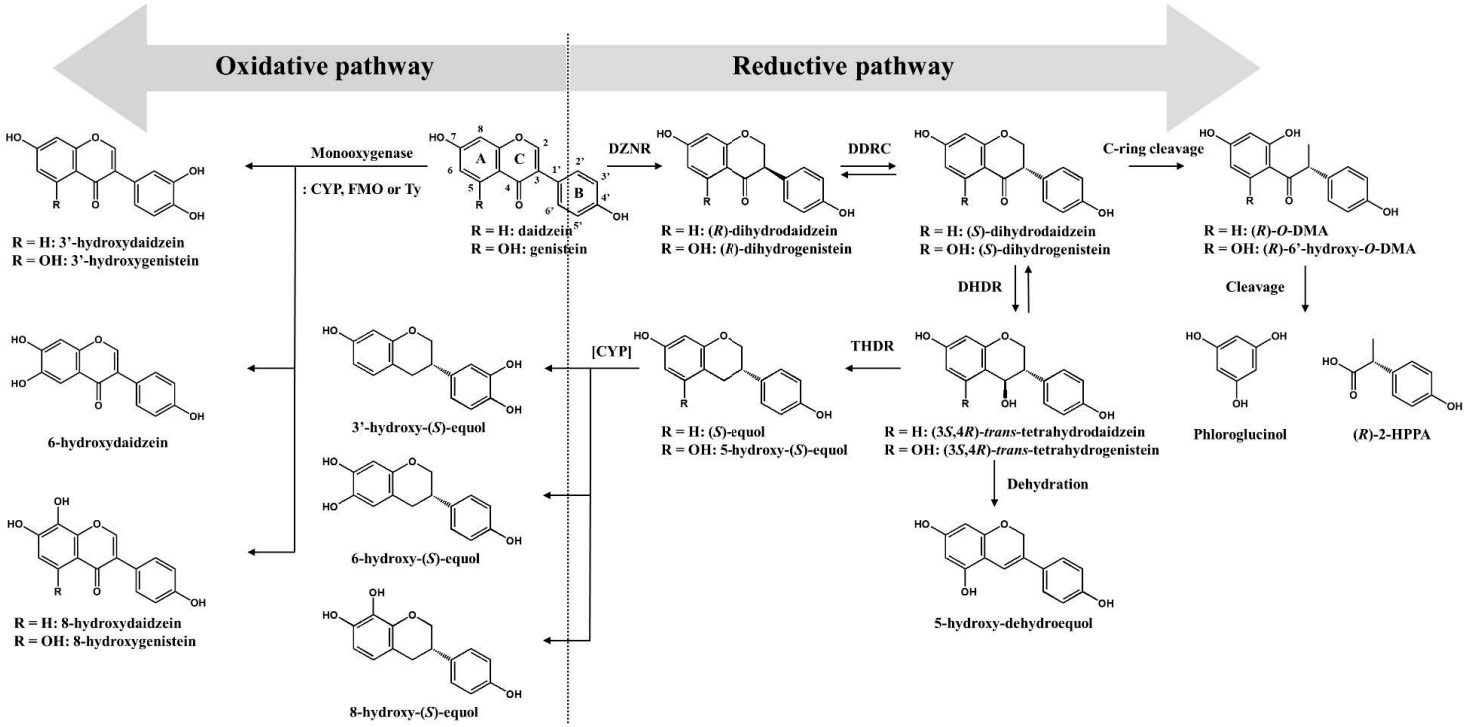

Figure 1.1 Oxido-reductive modification pathways of isoflavone denoted with possible biocatalysts.

Each abbreviation indicates as follows: CYP: cytochrome P450, FMO: flavin-containing monooxygenase, Ty: tyrosinase, DZNR: daidzein reductase, DDRC: dihydrodaidzein reductase, DHDR: dihydrodaidzein reductase, THDR: tetrahydrodaidzein reductase, *O*-DMA: *O*-desmethylangolensin, 2-HPPA: 2-(4-hydroxyphenyl)propionic acid. (*S*)-equol is converted into hydroxy-equols by potential CYPs.

1.2 Microbial Synthesis of isoflavone derivatives

1.2.1 Equol synthesis

Over the past decade, equol-producing bacteria have been thoroughly isolated and classified, and the bacterial species comprise a variety class of microorganisms including *Coriobacteriaceae* (i.e. *Slackia*, *Eggerthella*, *Adlercreutzia)*, *Lactococcus*, *Lactobacillus*, *Bifidobacterium*, *Pediococcus* genus, *etc* (**Table 1.1**). Most of the equol-producing bacteria are strictly anaerobes with one recent exceptional study: *Pediococcus*, *Lactobacillus* sp. (Kwon et al. 2018). Equol-producing capacity is quite different among the equol-producing bacteria, even though they are speculated to share the same enzymatic pathway. Microbial species which show relatively higher equol production yields and productivities, predominantly belong to Coriobacteriaceae family in general (**Table 1.1**). In contrast, equol-producing *Bifidobacterium* and *Eubacterium* tends to show poor yield or productivity (Tsangalis et al. 2002; Yu et al. 2008). This kind of tendency could be also found in the previous patents. A patent claimed a lactic acid bacterium producing equol, which is now classified as *Lactococcus garvieae* strain (Shimada et al. 2010; Uchiyama et al. 2006). The inventors could achieve 57 mg/L of anaerobic equol production during 96 h of soymilk fermentation. On the other hand, another Japanese patent claimed that the fermentation exploiting *Slackia sp.* YIT 11861 converted about 100 mg daidzein into (*S*)-equol with 94% conversion yield in 24 h, which is quite superior to the previous fermentation using *Lactococcus* strain (Tsuji et al. 2013). The same bacteria also tolerated 10 L anaerobic fermentation to give 2.4 g of equol from 2.5 g of daidzein, which made the *Slackia* strain more acceptable for

industrial application. In addition, *Coriobacterium*, mainly *Slackia* species, is the unique microorganism producing 5-hydroxy-equol from genistein, whereas other equol-producing bacteria do not (Matthies et al. 2009; Matthies et al. 2008; Xie et al. 2015). It is very likely that the isoflavone reductive pathway in *Slackia* has better potency and broad substrate specificity.

Recently, *Pediococcus* and *Lactobacillus* strains were isolated from human feces and they were also shown to produce equol from daidzin, daidzein and dihydrodaidzein in aerobic fermentation (Kwon et al. 2018). This is the first observation of aerobic production of equol by naturally isolated gut bacteria with high efficiency. Such bacteria are promising candidates for future development of industrial aerobic fermentation process, which would lead low-cost equol production and its successful commercialization, since food industry still mainly requires non-GMO (genetically modified organism) products.

On the other hand, other studies identified a gene cluster responsible for equol-producing activity of the bacteria. The gene cluster encodes 3 to 8 homologous open-reading frames (ORF) varying among microbial species. However, only four genes encoding DZNR, DDRC, DHDR and THDR are identified as key factors in the reductive isoflavone pathway (KAWADA et al. 2016; Schroder et al. 2013; Tsuji et al. 2012). Isoflavone reduction is firstly achieved by daidzein reductase (DZNR) which gives a saturated CC single bond between C2 and C3 of daidzein or genistein to produce dihydrodaidzein (DHD) or dihydrogenistein (DHG), respectively (Schroder et al. 2013; Shimada et al. 2010). The tautomerization at C4 ketone and dihydrodaidzein racemase (DDRC) easily isomerizes and produces racemic mixture

of DHD (Park et al. 2011; Shimada et al. 2012). Both DHD isomers are reduced at C4 ketone to alcohol by dihydrodaidzein reductase (DHDR) generating (3*S*,4*R*)-*trans*-tetrahydrodaidzein (THD) and (3*R*,4*R*)-*cis*-THD, respectively. Finally, only (3*S*,4*R*)-*trans*-THD is metabolized into (3*S*)-equol by tetrahydrodaidzein reductase (THDR) (Shimada et al. 2011). Because the metabolism of daidzein into equol is dependent on three reductases and an isomerase, the metabolic process is highly dependent on intracellular reducing power. In practice, DZNR and DHDR consume NADPH as an electron donor to reduce isoflavonoid substrates, whereas DDRC and THDR are verified as cofactor-independent enzymes (Shimada et al. 2012; Shimada et al. 2011). However, low catalytic activity of THDR in *in vitro* assay and thermodynamically speculated existence of extra reducing power strongly insist that unknown reduction mechanism is still remained to be seen (Schroder et al. 2013). Only putative catalytic mechanisms including a route via radical-intermediate or dismutase activity (sacrificing one THD to DHD for production of one equol) were suggested without experimental confirmation (KAWADA et al. 2016; Kim et al. 2010a).

Table 1.1 Bacterial species for production of equol and 5-hydroxy-equol and their production efficiency.

Species	Reaction	Substrate	Product	Initial substrate conc. [mg/L]	Titer [mg/L]	Productivity [mg/L/h]	Reference
Bifidobacterium pseudolongum	reduction	of 100ml soy milk	equol	n.d*.	4.6	0.1	(Tsangalis et al. 2002)
Bifidobacterium longum-a				n.d.	5.1	0.1	
Bifidobacterium animalis				n.d.	5.4	0.1	
Pediococcus pentosaceus CS1		of 2%(w/v) P. lobata extract		n.d.	246.0	3.4	(Kwon et al. 2018)
Lactobacillus sp. CS2				n.d.	144.0	2.0	
Lactobacillus sp. CS3				n.d.	158.0	2.2	
Slackia isoflavoniconvertens JCM16059		daidzein		38.1	31.1	0.3	(Jin et al. 2008)
Slackia sp. YIT 11861				102.0	96.9	1.0	(Tsuji et al. 2013)
Lactococcus garvieae 20-92				80.0	57.0	0.6	(Uchiyama et al. 2006)
slackia sp. TM-30				12.5	6.2	<0.1	(Tamura et al. 2014)
Eggerthella sp. YY7918				12.7	12.1	0.2	(Yokoyama and Suzuki 2008)
Slackia isoflavoniconvertens DSM22006				21.4	12.6	0.9	(Matthies et al. 2009)
Slackia sp. NATTS				102.0	91.1	3.8	(Tsuji et al. 2010)
Eggerthella sp. Julong 732, Lactobacillus sp. Niu-O16				305.0	183.0	7.6	(Wang et al. 2007)
Eubacterium sp. D1				200.0	3.4	<0.1	(Yu et al. 2008)
Eubacterium sp. D2				200.0	3.6	<0.1	
Asaccharobacter celatus gen,nov.sp. nov do03				49.0	33.6	0.4	(Minamida et al. 2006), (Minamida et al. 2008)
Coriobacteriaceae sp. Mt1B8				25.4	17.0	0.9	(Matthies et al. 2008)
Escherichia coli strain tDDDT, recombinant				254.0	206.0	51.5	(Lee et al. 2016a)
strain Julong 732		DHD*		103.0	84.8	0.9	(Wang et al. 2005a)
Slackia sp. NATTS				25.6	20.4	0.9	(Tsuji et al. 2010)
Slackia isoflavoniconvertens DSM22006		genistein	5-OH-equol*	22.7	8.0	0.2	(Matthies et al. 2009)
Coriobacteriaceae sp. Mt1B8				27.0	15.5	0.5	(Matthies et al. 2008)
Escherichia coli strain tDD and tDT, recombinant				270.0	230.0	38.0	(Lee et al. 2017)
Slackia equolifaciens AUH-JLC257				162.0	129.0	1.8	(Xie et al. 2015)

***5-OH-equol**: 5-hydroxy-equol, **DHD**: dihydrodaidzein, **n.d.** not determined.

1.2.2 Regioselective bioconversion of ODIs

Historically, isolation of ODIs was firstly achieved by biotransformation using fungal and microbial species as living catalysts (Umezawa et al. 1975). Especially, Aspergillus and Streptomyces isolated from traditional soybean fermented foods are known for potent target species for ODI production. For example, *Aspergillus oryzae* is a powerful species to prepare 8-ODIs with strict regioselectivity and fine yield (i.e. ~100 mg/L) (Seo et al. 2013a; Wu and Chang 2016; Wu et al. 2015). It is noteworthy that these fungal strains are compatible with large-scale fermentation (3~7 L), which makes these strains highly promising candidates for industrial application. Streptomyces, another class of isoflavone hydroxylating microorganisms, has been also recognized as a potent ODI producing strain. Komiyama *et al*. observed diverse hydroxylated isoflavone products from fermentation broth of *Streptomyces* sp. OH-1049, which included 3'-OHD and 8-OHD (Funayama et al. 1989; Komiyama et al. 1989). Afterward, Roh *et al*. screened diverse microbial strains including *Actinomyces*, *Bacillus* spp. and several fungal strains for their ability to hydroxylate daidzein and genistein, then *Streptomyces avermitilis* MA-4680 represented efficient conversion rate with regioselective production of 3'-OHD (37.5 mg/L) and 3'-OHG (22.9 mg/L) (Roh et al. 2009b).

Afterward, scientists took a different route to prepare target ODIs using cloned monooxygenases and recombinant strains to enhance low ODI productivity, yield and regioselectivity of natural microorganisms. Mainly cytochrome P450s, flavin-dependent monooxygenase and recently tyrosinase have been adopted for efficient isoflavone hydroxylation. Among them, cytochrome P450s are the most

investigated biocatalyst for ODI synthesis. Those studies are mainly performed by our group and Te-Sheng Chang's group. The P450 study for ODI production was conducted in five major directions of P450 identification, redox protein coupling, NAD(P)H cofactor supply, P450 engineering, and host development. At first, our group focused on screening of functional bacterial species with isoflavone hydroxylation activity, then could find out two microbial species, *Streptomyces avermitilis* MA4680 and *Nocardia farcinica* IFM10152, which predominantly perform B-ring and A-ring *ortho*-specific hydroxylations, respectively (Choi et al. 2009; Roh et al. 2009b). These two bacterial strains showed outstanding hydroxylation character compared to previously reported microbial genera including *Arthrobacter* and *Micrococcus* (Klus and Barz 1995). Then, their hydroxylation activity was revealed mainly due to endogenous cytochrome P450 monooxygenases: CYP105D7/CYP107Y1 from *S. avermitilis* MA4680 and Nfa12130/Nfa33880 from *N. farcinica* IFM10152, respectively (Choi et al. 2009; Pandey et al. 2011; Pandey et al. 2010). In addition, when the cytochrome P450s were artificially overexpressed with non-native promoters, the microbial catalysts produced significantly high yield of ODIs (37.5 mg/L of 3'-OHD; (Pandey et al. 2010), 7.2 mg/L of 3'-OHG; (Pandey et al. 2011)). Meanwhile, the catalytic efficiency of the cytochrome P450s could be improved by heterologous overexpression in *Streptomyces* host, co-expression with the innate redox partners, or artificial fusion with redox protein for self-sufficient electron supply (Choi et al. 2012a; Choi et al. 2014; Pandey et al. 2014). On the other hand, Te-Sheng Chang *et al*. thoroughly investigated fungal cytochrome P450s and their heterologous expression in recombinant yeast strains which were recognized as

valuable microbial cell factories for functional expression of membrane-anchored eukaryotic cytochrome P450s. At first, they selected a cytochrome P450, CYP57B3 previously isolated from *A. oryzae*, which played a major catalytic role in forming *ortho*-hydroxylation of genistein (Nazir et al. 2011). When the CYP57B3 was artificially fused with the reductase domain of CYP102A1 (BM3) from *Bacillus megaterium*, the recombinant *Pichia pastoris* harboring the chimeric P450 showed 9.1 mg/L of 6-OHD, which is the highest production level reported ever (Chang et al. 2013). The same group also performed several other constructions of chimeric CYP-CPRs (cytochrome P450 reductases) for preparation of versatile ODIs. Then, CYP57B3-sCPR (CPR from *Saccharomyces cerevisiae*) in *P. pastoris* was verified for efficient production of 3'-OHG with 3.5 mg/L yield, which was further improved to 23.0 mg/L by a following study in which the recombinant yeast was subjected to laboratory evolution during periodic hydrogen peroxide-shocking (Ding et al. 2015; Wang et al. 2016). Meanwhile, another chimeric enzyme was constructed with a fusion of transmembrane domain (from CYP57B3), CYP105D7 (from *S. avermitilis* MA4680) and CPR (from *S. cerevisiae*), then recombinant *P. pastoris* harboring the chimera enzyme achieved 7.5 and 15.0 mg/L yields for 6-OHD and 3'-OHG in 5 L scale fermentation, respectively (Chiang et al. 2016a). According to these pioneering studies performed by the two groups, *Streptomyces* and *Pichia* strains were potent hosts for ODI production, since they preserve high redox potentials in the cell during biotransformation, tolerate organic solvents and large-scale fermentation, and act as a good platform for heterologous expression of recombinant (membrane) proteins (Choi et al. 2014; Schwarzhans et al. 2017).

Even though the abovementioned investigations enabled microbial production of ODIs in semi-preparative scale, low catalytic efficiency of ODI monooxygenase, mainly cytochrome P450, resulting low productivity is far below the requirements of industry for sufficient high concentration and high yield preparation of valuable ODIs. Motivated by such problems, they tried to enhance the enzyme specific activity by random or directed evolution. CYP102D1, a single self-sufficient P450 identified as long chain fatty acid hydroxylase from *S. avermitilis* MA4680, was a target for protein engineering, and F96V/M246I mutations increased 15-fold in catalytic efficiency for daidzein to ODI conversion (Choi et al. 2012b). The mutant became a template for second generation saturation mutagenesis, then additional A273S/T277R mutations redirected its regioselectivity over the 3'/6-position by 3-fold with 23-fold improved hydroxylation activity (ODIs, 48.4 mg/L) (Choi et al. 2015). Another well-known self-sufficient bacterial P450, CYP102A1 (BM3) from *B. megaterium*, was also virtually screened to obtain isoflavone hydroxylation activity, which finally generated several improved variants with mutations at substrate access channel entrance and substrate binding sites. CYP102A1 F87A was able to produce ODI and additional mutation of Y51A changed regioselectivity favorable C3' over C6 position (Ko et al. 2015). For CYP57B3, a potent fungal P450 for ODI hydroxylation, a variant with single substitution of V138I was recently screened for 14-fold higher production of 3'-hydroxygenistein (Hatakeyama et al. 2017).

Even though these extensive studies offer a cytochrome P450-based biotransformation platform for regioselective production of ODIs, their yield and

productivity were still insufficient for the industrial application. The major drawback of the biotransformation is chronic disadvantages of cytochrome P450: low catalytic activity, stability, and cofactor dependency (Urlacher and Girhard 2012). The habitual obstacle was partially overcome by exploiting a non-heme flavin-dependent monooxygenase, Sam5 from *Saccharothrix espanaensis* as an efficient regioselective biocatalyst for 3'-hydroxydaidzein production (75 mg/L in yield, 3.1 mg/L/h in productivity) (Lee et al. 2014). The researchers adopted *E. coli* whole-cell biotransformation system, because the hydroxylase is also highly dependent on the available cellular reducing cofactor, i.e. NAD(P)H. Next, the ODI production underwent dramatic breakthrough by introduction of tyrosinase-catalyzed reaction system in recent years. At first, tyrosinase seemed not to be a good catalyst for the *ortho*-hydroxylation, since its catecholase activity oxidizes catechol compounds to quinones and finally melanin complex, preventing selective ODI production. In a previous microbial production, a tyrosinase (MelC2) from *Streptomyces avermitilis* MA4680, therefore, was a deletion target to increase ODI yield in cytochrome P450-mediating hydroxylation system (Pandey et al. 2014). On the other hand, monophenolase activity of tyrosinase was successfully exploited to give *ortho*-hydroxylation of aromatic substrates by supplementation with additional reducing agents (Lee et al. 2015). In this study, additions of catechol, NADH, and ascorbic acid sacrificially inhibited melanin formation, resulting efficient bioconversion of *trans*-resveratrol into piceatannol (3'-hydroxy-*trans*-resveratrol). In next, the same tyrosinase was used to convert daidzein to 3'-OHD. However, another tyrosinase with different microbial origin (*B. megaterium*) was superior for the production of

3’-ODI (Lee et al. 2016b). In the study, borate chelation at basic pH was strategically adopted to inhibit diphenolic 3’-ODI oxidation to quinone or melanin. The reaction system also increased 3’-OHD and 3’-OHG (orobol) with remarkable yields: 1.35 and 0.27 g/L, respectively (Lee et al. 2016b). The productivities and yields of ODIs highly exceeded the previous levels achieved by cytochrome P450s. The dramatic breakthrough seems due to no reductive cofactor requirement and higher enzymatic activity, i.e. more than 10~100 fold. Similarly, Te-Sheng Chang group adopted the same catalyst and chelating system to prepare 3’-ODI glycosides with fine yields, suggesting the microbial tyrosinase has broad substrate specificity (Chiang et al. 2016b). However, the tyrosinase was abandoned to produce different regiomeric ODIs rather than 3’-ODI. Its limited regioselectivity might be caused by inhibitory mechanism of the ODIs against the tyrosinase (Park et al. 2010). In fact, 6-ODI and 8-ODI are potent competitive and suicide tyrosinase inhibitors, respectively (Chang 2007; Chang et al. 2005). In addition, A-ring of isoflavone is more reluctant to hydroxylation than its B-ring owing to its structural bulkiness and higher pK_a value of the phenolic group at C7 over C4’. Therefore, the preparation of ODIs with specific hydroxylation at A-ring is recommended to use other enzymes such as cytochrome P450 rather than tyrosinase. The overall ODI production methods and microbial species are systematically summarized in **Table 1.2**.

Table 1.2 Production of *ortho*-dihydroxyisoflavones by microorganisms harboring monooxygenase.

Enzyme (recombinant host)	Microbial resources	Substrate	Product	Initial substrate conc.[mg/L]	Titer [mg/L]	Productivity [mg/L/h]	Reference
CYP107H1-CamA-CamB^{C} (*E. coli* BL21(DE3))	*B. subtilis* 168 *P. putida* ATCC17453	daidzein	3'-OHD*	12.7	<0.1	<0.1	(Roh et al. 2009a)
CYP57B3-bmCPR*^{F} (*P. pastoris* X-33)	*A. oryzae* BCRC32288 *B. megaterium* ATCC14581			25.4	0.2	<0.1	(Chang et al. 2013)
CYP154-CamA-CamB^{C} (*E. coli* BL21(DE3))	*N. farcinica* IFM10152			25.4	1.0	0.1	(Choi et al. 2010)
CYP102A1 (Y51L/F87A) (*E. coli* BL21(DE3))	*B. megaterium* ATCC10778			25.4	1.0	0.1	(Choi et al. 2010)
CYP105D7-saCPR^{F} (*S. avermitilis* MA4680)	*S. avermitilis* MA4680			25.4	9.3	<0.1	(Choi et al. 2012a)
Nfa33880-Nfa33870-Nfa33860^{C} (*E. coli* BL21(DE3))	*N. farcinica* IFM10152			25.4	0.11	<0.1	(Choi et al. 2009)
CYP105D7-FdxH-FprD^{C} (*S. avermitilis* MA4680)	*S. avermitilis* MA4680			76.2	10.0	1.3	(Pandey et al. 2014)
CYP102D1 G1 (A273H/G274E/T277G) (*E. coli* BL21(DE3))	*S. avermitilis* MA4680			127	13	0.3	(Choi et al. 2013)
CYP102D1 M8 (F96V/M246I/A273S/T277R) (*E. coli* BL21(DE3))	*S. avermitilis* MA4680			127	35-40	0.8	(Choi et al. 2015)
CYP105D7-FdxH^{C} (*S. avermitilis* MA4680)	*S. avermitilis* MA4680			127	37.5	2.5	(Pandey et al. 2010)
Sam5-osCPR^{C} (*E. coli* BL21(DE3))	*S. espanaensis* DSM44229 *O. sativa*			101.6	75	3.1	(Lee et al. 2014)
Tyrosinase (*E. coli* BL21(DE3))	*B. megaterium* ATCC10778			1270	1350	900	(Lee et al. 2016b)
-	*S. avermitilis* MA4680			127	37.5	1.3	(Roh et al. 2009b)
-	*N. farcinica* ATCC3318			127	9.6	0.4	
-	*S. lincolnesis* ATCC25466			127	7.9	0.3	
-	*S. avermitilis* MA4680	genistein	3'-OHG*	135	22.9	1.0	
CYP107Y1 (*S. avermitilis* MA4680)	*S. avermitilis* MA4680			27	7.2	0.1	(Pandey et al. 2011)
CYP57B3-scCPR^{F} (*P. pastoris* X-33)	*A. oryzae* BCRC32288 *S. cerevisiae* BCRC57896			27	3.5	<0.1	(Ding et al. 2015)
aoTMD*-CYP105D7-scCPR^{F} (*P. pastoris* X-33)	*A. oryzae* BCRC32288 *S. avermitilis* MA4680 *S. cerevisiae* BCRC57896			27	15	0.2	(Chiang et al. 2016a)
CYP57B3-scCPR^{F} (*P. pastoris* X-33(P2-D14-5))	*A. oryzae* BCRC32288 *S. cerevisiae* BCRC57896			135	23	0.3	(Wang et al. 2016)

Table 1.2 (*continued*)

Enzyme (recombinant host)	Microbial resources	Substrate	Product	Initial substrate conc.[mg/L]	Yield [mg/L]	Productivity [mg/L/h]	Reference
Tyrosinase (*E. coli* BL21(DE3))	*B. megaterium* ATCC10778	genistein	3'-OHG	270	271.7	271.7	(Lee et al. 2016b)
Tyrosinase (*E. coli* BL21 (DE3))	*B. megaterium* BCRC10608	daidzin	3'-OHDI*	~800	175	116.7	(Chiang et al. 2016b)
		genistin	3'-OHGI*	~800	160	106.7	
Nfa33880-CamA-CamB[C] (*E. coli* BL21 (DE3))	*N. farcinica* IFM10152	daidzein	6-OHD*	25.4	0.6	<0.1	(Choi et al. 2009)
Nfa12130-Nfa12140-Nfa12150[C] (*E. coli* BL21 (DE3))				25.4	0.8	<0.1	
CYP102D1 (F96V/M246I) (*E. coli* BL21 (DE3))	*S. avermitilis* MA4680			127	1.8	<0.1	(Choi et al. 2013)
Nfa12130-saCPR[F] (*S. avermitilis* MA4680)	*N. farcinica* IFM10152 *S. avermitilis* MA4680			25.4	2.3	<0.1	(Choi et al. 2014)
CYP102A1 (F87A/Y51L) (*E. coli* BL21(DE3))	*B. megaterium* ATCC10778			25.4	3.6	0.1	(Ko et al. 2015)
CYP57B3-bmCPR[F] (*P. pastoris* X-33)	*A. oryzae* BCRC32288 *B. megaterium* ATCC14581			25.4	9.1	<0.1	(Chang et al. 2013)
CYP102D1 M8 (F96V/M246I/A273S/T277R) (*E. coli* BL21 (DE3))	*S. avermitilis* MA4680			127	13.4	0.3	(Choi et al. 2015)
CYP102D1 (L95I/F96V) (*E. coli* BL21 (DE3))	*S. avermitilis* MA4680			25.4	1.6	<0.1	(Choi et al. 2012b)
aoTMD*-CYP105D7-scCPR[F] (*P. pastoris* X-33)	*A. oryzae* BCRC32288 *S. avermitilis* MA4680 *S.cerevisiae* BCRC57896			25.4	7.5	0.1	(Chiang et al. 2016a)
CYP57B3-bmCPR[F] (*P. pastoris* X-33)	*A. oryzae* BCRC32288 *B. megaterium* ATCC14581	daidzein	8-OHD*	25.4	0.6	<0.1	(Chang et al. 2013)
Nfa33880-CamA-CamB[C] (*E. coli* BL21 (DE3))	*N. farcinica* IFM33880			25.4	0.8	<0.1	(Choi et al. 2009)
Nfa33880-Nfa33870-Nfa33860[C] (*E. coli* BL21 (DE3))	*N. farcinica* IFM33880			25.4	<0.1	<0.1	
CYP102D1 (F96V/M246I) (*E.coli* BL21 (DE3))	*S. avermitilis* MA4680			25.4	2.2	<0.1	(Choi et al. 2012b)
-	*A. oryzae* BCRC32288			200	52	0.4	(Wu et al. 2015)
-	*A. oryzae* KACC40247			1248	160	4.4	(Seo et al. 2013a)
-	*A. oryzae* BCRC32288	genistein	8-OHG	200	83	3.5	(Wu and Chang 2016)

[C] : co-expressed proteins, [F] : fused proteins, * **CPR** : cytochrome reductase, **TMD** : transmembrane domain, **3'-OHD** : 3'-hydroxydaidzein, **3'-OHG** : 3'-hydroxygenistein, **3'-OHDI** : 3'-hydroxydaidzin, **3'-OHGI** : 3'-hydroxygenistin, **6-OHD** : 6-hydroxydaidzein, **8-OHD** : 8-hydroxydaidzein.

1.3 The scope of thesis

The purpose of this thesis is mainly to provide the biological synthetic methods of two different isoflavone derivatives, equol and ODI. Equol, a reductive isoflavone metabolite, is prepared by whole-cell biotransformation exploiting recombinant equol-producing *E. coli*. Engineering skills on enzymes, whole-cells and reaction solvent to enhance equol-forming activities were performed and discussed in Chapter 2, 3 and 4. The second theme includes protein engineering for regioselective production of ODIs. In Chapter 5, a bacterial tyrosinase was selected as the efficient biocatalyst to prepare ODIs and comprehensive engineering including circular permutation and site-saturation mutagenesis supported by computationally information, was presented.

First, the equol-producing artificial strain was constructed based on the previously reported sequence information of equol-forming enzymes (Chapter 1, a full reprint of a published article: Lee *et al*., *Applied and Environmental Microbiology,* 2016, 82(7): 1992-2002). Due to the outstanding equol producing activities, *Slackia isoflavoniconvertens* DSM22006 previously identified to synthesize equol and 5-hydroxy-equol was selected for exploring transplantation of its equol-producing activity to recombinant *E. coli,* and for enhancement of the reaction efficiency by enzyme engineering, in which an enzyme of rate-determining step was targeted for rational mutagenesis.

In Chapter 3, the same recombinant bacteria were used as whole-cell catalyst to prepare 5-hydroxy-equol from genistein. Because there was a unprecedented by-product, 5-hydroxy-dehydroequol, cellular compartmentalization

was exploited to enhance production selectivity and productivity (a full reprint of a published article: Lee *et al*., *ACS Chemical Biology,* 2017, 12: 2883-2890). In this study, estrogen receptor binding affinity of the biosynthesized 5-hydroxy-equol was firstly investigated.

In Chapter 4, g/L level production of equol and 5-hydroxy-equol was aimed. The limited titer of equols was firstly speculated by low solubility of isoflavone, not by low activities or poor expression of enzymes. Therefore, an isoflavone solubilization strategy compatible with whole-cell biotransformation was needed that supplementation of hydrophilic polymers was adopted in this study. In addition, tetrahydrodaidzein reductase (THDR) was recognized as the key enzyme to restrict the high conversion efficiency, computationally predicted active site residues of THDR were picked for mutagenesis to enhance 5-hydroxy-equol biotransformation titer.

In contrast to the previous chapters, chapter 5 is comprised of the studies for oxidative modification of isoflavone. Especially, ODIs were aimed for regioselective production using tyrosinase biocatalysts with enhanced catalytic performance. In order to overcome poor isoflavone hydroxylation characters of wild-type tyrosinase, circular permutation and site saturation mutagenesis were extensively investigated for 3'-hydroxylation and 6 or 8-hydroxyaltion, respectively. Furthermore, *ortho*-hydroxylation of equols was set to the second goal. Even though there was lack of known biological benefits of the compounds, they were recognized as important metabolites of equol in human body. To fulfill the novel biosynthesis, combinatorial biotransformation of tyrosinase (for hydroxylation) and whole-cells

(for reduction) was under investigation for regioselective preparation of OHEs. Finally, the studies in this chapter provides the valuable biocatalytic platforms for preparation of versatile oxidative or reductive isoflavone derivatives with high production yield.

Chapter 2.

Construction of equol-producing recombinant *Escherichia coli* and production of (*S*)-equol with enhanced dihydrodaidzein reductase mutant P212A

A full reprint of the paper published in *Applied and Environmental Microbiology* (2016) 82(7): 1992-2002.

2.1 Introduction

The daidzein metabolite (*S*)-equol is produced by human gut microbiota, and it has drawn a significant amount of attention as a result of its estrogenic properties in the human body that lessen postmenopausal symptoms in female patients (Jenks et al. 2012). (*S*)-equol binds effectively to the type-β estrogen receptor, but not to the type α, preventing menopausal symptoms without increasing the incidence rate of breast cancer. Since many other estrogenic chemicals that have been used to reduce menopausal symptoms have increased the incidence rate of breast cancer, such selectivity for the receptor subunit is critical to develop any estrogenic reagents (Muthyala et al. 2004; Setchell et al. 2005).

Most (*S*)-equol-producing bacteria (Tsuji et al. 2010; Uchiyama et al. 2007; Yokoyama and Suzuki 2008) that are known to convert daidzein to equol belong to Coriobacteriaceae, including *Slackia, Eggerthella* and *Adlercreutzia* (Kim et al. 2009; Matthies et al. 2009; Tsuji et al. 2010). However, the first gene identification for the equol metabolism was reported in the non-Coriobacteriaceae microbe, *Lactococcus* sp. strain 20-92 (Shimada et al. 2012; Shimada et al. 2011; Shimada et al. 2010). Similar identifications of equol metabolism in *Slackia* sp. have also been reported (Schroder et al. 2013; Tsuji et al. 2012). According to these reports, daidzein is converted to (*S*)-equol by four enzymes (**Fig. 2.1**): daidzein reductase (DZNR), dihydrodaidzein reductase (DHDR), tetrahydrodaidzein reductase (THDR), and dihydrodaidzein racemase (DDRC). DZNR reduces daidzein to (*R*)-dihydrodaidzein (DHD) enantioselectively (Shimada et al. 2012; Shimada et al. 2010). (*R*)-DHD is subsequently racemized either to (*S*)-DHD through tautomerization at C-3 or by

DDRC activity (Shimada et al. 2012). DHDR is involved in the reduction of both (*S*) and (*R*)-DHD to *trans*- and *cis*-tetrahydrodaidzein (*trans*- and *cis*-THD), respectively (Shimada et al. 2011). Here, only *trans*-THD can be converted enantioselectively to (*S*)-equol by THDR (Kim et al. 2009). In the case of THDR, a radical mechanism was suggested to produce (*S*)-equol from (3*S*,4*R*)-*trans*-tetrahydrodaidzein (Kim et al. 2010a).

The production of (*S*)-equol by use of gut bacteria was previously reported in some papers or patents (Elghali et al. 2012; Minamida et al. 2006; Tsuji et al. 2013; Uchiyama et al. 2013). According to these reports, *Slackia* sp. YIT 11861 is more productive than any of the other strains, including *Slackia* spp. TM-30, *Lactococcus garvieae* strain 20-92 or gram-positive bacterium do03 (Tsuji et al. 2013). However, the use of any equol-producing bacteria has a common disadvantage in that they exhibit oxygen-sensitive growth. Even though experiments have been carried out to overcome such oxygen labile properties of cell growth to produce dihydrodaidzein using a laboratory evolution method, the oxygen sensitivity is still serious and the cell growth rate is quite low, so production is difficult to achieve at an industrial scale (Zhao et al. 2011). Recombinant strains were constructed that are able to convert daidzein to (*S*)-equol or its precursors (Shimada et al. 2010; Tsuji et al. 2012). But those studies have only identified and/or characterized the enzymes involved in each step of the biosynthesis of (*S*)-equol, and since then, no reports have focused on producing (*S*)-equol using recombinant strains.

In this study, we develop a recombinant strain that can produce (*S*)-equol from daidzein under aerobic condition (**Fig. 2.1**). The enzyme expression and

reaction conditions for (*S*)-equol production using whole cell bioconversion were examined and optimized, and to increase the yield and productivity of (*S*)-equol, a mutation was attempted on DHDR to improve its reactivity and/or to shift its enantioselectivity toward (*S*)-DHD away from (*R*)-DHD. The P212A mutant was identified to improve the (*S*)-equol productivity, and the DHDR P212A mutant was characterized, which revealed that the mutation improved not only (*S*)-equol productivity but also the (*S*)-DHD selectivity. Using this unintentional advantage of the mutant, we suggested a novel preparation method for *trans*-THD and *cis*-THD with high enantioselectivity. The results were analyzed in terms of the pH dependency, enantioselectivity, and stereochemistry of the products. Furthermore, the improvement in productivity rather than in the final yield of (*S*)-equol implies other enzyme reaction steps might be the rate-determining steps in reactions with higher substrate concentrations.

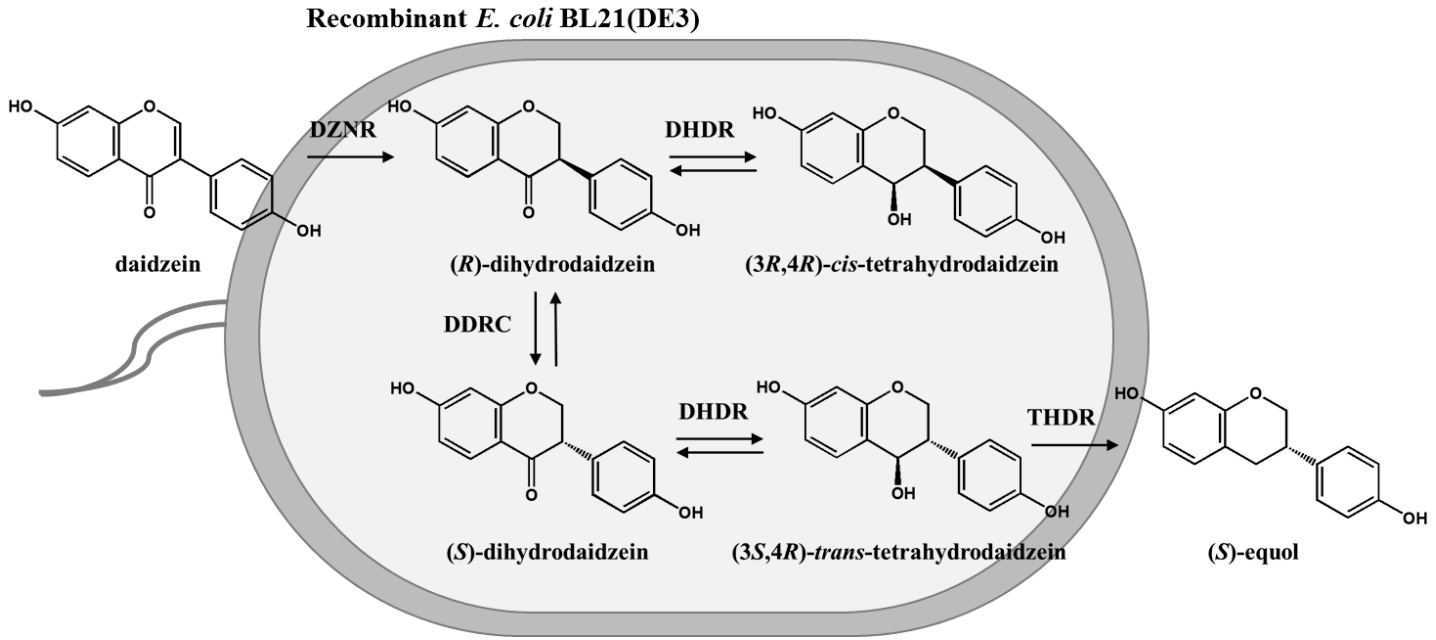

Figure 2.1 Reaction scheme of daidzein-to-equol by recombinant *E. coli*.

E. coli BL21(DE3) strain harboring the two plasmids was named as tDDDT. DZNR: daidzein reductase; DDRC: dihydrodaidzein racemase; DHDR: dihydrodaidzein reductase; THDR: tetrahydrodaidzein reductase.

2.2 Materials and Methods

2.2.1 Chemicals

Daidzein, and dihydrodaidzein were purchased from Sigma Aldrich and Toronto Research Chemicals Inc. (North York, Ontario, Canada), respectively. All other chemicals were purchased from Sigma Aldrich. Dihydrodaidzein racemate was separated and prepared using an HPLC equipped with a CHIRALCEL OJ-H column (Daicel Chemical Industries, Japan). Each enantiomer was confirmed with chiral HPLC analysis, and no tautomerization and racemization of the separated DHD enantiomers were detected in hexane or ethanol. The (*S*)-DHD and (*R*)-DHD had retention times of 10 min with a sharp peak and 39 min with a broad peak, respectively, in the eluent (hexane : ethanol = 60 : 40) at 1 ml/min flow rate. The unusually large difference in their retention times arose from using a different chiral column, CHIRALCEL OJ-H column working under normal phase condition, whereas most of other researchers utilized other chiral columns which worked under reversed phase condition. The researchers claimed that (*S*)-DHD was eluted first, followed by (*R*)-DHD (Park et al. 2011; Shimada et al. 2012). Additionally, comparison with the retention times of (*R*)-DHD produced by purified DZNR and (*S*)-DHD racemized from (*R*)-DHD by purified DDRC confirmed the assignment. Chiral analysis for THDs was also performed under the same conditions as that for DHD analysis.

2.2.2 Cloning and construction of recombinant strain

S. isoflavoniconvertens DSM 22006 was cultured on Columbia blood agar plate with 5% sheep blood at 37°C under anaerobic condition. *S. isoflavoniconvertens* genomic DNA was extracted with an Exgene^{TM} Cell SV genomic DNA purification kit (Geneall, South Korea) and was used as a PCR template. The four genes, *dzr* (Gene ID: 409131878) encoding DZNR, *ddr* (Gene ID: 409131876) encoding DHDR, *tdr* (Gene ID: 409131875) encoding THDR and *ifcA* (Gene ID: 409131872) encoding DDRC, were amplified by PCR using a set of designed primers, and the PCR products were cloned into the pRSFDuet-1 (*dzr/ifcA*) and pCDFDuet-1 (*ddr/tdr*) expression vectors with specific restriction enzyme sites at multi-cloning sites 1 and 2, respectively (**Fig. 2.2** and **Table 2.1**). All the cloned genes were verified for their sequences with no errors compared to their gene sources. The two expression vectors were transformed simultaneously into *E. coli* BL21 (DE3) (Novagen) by heat shock, and the transformed colonies were selected on a kanamycin (50 μg/ml) and streptomycin (50 μg/ml) LB agar (tryptone 10.0 g/L, yeast extract 5.0 g/L, sodium chloride 10.0 g/L and 15.0 g/L of agar in the case of solid media) plate. A single colony was inoculated with 3 ml of LB with two antibiotics and was grown overnight. The transformants were named as tDDDT-WT or tDDDT-PA depending on the presence of the P212A mutation on the pCDFDuet-1 vectors. The transformants were then used for the whole cell reaction. For the enzyme purification, *ddr* and *ifcA* were individually cloned into pCDFDuet-1 and pET24a, respectively, and transformed into BL21 (DE3). The description and notation for all transformants are listed in **Table 2.1**.

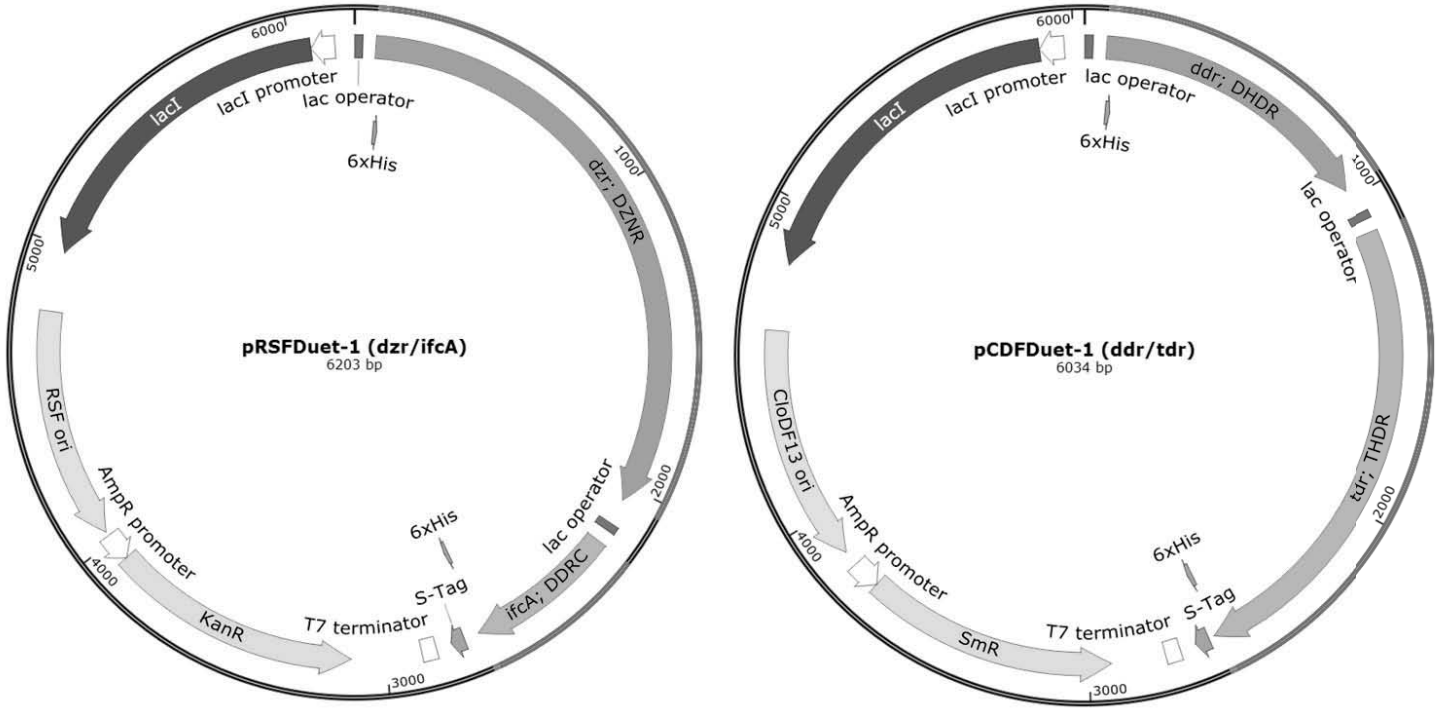

Figure 2.2 Designed plasmids containing equol forming genes.

All the genes: *dzn*, *ifcA*, *ddr*, and *tdr* encoding DZNR, DDRC, DHDR and THDR, respectively were cloned from *Slackia isoflavoniconvertens* DSM22006.

2.2.3 Site-directed mutagenesis of DHDR

A previously-established protocol (Zheng 2004) was used to make amino acid mutations at P212, H182 residues of DHDR. The mutations were introduced into the pCDFduet-1-*ddr* construct by PCR (Herculase II fusion DNA polymerase) using the specific mutagenesis primers (**Table 2.1**), and all constructs were confirmed by sequencing.

Table 2.1 Cloning, transformation and site-directed mutagenesis information.

dzr and *ifcA* were cloned to pRSFDuet-1 vector at multi-cloning sites 1 and 2, respectively. *ddr* and *tdr* were cloned to pCDFDuet-1 vector at multi-cloning sites 1 and 2, respectively. *dzr* and *ddr* have N-terminal 6xHis tag sequence. Whereas, *ifcA* and *tdr* have 6xHis tag at their C-terminus, followed by stop codon. In the case of sole cloning of *ifcA*, pET24a vector was used and C-terminal cloning primer was modified by substituting the EcoRV restriction site with a HindIII restriction site. All genes are expressed under T7 promoter.

Cloning information		
Genes	**Cut sites**	**Primer sequences (5' to 3')**
dzr	BamHI	ATAAGGATCCGATGCAGCACGCGAAATA
	NotI	ATATAGCGGCCGCTACACCATGCGCGCTAC
ifcA	NdeI	ATAATCATATGAAAGCTCAACTGAATC
	EcoRV	ATAAGATATCCTAGTGGTGATGATGGTGATGCTCAGCGTCCACGTC
ddr	BamHI	ATAAGGATCCGATGGCACAAGAGGTTAAG
	NotI	ATATAGCGGCCGCTTAGGCGATTTCGCCCTG
tdr	NdeI	ATAATCATATGGCAGAATTCGACGTTG
	KpnI	ATAAGGTACCTCAGTGGTGGTGGTGGTGGTGCATGTTTGCAATCGCGTG
Transformant notation		
Name	**Plasmid description**	
tDDDT-WT	pRSFDuet-1(*dzr/ifcA*) + pCDFDuet-1(*ddr/tdr*)	
tDDDT-PA	pRSF Duet-1(*dzr/ifcA*) + pCDF Duet-1(*ddr P212A/thdr*)	
tDHDR-WT	pCDF(*ddr*)	
tDHDR-PA	pCDF(*ddr P212A*)	
tDDRC	pET24a(*ifcA*)	
Site-directed mutagenesis of DHDR		
Primer	**Primer sequences (5' to 3')**	
P212A_F	CCGTGACCGCCGGCCTGGTGTG	
P212A_B	CCAGGCCGGCGGTCACGGAATTG	
H182Y_F	CAGGCATGCTACGCCGCCGCCAAG	
H182Y_B	GGCGGCGGCGTAGCATGCCTGCGG	

2.2.4 Whole-cell reaction with (*S*)-equol producing recombinant *E. coli*

Transformants tDDDT-WT or tDDDT-PA were grown in LB broth medium (50 ml) containing 50 μg/ml of kanamycin and streptomycin at 37 °C until reaching an optical density of 0.6-0.8 at 600nm (OD_{600}). Isopropyl-thio-β-D-galactopyranoside (IPTG) was then added to a final concentration of 0.1 mM along with 0.1 mM $FeSO_4$ as the source of the iron sulfur cluster of DZNR. After the IPTG induction, cells were grown at 18 °C for 12 hr and were subsequently harvested by centrifugation, washed with phosphate buffer saline (PBS: sodium chloride 8.00 g/L, potassium chloride 0.20 g/L, disodium hydrogen phosphate 12-water 3.58 g/L and potassium dihydrogen phosphate 0.27 g/L, pH 7.2), and resuspended in 200 mM of potassium phosphate buffer (KPB) (pH 8.0). The pH of the reaction buffer in the whole-cell reaction was first optimized for the highest equol production, because the whole-cell reaction includes four enzyme reactions and many other reaction parameters such as substrate/product solubility, cell viability, and redox balance also depend on the pH of the reaction solution (**Fig. 2.3**). After the each whole-cell reaction, pH of reaction solution was measured and no change was observed. The initial OD_{600} was set to 10 with 2% (w/v) glucose as a carbon source for cells and isoflavonoid substrate, and the biotransformation with the resting cell was executed with 5 ml of reaction volume in a 20 ml glass vial with gentle shaking (100 rpm) at 30 °C. At different time points during the reaction, 200 μl aliquots were sampled from the reaction mixture, and the reaction was stopped by the addition of 200 μl of ethyl acetate (EA) with vigorous vortexing. After centrifugation at 14000 x g for 5 min, 140 μl of the EA layer were

evaporated using a centrifugal vacuum concentrator (Biotron, South Korea). The samples were then dissolved in 140 μl of methanol for HPLC analysis.

2.2.5 HPLC analysis

The reaction samples prepared from the whole cell reaction or enzyme assay were analyzed via HPLC (YoungLin, South Korea) equipped with a C_{18} column (5 μm, particle size, 4.6 by 250 mm; Vydac, US). 20 μl of reaction sample was injected for the HPLC analysis. The mobile phase was composed of a mixture of solvent A (0.1% trifluoroacetic acid water) and solvent B (acetonitrile), and each metabolite was separated by increasing the concentration of solvent B under the following conditions: an isocratic elution for 5 min with 10% solvent B, a linear gradient for 15 min with 10 to 25% solvent B, an isocratic elution for 9 min with 25% solvent B, a linear gradient for 2 min with 25 to 10% solvent B, an isocratic elution for 5min with 10% solvent B at a flow rate of 1 ml/min and then detected with UV at 280 nm.

For the statistical comparison of (*S*)-equol production between wild-type and P212A mutant strains, a *T*-test was used and a difference was considered significant when $P < 0.05$.

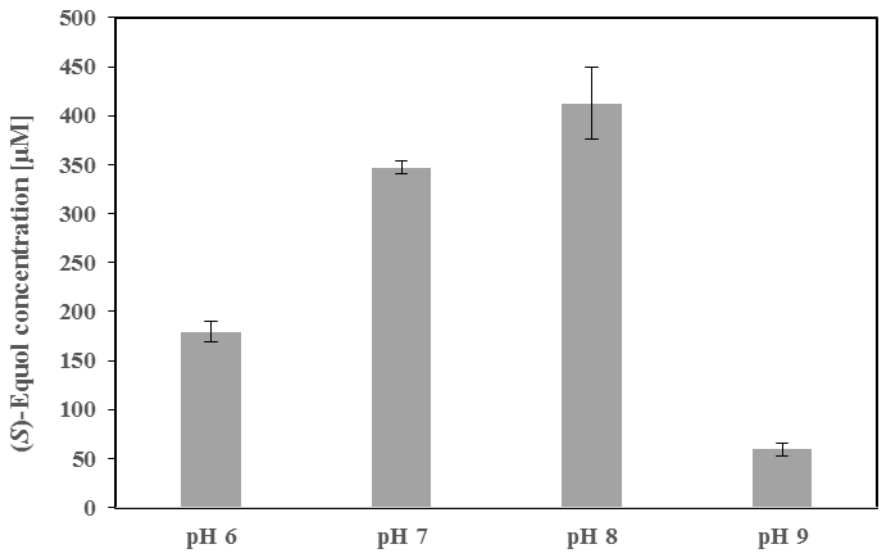

Figure 2.3 Equol production rate comparison varying reaction buffer pH.

Induction temperature was set to 18 °C varying reaction buffer pH. 200mM Potassium phosphate buffer were tested for pH 6 to 8 and 200 mM Tris-HCl buffer was used for pH 9. All other reaction conditions followed '*Materials and Methods*'.

2.2.6 Recombinant enzyme expression and purification

The transformants, tDHDR-WT, tDHDR-PA or tDDRC, were grown in LB broth medium until OD_{600} reached 0.6, and IPTG was added up to a final concentration of 0.1 mM. After IPTG induction, the cells were cultured for 4 hr at 30 °C, and then the cells were harvested by centrifugation and were subsequently washed with PBS. The prepared cells were resuspended in 100 mM of KPB (pH 7.0) containing 1 mM phenylmethylsulfonyl fluoride and were disrupted using a sonicator (Misonix, US) in an ice-cooled bottle. The total pulsing time was 5 min (3 sec on, 8 sec off) with 21 W powered micro-tip. The cell lysates were centrifuged in 14000 x g for 30 min at 4 °C, and supernatant samples were prepared for enzyme purification. The enzymes were purified using Ni-NTA his-tag purification kit (QIAGEN Korea Ltd, Seoul, South Korea), and purification was then carried out utilizing the Ni-NTA resin. The Ni-NTA bound enzymes were washed twice with 50 mM sodium phosphate buffer (pH 8.0) containing 300 mM NaCl, 10 mM imidazole and 0.1 % (v/v) Tween 20, and were further washed with the same buffer containing 30 mM imidazole. The enzymes were eluted with the same buffer containing 250 mM imidazole, and finally, the eluents were dialyzed to remove imidazole, NaCl and Tween 20 against 100 mM KPB (pH 8.0). Purified enzymes were subjected to 12% sodium dodecyl sulfate-polyacrylamide gel electrophoresis (SDS-PAGE) to confirm purity of the enzymes (**Fig. 2.4**), and the enzyme concentrations were determined according to the Bradford assay with bovine serum albumin (BSA) as a standard (Bradford 1976).

Glucose dehydrogenase (GDH) from *Bacillus subtilis* was also cloned, expressed and purified according to the method reported elsewhere (23), for

regenerating NADPH in the enzyme assay. All purified enzymes were stored at -80 °C with 30% glycerol with the relevant buffer.

2.2.7 Enzyme assays

The assays were performed at 37 °C under aerobic conditions with a final volume of 200 µl. The solution contains 100 mM KPB (pH 6.0, the approximately optimum pH for reductase activity of DHDR), 0.5 mM NADPH, and purified enzyme with a final concentration of 0.5 µM. After 5 min of incubation at 37 °C for enzyme activation, the reaction was started by adding 2 µl of 10 mM stock solution of the DHD racemates or each enantiomer of DHD in dimethyl sulfoxide (DMSO). The reaction was stopped by adding 200 µl of ethyl acetate, which was followed by vigorous vortexing. After 5 min of vortexing and 5 min of centrifugation at 14000 x g, the solvent layer was evaporated using a centrifugal vacuum concentrator, and finally redissolved to methanol for HPLC analysis.

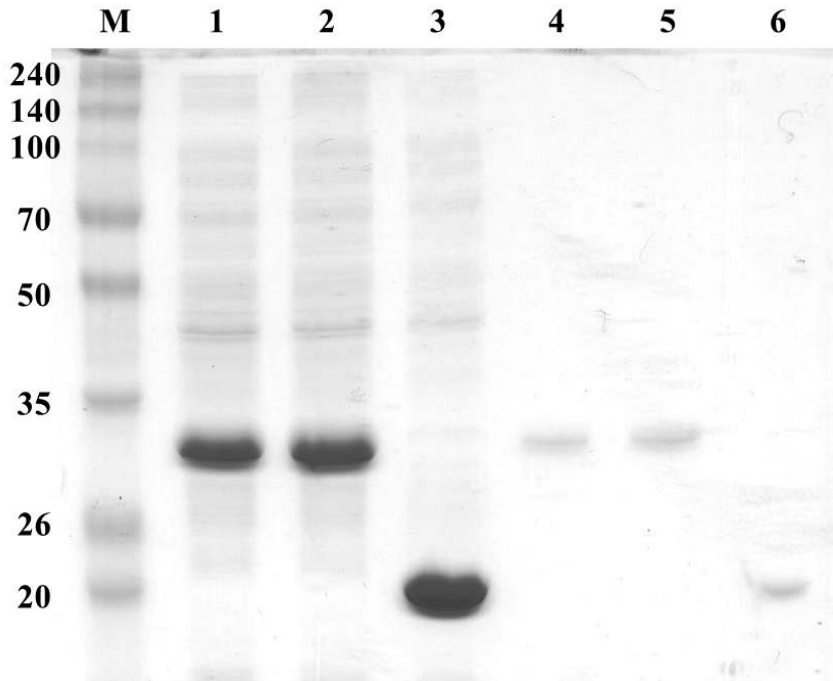

Figure 2.4 Protein expression level comparison between tDHDR-WT and tDHDR-PA and purified enzymes.

Three transformants, tDHDR-WT (line 1), tDHDR-PA (line 2), and tDDRC (line 3) were induced with 0.1mM of IPTG and incubated for 4hr at 30 °C, which gave great high level expression of recombinant proteins in their cytoplasm. Each His-tag purified enzyme was also loaded to confirm their purity on the line 5 (DHDR WT), line 6 (DHDR P212A), line 7 (DDRC). The theoretical His-tagged protein sizes are as such DHDR WT and P212A (30.4 kDa) and DDRC (17.8 kDa). The 10 μl of loaded samples were adjusted to 2 mg/ml in their protein concentration, except that 200 μg/ml of purified enzymes were loaded by 5 μl.

2.2.8 Enzymatic synthesis of *trans*- and *cis*-THD

trans- and *cis*-THD were enzymatically synthesized using (*S*)-DHD and (*R*)-DHD as substrates, respectively, while His-tag purified DHDR was used as a biocatalyst. The reaction conditions were almost the same as those for the enzymatic assay protocol. In addition, 0.25 U/ml of GDH were added to ensure efficient NADPH regeneration with 20 mM of glucose as a substrate (Yun et al. 2005; Yun et al. 2003). The reaction samples were extracted with two volumes of ethyl acetate, and the extracts were concentrated using a rotary evaporator for further chromatography separation. Enzymatically synthesized THD enantiomers were analyzed and confirmed via HPLC with a chiral column. Then, the THD enantiomers were derivatized with N,O-bis(trimethylsilyl)trifluoroacetamide (BSTFA) at 50 °C for 5 min and were analyzed with GC/MS equipped with an electron impact (EI) ionization source for their identification according to a previously described method with some modification (Bae et al. 2014). The GC oven temperature started at 65 °C, was held for 5 min, and then increased by 3 °C/min to 250 °C, holding for 10 min. The ionizing-electron energy was of 70 eV and the collected mass range was 50-600 amu. The retention times for *trans*-THD and *cis*-THD were 15.5 min and 15.9 min, respectively. The relative intensity of the fragmental peaks for each THD diastereomer were recorded and compared with previously reported data (Joannou et al. 1995) (**Fig. 2.5**). HPLC and GC/MS analysis confirmed the purity of each THDs to be more than 95%. To determine the stereochemistry of the enzymatically produced THDs, each THD stereoisomer was dissolved in methanol and CD spectra

were obtained in the range from 220 to 300 nm using a Chirascan^{TM}-plus CD spectrometer (Applied Photophysics, UK).

(3*S*,4*R*)-*trans*-THD (RT= 15.5 min)

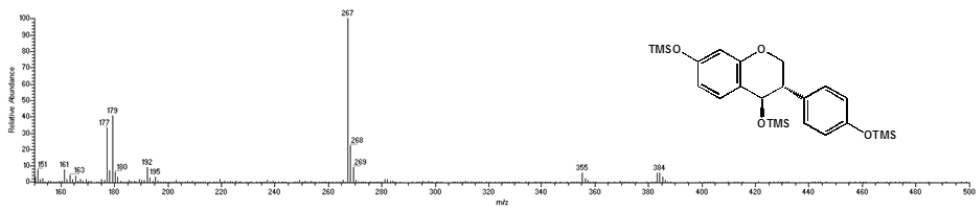

(3*R*,4*R*)-*cis*-THD (RT= 15.9 min)

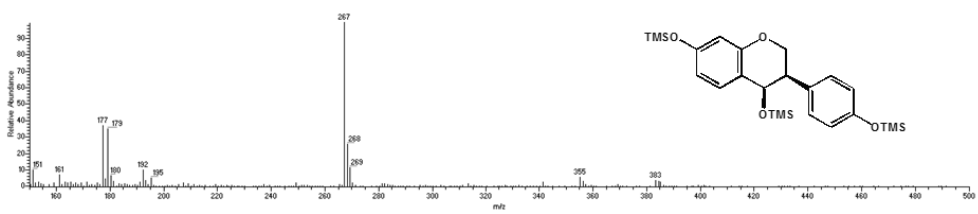

Figure 2.5 Mass Spectra of (3*S*,4*R*)-*trans*-THD and (3*R*,4*R*)-*cis*-THD synthesized by recombinant purified DHDR.

The two THDs displayed same patterns of mass spectra with prominent ions at m/z 383, 355, 267, 192, 179, 177, 161. And they were identified as tetrahydrodaidzein compared with MS patterns. GC/MS analysis was performed after derivatization of the THDs with N,O-BSTFA.

2.3 Results

2.3.1 Daidzein to (*S*)-equol biosynthesis using recombinant *E. coli* BL21 (DE3)

Soluble co-expression of four recombinant enzymes (i.e. DZNR, DDRC, DHDR and THDR) was confirmed via SDS-PAGE. Despite their heterologous expression in *E. coli*, four enzymes were successfully overexpressed at 18, 25, and 30 °C (**Fig. 2.6A**). However, the expression levels of DZNR and DHDR were lower at 30 °C than at 18 or 25 °C, whereas the DDRC expression was the opposite. Since lower conversions of daidzein to (*S*)-equol were observed for the cells grown at 25 and 30 °C, further induction experiments were carried out at 18 °C as the optimum (**Fig. 2.6B**). The heterologous expression of DZNR from *Lactococcus* strain 20-92 in *E. coli* that was grown aerobically resulted in a somewhat low enzyme activity (Shimada et al. 2010), and similarly, in our case, no conversion of daidzein was detected under vigorous shaking conditions (200 rpm with airation) or in a whole cell reaction at 37 °C (data not shown), suggesting that the DZNR catalytic activity is vulnerable to oxygen or to high temperatures. However, no significant decrease in DZNR expression was observed in the recombinant strain under an aerobic growth condition during induction. To overcome the problem of the DZNR activity, a biotransformation reaction was carried out using a fixed cell density (OD_{600}=10) of resting cells under gentle shaking conditions of 100 rpm at 30 °C, which achieved an effective reduction condition for the whole cell conversion without the loss of DZNR activity.

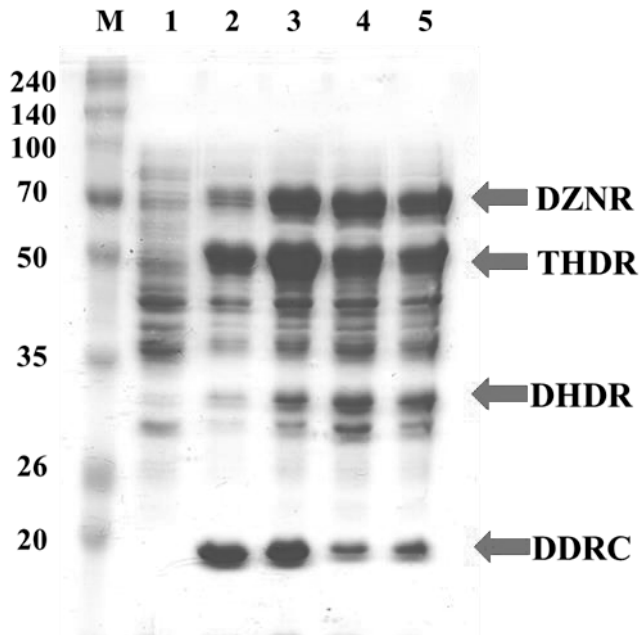

A.

Figure 2.6 Temperature effect in enzyme expression and equol production rate.

A. SDS PAGE of coexpression DZNR/DDRC in pRSFDuet-1 and DHDR/THDR in pCDFDuet-1 vector. Line 1: cell extract of *E. coli* BL21 (DE3) strain containing empty vectors as a control. Line 2 to 4: soluble fractions of tDDDT-WT of which induction temperatures were 30 °C (Line 2), 25 °C (Line 3), and 18 °C (Line 4). Line 5: soluble fraction of tDDDT-PA that was induced at 18 °C. The theoretical His-tagged protein sizes are as follows: DZNR (70.8 kDa), DDRC (17.8 kDa), DHDR (30.4 kDa) and THDR (52.4 kDa). The 10 µl of each soluble fraction was loaded with 3 mg/ml protein concentration.

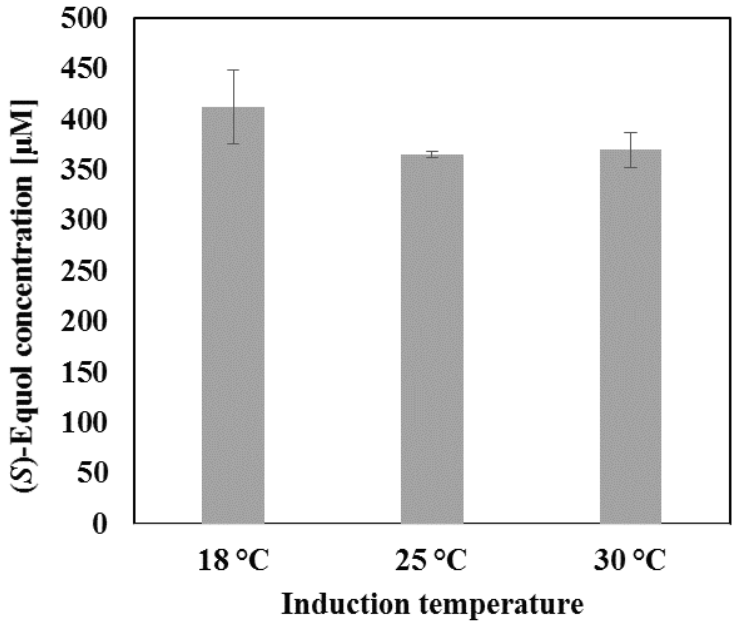

B.

B. Equol production rate comparison varying induction temperature: 18, 25 and 30 °C. When induction temperature was varied, buffer pH was set to pH 8 (the optimal pH point). All other reaction conditions followed '*Materials and Methods*'.

The recombinant *E. coli* tDDDT-WT was used to convert between 0.2 mM and 5 mM daidzein to (*S*)-equol with a high conversion yield (**Fig. 2.7A**). The conversion to (*S*)-equol was high (over 85%) at below 1 mM daidzein. However, when daidzein concentration went over 2 mM, the reaction was severely inhibited and the (*S*)-equol yield was quite low. Even when the reaction time was extended up to 8 hr for the reactions at 2 and 5 mM daidzein, the low conversion problem was not changed, and daidzein was not converted into DHD or (*S*)-equol any more after 4 hr. Furthermore, no DHD and THD were detected at 4~8 hr reaction time points, and daidzein concentration was not decreased anymore.

To determine a rate determining step (RDS) at below 1 mM concentration range, the concentration profiles of the daidzein metabolites, i.e., daidzein, DHD, *trans*-THD and (*S*)-equol were recorded during the whole cell biotransformation, which suggested that DHDR reaction is the RDS among the series enzyme reactions (**Fig. 2.7B**). The *trans*-THD concentration was generally low (less than 50 μM) during the reaction time, and DHD appeared to have accumulated to a great extent and then gradually decreased. Moreover, *trans*-THD was rarely detected on HPLC elution profile of reactions done with lower daidzein concentrations than 500 μM, suggesting that DHDR catalyzing DHD to *trans*-THD was the RDS for (*S*)-equol production. In addition, the accumulated DHD was detected in its fully racemized form with 0 ee (%) (data not shown), indicating that DDRC was not a limiting step. The expression level of DHDR appeared to be lower than that of other enzymes (**Fig. 2.6A**), but its expression was optimized by varying induction temperature. Additionally, the sole overexpression of DHDR in tDHDR-WT did not increase the

THD over the DHD levels, suggesting that DHDR overexpression cannot simply increase THD production. After the findings to increase the THD level in *E. coli* cytoplasm, protein engineering was attempted to enhance reductase catalytic activity of DHDR to increase cytoplasmic THD level. The engineering results were described later.

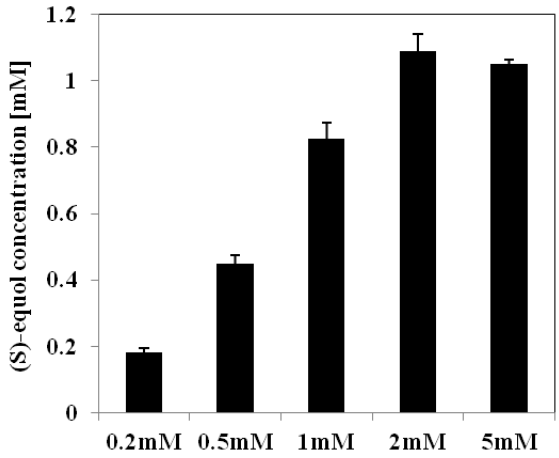

A.

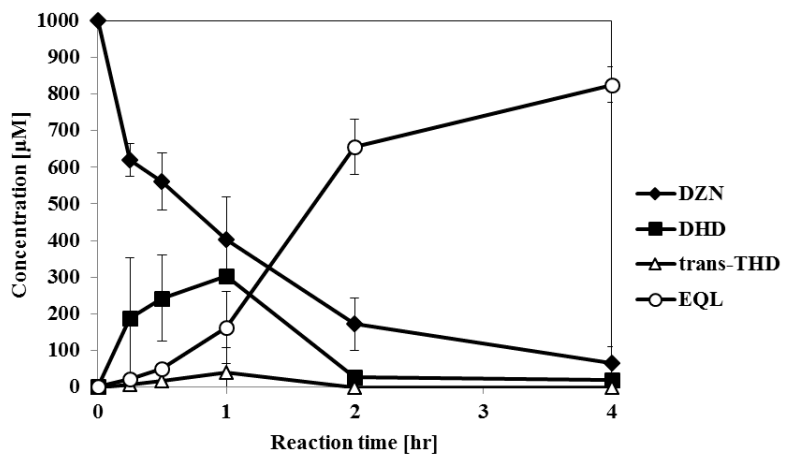

B.

Figure 2.7 (*S*)-equol production by recombinant *E. coli* BL21 (DE3) strain (tDDDT-WT).

A. Yield along initial daidzein concentration (0.2 to 5 mM). **B.** Concentration of four metabolites including daidzein (DZN), dihydrodaidzein (DHD), *trans*-tetrahydrodaidzein (*trans*-THD) and (*S*)-equol (EQL). 1 mM Daidzein was used as a substrate, and the concentrations along the reaction time were recorded.

2.3.2 pH effect and kinetics of DHDR

Prior to DHDR engineering, the effect of pH on DHDR activity, as well as DHDR's kinetic parameters and enantioselectivity were characterized. Since DHDR belongs to the SDR family, the reaction was expected to be reversible, and the pH optima of the reduction and dehydrogenation would be different, as for other SDR enzymes. In order to determine the optimum pH for the reductase activity, an enzyme assay was performed in the range of pH 5 to 7 with 0.5 interval units. DHDR showed the highest reductase activity at around a pH of 6.0 (**Fig. 2.8**). To measure the backward dehydrogenase activity, purified DHDR was reacted with (3*S*,4*R*)-*trans*-THD as substrate in the pH range from 6.5 to 8.5, and its optimum was identified at pH 7.5. In the pH range from 5.0 to 6.5, the reductase activity of DHDR is dominant over its dehydrogenase activity, and the dehydrogenase activity dominates at pH above 7, according to **Fig. 2.8**.

According to several previous studies, the cytoplasmic pH of *E. coli* was maintained at between 7.2 and 7.8, owing to its pH homeostasis enacted by the prokaryotic primary proton pumps on membrane (PADAN et al. 1976; Salmond et al. 1984; Slonczewski et al. 1981; Zilberstein et al. 1984). Rapid measurement of pH of the cytoplasm and periplasm on *Escherichia coli* by green fluorescent protein fluorimetry enabled to observe that pH perturbation by HCl addition was recovered in several minutes again to reach the initial pH 7.6 (Wilks and Slonczewski 2007). Therefore, it was expected that DHDR was rather a dehydrogenase than a reductase under the condition of *E. coli* cytoplasm. This inference was confirmed by an *E. coli* transformant, tDHDR-WT, to see which reaction, between reduction and

dehydrogenation, is more favorable in cytoplasm. tDHDR-WT showed a low conversion of DHD to *trans*- and *cis*-THD (**Fig. 2.9A**). When 100 μM of DHD racemates were used, tDHDR-WT yielded 10 μM *trans*-THD from 50 μM (*S*)-DHD (20% yield for (*S*)-DHD) and about 4 μM *cis*-THD from 50 μM (*R*)-DHD (8% yield for (*R*)-DHD).

The kinetics of the DHDR was analyzed at pH 6, i.e., the optimum pH for reductase activity. Since it was reported that DHDR could convert the (*S*) and (*R*) enantiomers of DHD to *trans*- and *cis*-THD, respectively, the kinetic parameters were separately measured with each enantiomer separately (**Table 2.2**). The k_{cat} for (*S*)-DHD was about 9.5 times larger than that for (*R*)-DHD, and the K_m value for (*S*)-DHD was 3.6 times smaller than that for (*R*)-DHD. DHDR wild-type has a catalytic efficiency that is higher by a factor of about 23.5 for (*S*)-DHD over (*R*)-DHD in terms of the k_{cat}/K_m ratio. We confirmed that DHDR prefers (*S*)-DHD to (*R*)-DHD as its substrate (Schroder et al. 2013; Shimada et al. 2012).

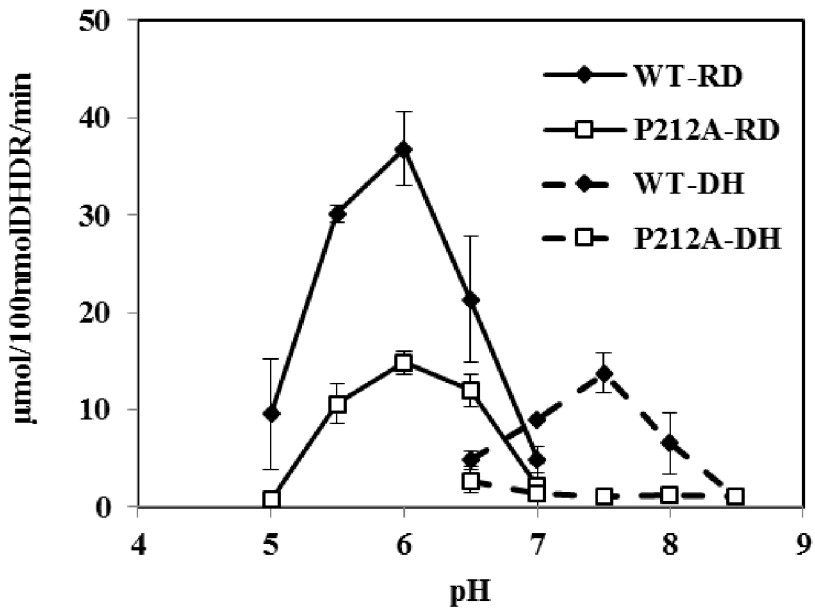

Figure 2.8 Effect of pH on DHDR activity.

The reduction reactions (RD) of wild-type (WT) and P212A mutant were performed at pH 5.0-7.0. The dehydrogenation reactions (DH) wild-type (WT) and P212A mutant were performed at pH 6.5 to 8.5.

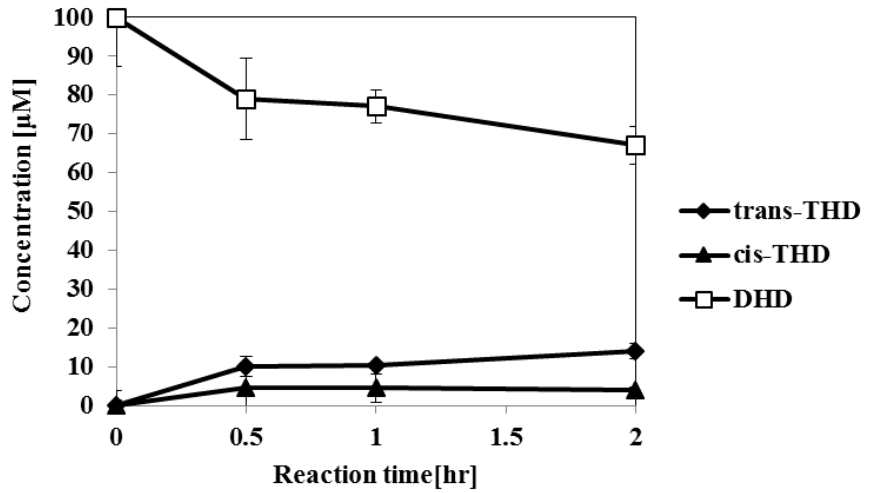

A.

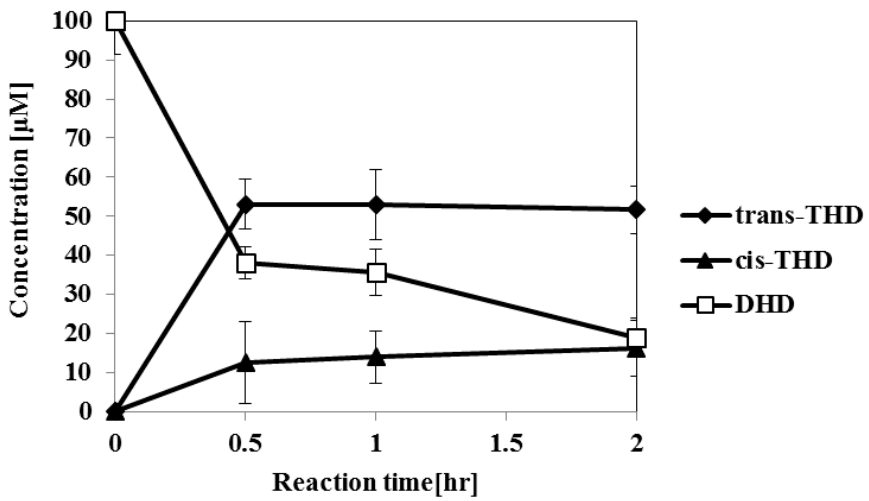

B.

Figure 2.9 DHDR reduction reaction by whole cell biocatalyst.

A. tDHDR-WT and **B**. tDHDR-PA with 100 μM of initial dihydrodaidzein racemates. Metabolite concentrations were recorded along the reaction time. All the data points have standard deviation indicated with error bars.

Table 2.1 Kinetic parameters of purified DHDR wild-type and P212A mutant.

	(*S*)-DHD†			(*R*)-DHD†		
Strain	$K_{M,S}$ (μM)	$k_{cat,S}$ (min^{-1})	$k_{cat,S}/K_{M,S}$ (min^{-1} μM^{-1})	$K_{M,R}$ (μM)	$k_{cat,R}$ (min^{-1})	$k_{cat,R}/K_{M,R}$ (min^{-1} μM^{-1})
Wild type	28.3 ± 6.9	328.1 ± 23.5	12.00 ± 3.31	102.4 ± 7.6	34.7 ± 1.2	0.51 ± 0.05
P212A	60.7 ± 4.9	216.4 ± 44.7	3.60 ± 0.95	n.d.‡	n.d.	n.d.

† (*S*), (*R*)-Dihydrodaidzein enantiomer were used as a substrate, respectively. All enzyme assays were performed at 37 °C and pH 6.0 in 100mM KPB. The results are presented as means ± the standard deviation with triplicates.
‡ No detection of any product formation by DHDR P212A mutant.

2.3.3 Construction and characterization of DHDR P212A mutant

In the previous section, we identified DHDR as a RDS in recombinant whole cell reaction system for (*S*)-equol production from daidzein. Based on this fact, enzyme engineering on DHDR was attempted in order to increase the DHDR activity in the whole cell reaction. For the engineering we chose a site-directed mutagenesis method based on a previous report about a SDR family enzyme. Previous mutations on 3α-hydroxysteroid dehydrogenase/carbonyl reductase (3αHSD) from *Comamonas testosteroni* (Hwang et al. 2013), which belongs to short-chain dehydrogenase/reductase (SDR) like DHDR, were mimicked to obtain mutants with changes in their substrate/product binding property or enantioselectivity. The reference suggested that when Pro185 (which was aligned to Pro212 in DHDR) was substituted with glycine or alanine with small alkyl group side chain, the substrate binding loop in 3αHSD appeared to have more flexibility, as measured according to the fluorescence of tryptophan on the substrate binding loop. Intrigued by the previous research, the DHDR P212A mutant was constructed using site-directed mutagenesis, and enzyme characterization was performed and the whole-cell reaction system with the overexpressed mutant was evaluated.

In a similar way as DHDR wild-type, the DHDR P212A mutant showed the highest reductase activity at pH 6. But its catalytic activity was reduced down to 66% in k_{cat} and its K_M increased by 214%, resulting in 30% decrease in k_{cat}/K_M for (*S*)-DHD (**Table 2.2**). Interestingly, the P212A mutant showed no activity toward (*R*)-

DHD, even with 1 μM purified enzyme and up to 500 μM substrate, suggesting that the DHDR P212A mutant is completely inactive on (*R*)-DHD. However, such observation was inconsistent with the result of the whole cell reaction, indicating that tDHDR-PA still shows some reductase activity for both (*S*) and (*R*)-DHD (**Fig. 2.9B**). One possible explanation is that the enzyme concentration in the cell after IPTG induction was much higher than 1 μM to show any remaining reductase activity, even for (*R*)-DHD. The time course reaction of the DHDR wild-type and P212A mutant revealed that the DHDR wild-type consumes (*S*)-DHD primarily, then (*R*)-DHD, which corresponds to its kinetic parameters of lower K_m value of (*S*)-DHD than that of (*R*)-DHD, while the DHDR P212A mutant consumes (*S*)-DHD only (**Fig. 2.10A and B**).

tDHDR-PA converted 50 μM (*S*)-DHD to 50 μM *trans*-THD (100% yield for (*S*)-DHD) and 50 μM (*R*)-DHD to 14 μM *cis*-THD (28% yield for (*R*)-DHD) (**Fig. 2.9B**). The preference to (*S*)-DHD over (*R*)-DHD was maintained in the tDHDR-PA mutant, and the ratio of product concentrations, *trans*-THD/*cis*-THD, at the 1 hr time point was 2.3 for wild-type and 3.8 for P212A mutant. These results appear to be inconsistent with the fact that DHDR P212A shows a poorer catalytic efficiency than wild-type DHDR (**Table 2.2**). However, in fact it is a reasonable result, since the kinetic study was performed at pH 6, where no dehydrogenase activity was displayed. In result, at pH 6.0, DHDR wild-type surely showed better reductase activity than DHDR P212A mutant. Whereas all the reactions of DHDs and THDs in the cytoplasm by tDHDR-WT or tDHDR-PA would be affected by the pH of the cytoplasm.

In addition, DHDR H182Y mutant was also constructed by site-directed mutagenesis to see the function or exchangeability of His182, which was expected to be a catalytic hydrogen donor in the case of DHDR, because most of SDR family enzymes have tyrosine as a catalytic hydrogen donor. The *S. isoflavoniconvertens* DHDR H182Y mutant showed no catalytic reductase and dehydrogenase activities, suggesting that His182 is the main catalytic functional residue and cannot be replaced (data not shown).

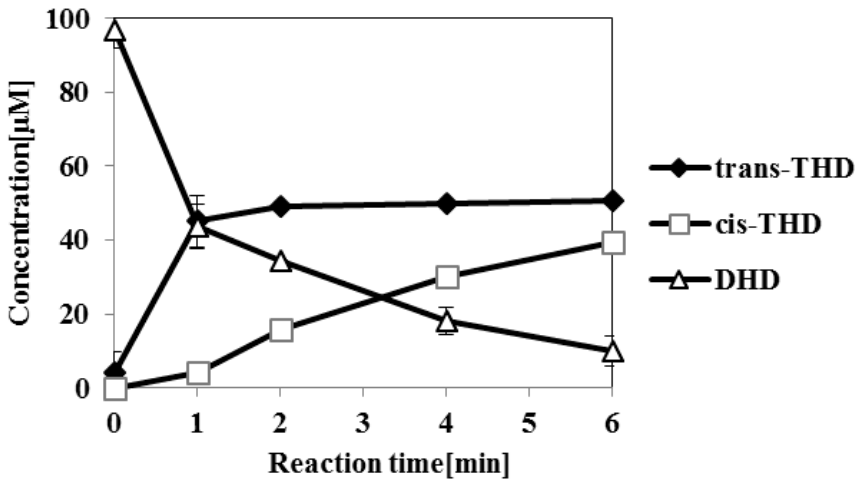

A.

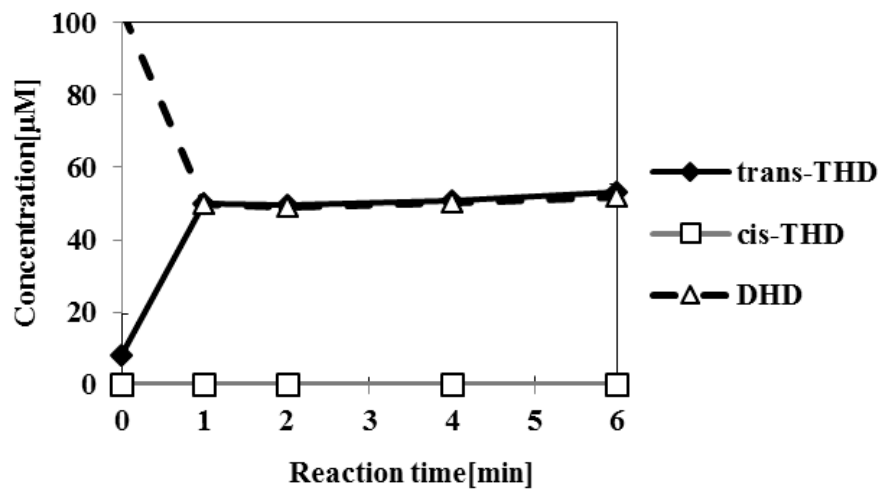

B.

Figure 2.10 Time course reaction of (A) purified DHDR wild-type and (B) DHDR P212A.

100 μM dihydrodaidzein racemate was used as a substrate with 0.5 μM of each purified enzyme. All the data points have standard deviation indicated with error bars.

2.3.4 Enantioselectivity of DHDR and production of (3*S*,4*R*)-*trans*-THD

Chiral analysis revealed that the biosynthetic products of DHDR consisted of two forms of diastereomeric THD, *trans*- and *cis*-THD, whereas chemical synthesis generates four forms of THD: (3*R*,4*S*), (3*S*,4*R*)-THD for *trans*-isomers and (3*R*,4*R*), (3*S*,4*S*)-THD for *cis*-isomers (**Fig. 2.11**). In **Fig. 2.11**, chiral separation of a chemical preparation of THD that yields about 30% *trans*- and 70% *cis*-THD generated two small peaks first, then two large peaks (Wähälä et al. 1997). Additionally, *trans*-THD had a shorter elution time than *cis*-THD on C18 HPLC column. Based on such facts, the first two peaks were assigned as *trans*-isomers and the last two peaks as *cis*-isomers. The DHDR P212A mutant also produced one enantiomer of *trans*-THD that had the same stereochemistry as that of a *trans*-isomer produced by DHDR wild-type. However, it was difficult to identify their exact stereochemistry by only using the HPLC retention time. To elucidate the stereochemistry of the THDs produced by DHDR, circular dichroism (CD) spectroscopy data were exploited (**Fig. 2.12**). According to the previous CD spectra of THDs, *trans*-THD and *cis*-THD were (3*S*,4*R*)-*trans*-THD and (3*R*,4*R*)-*cis*-THD, respectively (Kim et al. 2010b). Direct observation of the stereochemistry of THDs produced by DHDR was firstly reported in this study, and our result showed that (3*S*,4*R*)-*trans*-THD rather than (3*R*,4*S*)-*trans*-THD was a direct precursor of (*S*)-equol, which was the same as the one that was verified in a previous report (Kim et al. 2010a), and only (3*R*,4*R*)-*cis*-THD was generated as a by-product from (*R*)-DHD by DHDR.

Enantioselective (3*S*,4*R*)-*trans*-THD production was also confirmed by utilizing the stereospecificity of the DHDR P212A mutant. To achieve a 100% conversion using DHD racemate as a substrate, DDRC should be included in the enzyme reaction system. Due to the enantioselectivity of DHDR P212A, (*S*)-DHD was preferentially consumed, and then the remaining (*R*)-DHD was racemized to (*S*)-DHD by DDRC. Gradually, both enantiomers of DHD could be converted to (3*S*,4*R*)-*trans*-THD, and as a result, when 0.5 μM of DHDR P212A was used with 5 μM of DDRC, 100 μM of DHD racemates were converted to (3*S*,4*R*)-*trans*-THD with a 93% yield within 5 min and no (3*R*,4*R*)-*cis*-THD was detected during the reaction (**Fig. 2.13**).

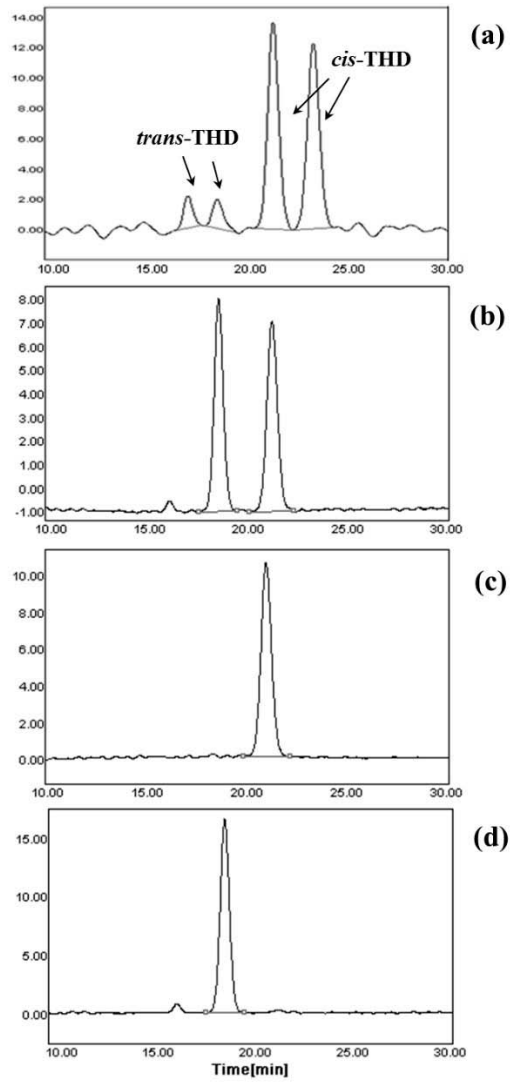

Figure 2.11 HPLC elution profiles of four THDs.

(a) four chemically synthesized THDs, and (b) enzymatically synthesized THDs by purified DHDR using (*R*,*S*)-DHDs as substrate. (c) and (d) are THDs produced by DHDR using (c) (*R*)-DHD and (d) (*S*)-DHD as substrates, respectively. Each THD was separated and detected on a chiral column, CHIRALCEL OJ-H, with an elution condition (hexane : ethanol = 60 : 40) at 1 ml/min flow rate.

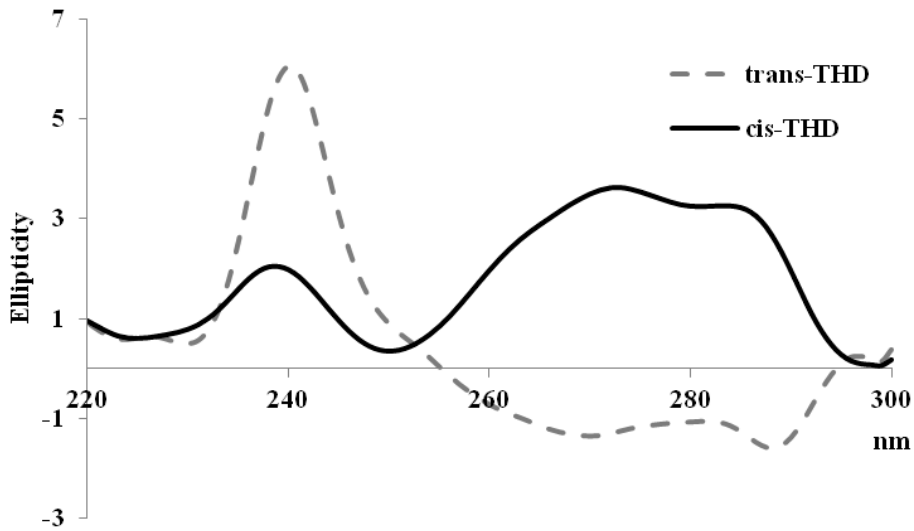

Figure 2.12 CD spectra of biosynthesized THDs.

Circular dichroism spectra of *trans*- and *cis*-THD produced by DHDR were generated using a CD spectrometer. Each THD was dissolved in methanol and CD spectra was recorded in the range from 220 to 300 nm.

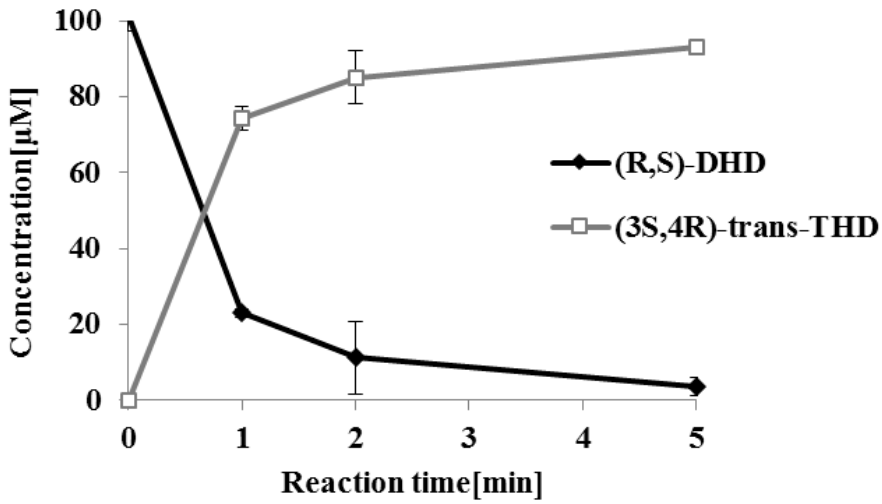

Figure 2.13 Time course production of (3*S*,4*R*)-*trans*-THD from (*R*,*S*)-DHD.

(3*S*,4*R*)-THD was enantioselectively produced in a co-catalyzing reaction using purified DHDR P212A and DDRC. 100 μM dihydrodaidzein racemate was used as a substrate with 0.5 μM DHDR P212A and 5.0 μM DDRC of each purified enzyme. All the data points have standard deviation indicated with error bars.

2.3.5 Efficient (*S*)-equol production using the DHDR P212A mutant

Integrating all the above findings, (*S*)-equol production was performed using two transformants, tDDDT-WT and tDDDT-PA. With 500 μM daidzein, the control strain, tDDDT-WT, exhibited an 83% (413 μM) yield of (*S*)-equol and 59.0 mg/L/h productivity. On the other hand, a mutant strain, tDDDT-PA, exhibited a 93% (466 μM) yield of (*S*)-equol and 69.8 mg/L/h productivity, which were 13% and 18% higher, than those of the control (**Fig. 2.14C**). Except the time point 0.5 hr, the higher yield was statistically significant at all time points. However, the improved productivity was only observed at below 500 μM of initial daidzein concentration, and the higher productivity of (*S*)-equol in the mutant strain seems to have been caused by the fast conversion of (*S*)-DHD to (3*S*,4*R*)-*trans*-THD without (*S* or *R*)-DHD accumulation (**Fig. 2.14A and B**). At a concentration of daidzein above 2 mM, however, DHD did not accumulate and daidzein consumption was severely reduced. In such a case, the control tDDDT-WT and mutant tDDDT-PA strain showed almost a similar profile of (*S*)-equol production, suggesting that another step rather than DHDR was likely to become a new rate-limiting step for (*S*)-equol biosynthesis (data not shown).

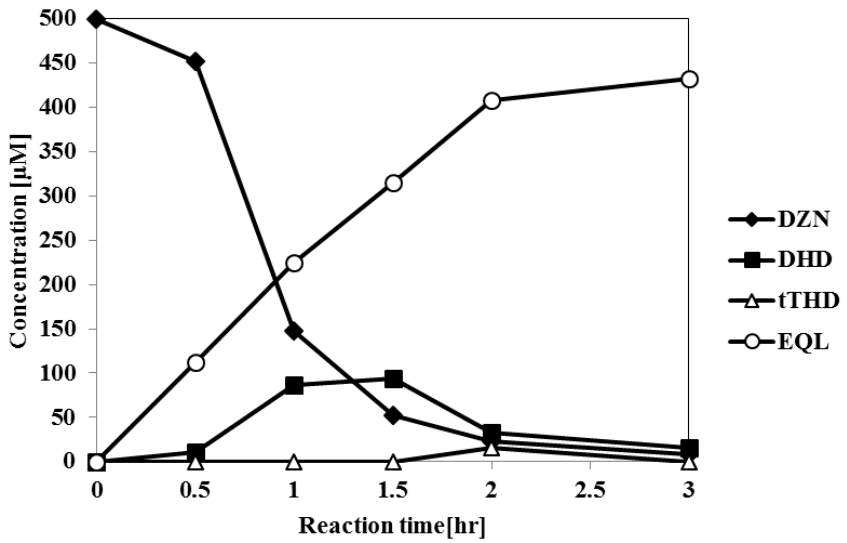
500
450
400
350
300
250
200
150
100
50
0
Concentration [μM]
0
0.5
1
1.5
2
2.5
3
Reaction time[hr]
DZN
DHD
tTHD
EQL

A.

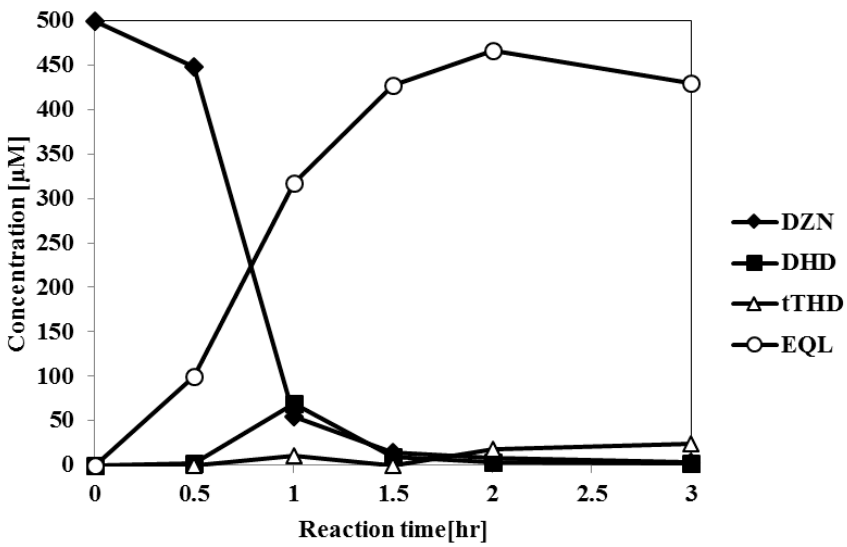
500
450
400
350
300
250
200
150
100
50
0
Concentration [μM]
0
0.5
1
1.5
2
2.5
3
Reaction time[hr]
DZN
DHD
tTHD
EQL

B.

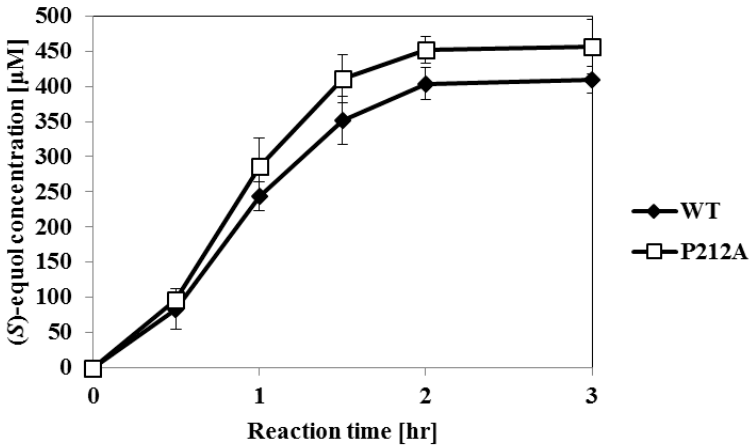

C.

Figure 2.14 Time course production of equol in tDDDT-WT and tDDDT-PA.

500 µM Daidzein was used as a substrate, and the concentrations were recorded along the reaction time. (A) tDDDT-WT as a control strain, (B) tDDDT-PA mutant, (C) comparison (*S*)-equol production between the control strain (WT) and the mutant strain (P212A). Graph (A) and (B) are representatives from each dataset. To confirm the statistical difference between tDDDT-WT and tDDDT-PA mutant, more than three repeated biotransformation were performed independently and shown as average values with standard deviation error bars.

2.4 Discussion

In this study, DHDR from *S. isoflavoniconvertens* was fully characterized in terms of its pH optimum, kinetic parameters and stereoselectivity. Although DHDRs from *S. isoflavoniconvertens* (Schroder et al. 2013) and from *Lactococcus* sp. Strain 20-82 (Shimada et al. 2011) were previously characterized on their kinetic parameters, cofactor specificity and preference to (*S*)-DHD, the analyses were restricted only to neutral pH, which restricted complete understanding of the DHDR characteristics. Moreover, previous studies (Schroder et al. 2013; Shimada et al. 2011) did not assess any of the kinetics of DHDR toward each DHD enantiomer nor the exact stereochemistry of *trans*- and *cis*-THD produced from each DHD enantiomer. It is worth mentioning that we only confirmed that (3*S*,4*R*)-THD was transformed to (3*S*)-equol by THDR in the biological system (Kim et al. 2010a). This study also reports the first direct measurement of stereochemistry of THDs produced by DHDR and the quantification of its (*S*)-DHD preference by kinetic values. The stereochemistry confirmed for the THDs revealed that no stereochemical inversion at C-3 occurs by the DHDR reaction, and DHDR introduces 4*R* stereochemistry at C-4 to both (*S*) and (*R*)-DHD.

DHDR is a novel enzyme that belongs to the short-chain dehydrogenase/reductase (SDR) family, and DHDR has a unique catalytic tetrad pattern (Asn, Ser and HXXXK) that is somewhat different from that of general SDR enzymes (Asn, Ser, and YXXXK) (Filling et al. 2002; Shimada et al. 2011). The catalytic tyrosine is a well-conserved residue in SDR as a proton donor, however, its replacement by histidine is observed in some SDR family proteins. According to the

Basic Local Alignment Search Tool (BLAST; http://www.ncbi.nlm.nih.gov/blast) result, more than 100 proteins were aligned to have the histidine as a potential catalytic residue, when DHDR protein sequence (Protein ID: AFV15451.1) was used as a template.

However, there were no scientific reports about those SDR proteins having a catalytic histidine residue. In the case of DHDR from *S. isoflavoniconvertens*, the role of tyrosine in most of the known SDR family enzymes seems to be substituted with histidine, for which imidazole ring (de)protonation would be engaged in substrate reduction or oxidation. The histidine is likely a catalytic residue that can affect pH optimal values of DHDR for its reductase and dehydrogenase activities. The optimal values are near a pH of 7 (i.e., 6 for reduction and 7.5 for dehydrogenation), which is similar to one of the pK_a values of the amine groups in the imidazole ring of histidine. In the case of other SDR family enzymes, such as mannitol dehydrogenase from *Candida magnolia* or D-arabitol dehydrogeanse from *Gluconobacter oxydans*, the optimal pH was around 6.5-7.5 for reduction, and 8.5-10 for dehydrogenation (Cheng et al. 2005; Lee et al. 2003). Therefore, the histidine residue would lower the pH optimum for dehydrogenase activity.

Interestingly, DHDR P212A lost its dehydrogenase activity at pH values above 7.0. Pro212 is likely to be positioned on the substrate binding loop according to its alignment to Pro185 in 3αHSD from *Comamonas testosteroni* (Hwang et al. 2013). P185A or G mutations make the loop flexible, increasing the product release and overall catalytic activity in 3αHSD (i.e., an increase in k_{cat}, K_M and K_{iNAD}), but there was no mention of any change in enzyme stereospecificity. As a result, P185A

and G changed its rate-limiting step from product release to hydride transfer. In the case of DHDR, the corresponding substitution resulted in different changes in the enzyme properties. The introduction of the P212A mutation caused DHDR to have decreased catalytic activity for both (*R*) and (S)-DHD, resulting in no (3*R*,4*R*)-THD formation. The underlying reason for the decreased activity is not clear, because it is the opposite conclusion of the previous report. One possible explanation is that the hydride transfer from NADPH to DHD can be prohibited by the P212A substitution. In contrast with 3αHSD, perhaps hydride transfer would be the primary rate-limiting step in DHDR, and then the P212A mutation might reduce the transfer rate even further.

As a result of the improved enantioselectivity of DHDR P212A, rapid enantioselective production of (3*S*,4*R*)-THD was possible with an enzymatic method using a combination of DHDR P212A and DDRC. In addition, the enantioselective production of (3*R*,4*R*)-*cis*-THD was also possible by using only purified (*R*)-DHD substrate and DHDR wild-type enzyme (**Fig. 2.11C**). Till now, there have been no ways to prepare chiral isoflavan-4-ols through chemical and/or enzymatic synthesis (Jokela 2011). Therefore, this is the first report to produce (3*S*,4*R*) and (3*R*,4*R*)-isoflavan-4-ols with a high enantiomeric excess (both above *ee* 99%).

Chiral THDs have the potential to be used as precursors for useful isoflavonoid compounds, such as (*S*)-equol or dehydroequol (Joannou et al. 1995; Kim et al. 2009; Wang et al. 2005b). (*S*)-Equol is well known for its estrogenic activity in the human body to treat postmenopausal symptoms, and a synthetic dehydroequol (or phenoxodiol) is currently undergoing phase II clinical trials as an

anticancer drug for prostate cancer (Gibney et al. 2010). In addition, the THDs themselves have anticancer activity to prostate cancer cells, and *trans*-THD was reported to be a more effective form than the *cis* form (Wähälä et al. 1997). Four stereoisomers of THD: *trans* (3*R*,4*S* and 3*S*,4*R*)- and *cis* (3*R*,4*R* and 3*S*,4*S*)- forms, have been known to be effective in suppressing vascular disease. *trans*-THD was reported to suppress neointimal hyperplasia by capturing superoxide anion (Kanellakis et al. 2004), and similarly, *cis*-THD inhibits ERK-1 activation and proliferation in human vascular smooth muscle cells (Ling et al. 2004). However, these results were acquired with chemically synthesized THDs that had both enantiomers of each diastereomer. Therefore, this biological method to prepare enantio-pure THDs might help understand their individual effects to treat vascular disease or prostate cancer in further detail.

2.5 Conclusion

Our goal was to develop a recombinant *E. coli* strain with an improved (*S*)-equol production capacity under aerobic condition. Compared to native anaerobic bacteria culture and reaction systems, this recombinant system enables aerobic microbial growth and reaction with higher productivity of (*S*)-equol enhanced by a DHDR mutant. The improvement in the (*S*)-equol productivity by introducing DHDR P212A could be explained through several reasons. First, the DHDR P212A mutation almost removed the dehydrogenase activity, and the reduction in DHD became dominant with the cytoplasmic pH. Second, the decrease in reductase

activity toward both (*S*) and (*R*)-DHD increased the selectivity for (*S*)-DHD over (*R*)-DHD. The increased selectivity can save the NADPH pool that should be used in DZNR or DHDR reactions for (*S*)-equol production.

Even though the improvement in the yield and productivity of (*S*)-equol were minor, this is the first report to construct recombinant strains for (*S*)-equol production. Several strategies can be suggested here to further improve the (*S*)-equol production using this recombinant strain. First, protein engineering to reverse the enantioselectivity of DZNR from the (*R*)-DHD preference to (*S*)-DHD preference would diminish the necessity of DDRC, which would eventually relieve the metabolic burden of the heterologous expression of four recombinant genes and increase the expression levels of the three other enzymes. Second, the maximization and balancing reducing powers in cell cytoplasm might possibly increase the (*S*)-equol production. Since the full reactions largely depend on NADPH supplied by the cell, the co-expression of NADPH-regenerating enzymes, such as glucose dehydrogenase, or metabolic engineering for strain development to increase NADPH concentration or to balance the concentration ratio of NAD(H)/NADP(H) would be helpful (Chemler et al. 2010; Kataoka et al. 1998). In addition, the identification of the rate-determining step at high daidzein concentrations, and resolution of the product inhibition by systematic approaches or protein engineering should be the next goal for future work.

Chapter 3.

Biosynthesis of (-)-5-hydroxy-equol and 5-hydroxy-dehydroequol from genistein using equol-producing recombinant *E. coli*

A full reprint of the paper published in *ACS Chemical Biology* (2017) 12: 2883-2890.

3.1 Introduction

Isoflavones such as daidzein and genistein are phytoestrogens abundant in soybean. Their structural similarity to endogenous human steroid hormone, 17β-estradiol, endows them with anticancer, antitumor and antioxidant effects (Setchell 1998). Structural modification of isoflavones by gut microbiota such as reduction to isoflavans such as (*S*)-equol enhanced estrogenic activities (Muthyala et al. 2004; Yokoyama and Suzuki 2008).

(*S*)-equol shows moderate estrogenic activity which can relieve post-menopausal symptoms such as hot flash (Jenks et al. 2012), reduce the incidence rate of osteoporosis, breast and prostate cancer (Duncan et al. 2000; Jackson et al. 2011; Lund et al. 2004; Setchell et al. 2005; Tousen et al. 2011). The antioxidant activity of equol is also of interest for cosmetic, medical and food applications (Lephart 2014; Lephart 2016; Setchell and Cole 2015). Recently, E. D. Lephart *et al.* insisted that racemic equol and (*R*)-equol have superior positive effect on dermal gene expression (inhibition of matrix metalloproteinase (MMP)s gene and stimulation of collagen (COL1A1) and elastin (ELN) gene) in anti-aging effects compared to (*S*)-equol. However, the same reference also suggested that (*S*)-equol or racemic equol stimulated tissue inhibitor of matrix metalloproteinase-1 (TIMP1) gene expression whereas (*R*)-equol did not (Lephart 2013). In addition, (*S*)-equol supplementation was verified to reduce wrinkle depth or area in a pilot randomized placebo-controlled trial (Oyama et al. 2012).

Most (*S*)-equol-producing bacteria are obligate anaerobes, but a few oxygen-tolerant bacterial strains were developed for the production of (*S*)-equol precursors such as *O*-desmethylangolensin, dihydrodaidzein and dihydrogenistein (Li et al. 2015; Wang et al. 2005a; Yokoyama and Suzuki 2008; Zhao et al. 2011). [15-17] A recombinant *E. coli* strain efficiently reduces 1 mM daidzein to (*S*)-equol with over 85% conversion yields even under aerobic conditions (Lee et al. 2016a). This strain expresses several reductases and a racemase from gut bacteria for daidzein to equol bioconversion (Schroder et al. 2013; Shimada et al. 2012; Shimada et al. 2011; Shimada et al. 2010; Tsuji et al. 2012).

In analogy to the reduction of daidzein to (*S*)-equol, the reduction of genistein, the most abundant isoflavone in soy, would yield 5-hydroxy-equol (**Fig. 3.1**) (Matthies et al. 2009; Matthies et al. 2008; Matthies et al. 2011). However, there is no report and direct evidence that 5-hydroxy-equol is produced along the reduction pathway. The gut bacteria *Coriobacteriaceae* strain Mt1B8 and *Slackia isoflavoniconvertens* convert both daidzein to equol and genistein to 5-hydroxy-equol anaerobically (Matthies et al. 2009; Matthies et al. 2008). In addition, intestinal reduction daidzein and genistein to equol and 5-hydroxy-equol in gnotobiotic rats further supports this metabolism of isoflavones (Matthies et al. 2011). However, the three reductases that reduce daidzein to (*S*)-equol, i.e. daidzein reductase (DZNR), dihydrodaidzein reductase (DHDR), tetrahydrodaidzein reductase (THDR), do not convert genistein into 5-hydroxy-equol (Schroder et al. 2013). The first enzyme DZNR reduced genistein to dihydrogenistein, but no further reduction occurred by

the other two reductases (Schroder et al. 2013). The reductive metabolic pathway of genistein is still unclear.

Organic synthesis of 5-hydroxy-equol yields racemic mixtures, which require additional separation steps to obtain pure enantiomers (Chang et al. 1995). To establish the biological and physiological properties of this potent phytoestrogen, good routes to pure enantiomers are needed. Herein, we converted genistein into 5-hydroxy-equol by using recombinant *E. coli* cells expressing the three reductases (DZNR, DHDR and THDR) and dihydrodaidzein racemase (DDRC). This pathway was used to produce (*S*)-equol from daidzein (Lee et al. 2016a). Interestingly, in the reaction pathway of 5-hydroxy-equol from genistein, we found that 5-hydroxy-dehydroequol was produced as a byproduct after DHDR reaction with unknown dehydration mechanism through the whole cell reaction. The structures were established by GC/MS and NMR, and the absolute configuration of 5-hydroxy-equol was estimated by circular dichroism and polarimeter. Moreover, estrogen receptor binding affinity of biosynthesized (-)-5-hydroxy-equol was evaluated and compared with that of other isoflavones and isoflavans to determine its applicability as a novel phytoestrogen.

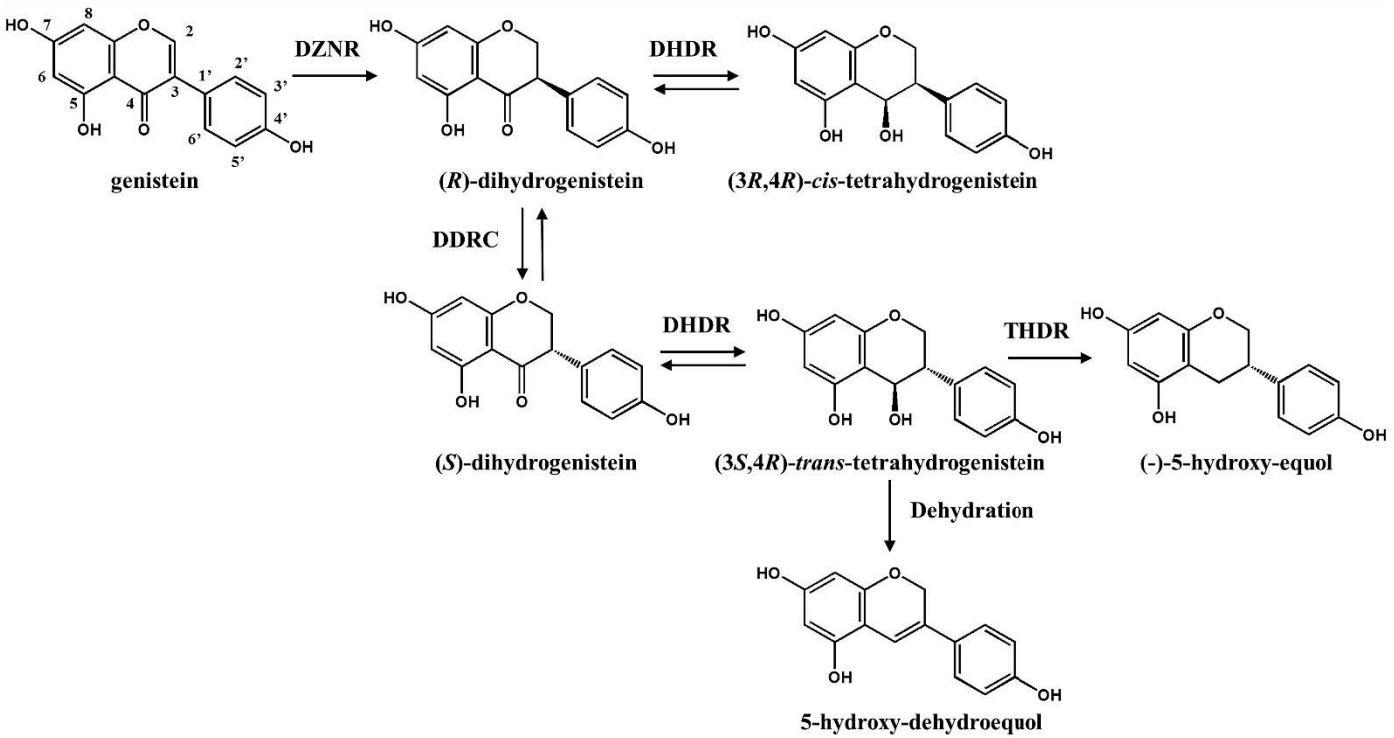

Figure 3.1 Suggested metabolic pathways of genistein to (-)-5-hydroxy-equol and 5–hydroxy-dehydroequol.

The recombinant strain expressed four enzymes from *Slackia isoflavoniconvertens*: DZNR, DDRC, DHDR and THDR.

3.2 Materials and Methods

3.2.1 Chemicals

Genistein, phenoxodiol and other chemicals were purchased from Sigma Aldrich. Dihydrogenistein was purchased from Toronto Research Chemicals Inc. (North York, Ontario, Canada) and 5-hydroxy-equol and 5-hydroxy dehydroequol were biosynthesized using whole cell catalysts.

3.2.2 Biotransformation and preparation of 5-hydroxy-equol and 5-hydroxy-dehydroequol

Resting cell reaction was performed following the previous reported protocol with slight modification (Lee et al. 2016a). Because the biotransformation system exploiting resting microbial cells can exclude unnecessary growing competition between the two different *E. coli* cells, all previous biotransformation experiments using compartmentalization reaction were performed using resting cells, which is distinct from co-culture using growing cells. If not mentioned, a basic recombinant strain (tDDDT) overexpressing DZNR, DDRC, DHDR, and THDR was used for the production of (-)-5-hydroxy-equol and 5-hydroxy-dehydroequol. Genistein was given as an initial substrate up to 500 μM final concentration from 100 mM DMSO stock. The reactor contained the mentioned recombinant cell (OD_{600} = 20), glucose 2% (w/v) and glycerol 1% (v/v) as carbon sources. After finishing the reaction, the solution was extracted with 2 x volume of ethyl acetate (EA), and the EA layer was evaporated for HPLC or GC-MS analysis. GC-MS and circular dichroism analysis

method was the same as previously reported (Lee et al. 2016a). For the preparation of bioconversion products, (-)-5-hydroxy-equol and 5-hydroxy-dehydroequol, the reaction solution was centrifuged with 4000 rpm for 10 min, and the supernatant was prepared and extracted with 2 x volume of ethyl acetate. The ethyl acetate layer was evaporated with rotary evaporator, and the final powder was dissolved in ethanol and purified with HPLC equipped with CHIRALCEL OJ-H column (Daicel Corporation). The purity of the final products was confirmed with GC-MS, HPLC and biosynthesized (-)-5-hydroxy-equol and 5-hydroxy-dehydroequol were analyzed with ^{1}H-NMR. Then, the biosynthesized chemicals were stored with 10 mM DMSO stock at -20 ºC.

(-)-5-Hydroxy-equol: ^{1}H-NMR [$(CD_3)_2CO$, 400 MHz] δ 2.73 (ddd, *J* = 1.6, 5.6, 16.4 Hz, 1H, H-4), 2.94 (m, 1H, H-3), 3.83 (t, *J* = 10.4 Hz, 1H, H-4), 4.03 (dd, *J* = 7.2, 14.4 Hz, 1H, H-2), 4.09 (ddd, *J* = 1.6, 3.2, 10.0 Hz, 1H, H-2), 5.70 (d, *J* = 2.0 Hz, 1H, H-8), 5.89 (d, *J* = 2.0 Hz, 1H, H-6), 6.71 (d, *J* = 8.4 Hz, 2H, H-3'), 7.10 (d, *J* = 8.4 Hz. 2H, H-2'), 8.92 (s, 1H, OH), 9.17 (s, 1H, OH), 9.25 (s, 1H, OH).

5-Hyroxy-dehydroequol: ^{1}H-NMR [$(CD_3)_2CO$, 400 MHz] δ 4.92 (s, 2H, H-2), 5.76 (d, *J* = 1.6 Hz, 1H, H-8), 5.92 (d, *J* = 2.4 Hz, 1H, H-6), 6.76 (d, *J* = 8.8 Hz, 2H, H-3'), 6.85 (s, 1H, H-4), 7.29 (d, *J* = 8.8 Hz. 2H, H-2'), 9.35 (s, 1H, OH), 9.50 (s, 1H, OH), 9.52 (s, 1H, OH).

3.2.3 HPLC and GC/MS analysis

To separate reaction samples, HPLC (YoungLin, South Korea) equipped with the COMOSIL $5C_{18}$-AR-II column (5 μm particle size, 4.6 by 150 mm; Nacalai tesque, Japan) was used, and each isoflavonoid was detected with UV at 280 nm. The mobile phase was composed of 50% methanol and 50% water containing 0.1% trifluoroacetic acid, and 0.7 ml/min isocratic flow was applied for 20 min. Isoflavonoid concentrations and final yields were determined using individual standard curves calculated from stock solutions. For the chiral analysis, CHIRALCEL OJ-H column (Daicel Chemical Industries, Japan) was used with the 1 ml/min isocratic mobile phase (hexane : ethanol = 70 : 30). For the identification of genistein metabolites of recombinant *E. coli* strain, purified metabolites were derivatized with N,O-bis(trimethylsilyl)trifluoroacetamide (BSTFA) at 50 °C for 5 min, and were analyzed with GC/MS equipped with an electron impact (EI) ionization source for their identification.

3.2.4 Chirality studies of biosynthesized 5-hydroxy-equol

To determine the absolute configuration of the biosynthetically prepared 5-hydroxy-equol, polarimetric and circular dichroism analysis were exploited. The specific rotation in ethanol was obtained with the JASCO *P-2000* digital polarimeter (Jasco Corp., Japan). For circular dichroism analysis, purified 5-hydroxy-equol was dissolved in methanol and CD spectra were obtained in the range from 210 to 320

nm using a Chirascan^{TM}-plus CD spectrometer (Applied Photophysics, UK). Pure methanol was used as a reference.

3.2.5 Estrogen receptor binding assay

To measure binding affinity of biosynthesized (-)-5-hydroxy-equol for human estrogen receptor (hER) α and β, the previous reported protocol was used with slight modification (Muthyala et al. 2004). Briefly, the pre-incubated each hER subtype with 0.5 nM of [^{3}H]estradiol was under competitive binding with $10^{-4 \sim -9}$ M of (-)-5-hydroxy-equol, then the reaction mixture was filtered and washed. The still bound [^{3}H]estradiol was determined to calculate IC_{50} and relative binding affinity (RBA) values, where estradiol has an affinity of 100%. Every assay was assessed in three independent experiments. K_i values to each hER subtype were calculated from the IC_{50} values using Cheng Prussof competitive equation (Wells 1992).

3.3 Results and Discussion

3.3.1 Conversion of genistein into 5-hydroxy-equol by tDDDT

To evaluate bioconversion capability of genistein into 5-hydroxy-equol by tDDDT strain, which harbors two plasmids containing four recombinant genes: *dzr* and *ifcA* in pRSFduet-1 plasmid and *ddr* and *tdr* in pCDFduet-1 plasmid (**Table 3.1**), the resting tDDDT cells were incubated with 0.5 mM of genistein in glucose supplemented KPB (potassium phosphate buffer). More than 99% of the genistein was consumed within 3 h, and the major metabolite was identified as dihydrogenistein (enol) by GC/MS analysis (m/z = 560, 545, 471, 369, 355, 207, 191), which matched well with those from EI-MS fragmentation patterns previously reported (**Fig. 3.2A, 3.3A**) (Joannou et al. 1995). After 6 h incubation, the dihydrogenistein was further metabolized to two unidentified peaks (*peak 1* and *2*, **Fig. 3.2B**), named for their order of elution from a reversed phase column (C18). The two peaks also eluted in the same order from a CHIRALCEL OJ-H column (**Fig. 3.2C**).

GC-MS analysis of unidentified *peak 1* revealed an m/z value of 474 and a fragmentation pattern that matches trimethylsilylated 5-hydroxy-equol (**Fig. 3.3B**). Analysis of *peak 2* revealed and m/z value of 472 (**Fig. 3.3C**) consistent with trimethylsilylated 5-hydroxy-dehydroequol. The fragmentation pattern resembles trimethylsilyl phenoxodiol (dehydroequol) which lacks a hydroxyl group at C5 (**Fig. 3.3D**). ^{1}H-NMR analysis confirmed their identification.

Table 3.1 Strains with plasmid information.

Strain	Plasmid(s)
tDDDT	pRSFDuet-1 (*dzr/ifcA*) + pCDFDuet-1 (*ddr/tdr*)
tDDDT-PA	pRSFDuet-1 (*dzr/ifcA*) + pCDFDuet-1 (*ddr P212A mutant/tdr*)
tDDD	pRSFDuet-1 (*dzr/ifcA*) + pCDFDuet-1 (*ddr*)
tDZDH	pRSFDuet-1 (*dzr*) + pCDFDuet-1 (*ddr*)
tDD	pRSFDuet-1 (*dzr/ifcA*)
tDT	pCDFDuet-1 (*ddr/tdr*)

dzr: daidzein reductase, *ifcA*: dihydrodaidzein racemase, *ddr*: dihydrodaidzein reductase, *tdr*: tetrahydrodaidzein reductase

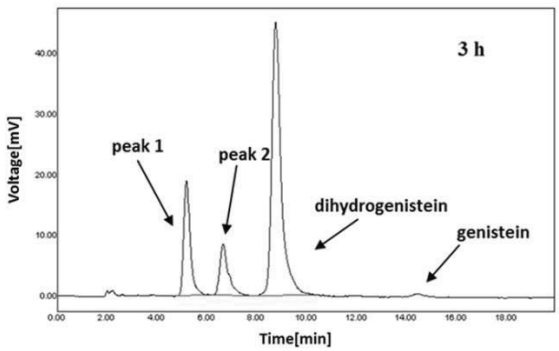

A.

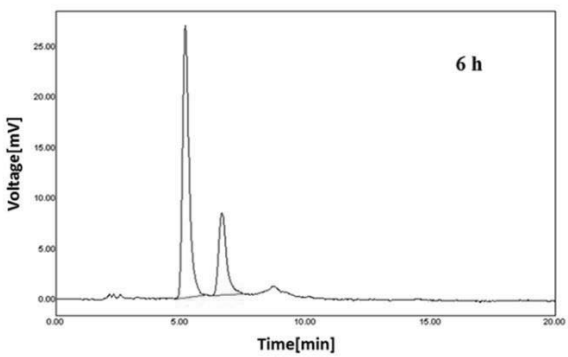

B.

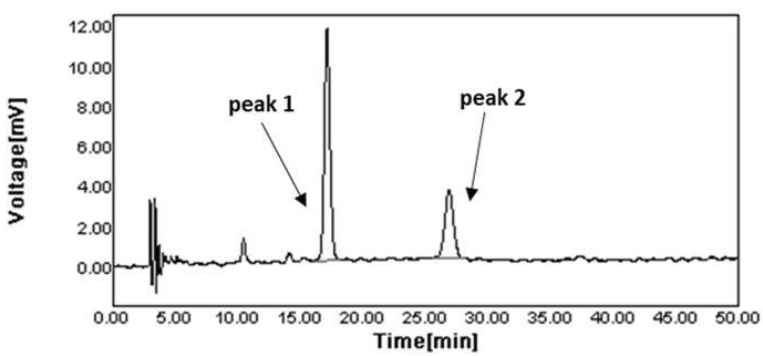

C.

Figure 3.2 HPLC elution profiles of genistein metabolites converted by recombinant tDDDT strain.

HPLC spectra of the reaction samples of (A) 3 h and (B) 6 h separated with COMOSIL C18 column, (C) HPLC spectrum of reaction sample of 6 h separated with CHIRALCEL OJ-H column.

A.

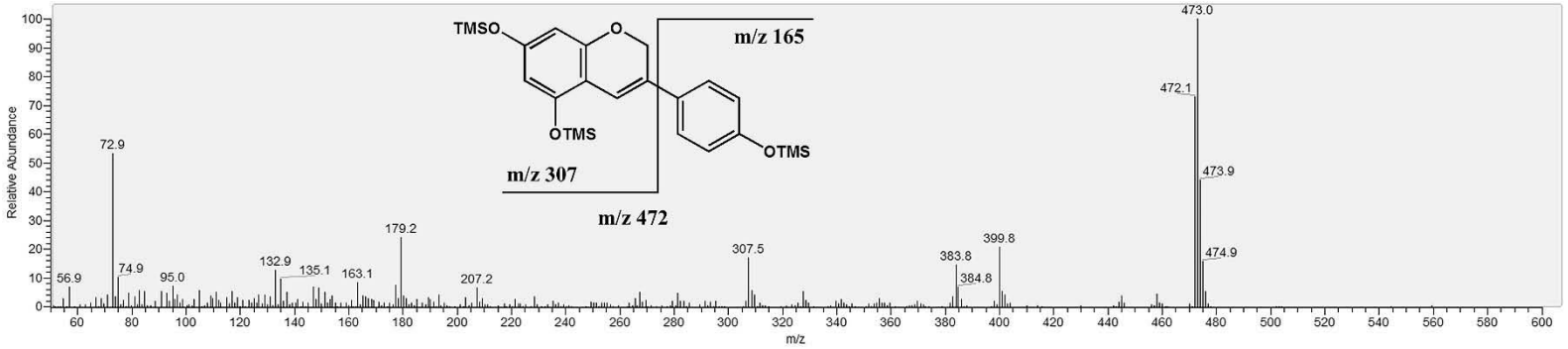
TMSO
O
OTMS
OTMS
m/z 165
m/z 307
m/z 472
Relative Abundance
m/z
72.9
56.9
74.9
95.0
132.9
135.1
163.1
179.2
207.2
307.5
383.8
384.8
399.8
472.1
473.0
473.9
474.9

B.

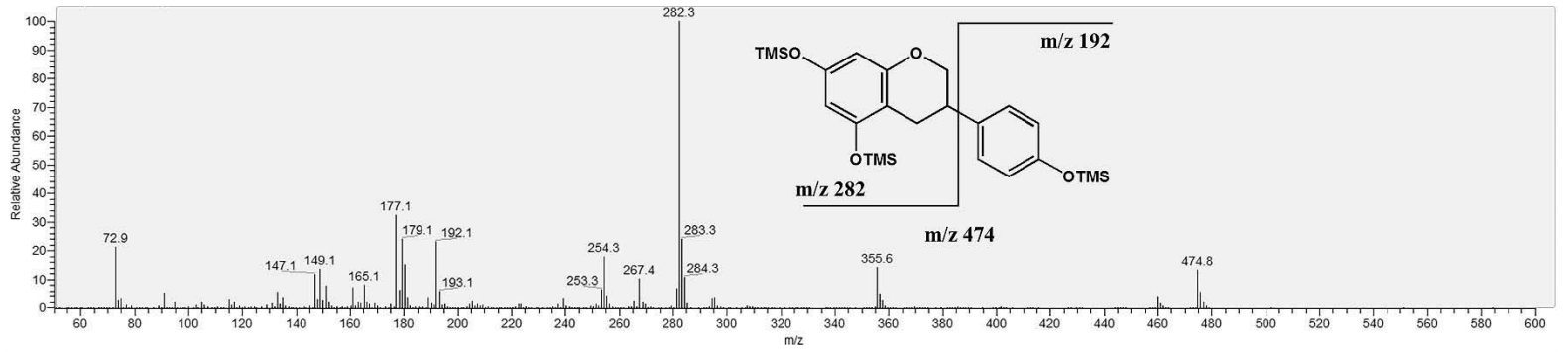
TMSO
O
OTMS
OTMS
m/z 192
m/z 282
m/z 474
Relative Abundance
m/z
72.9
147.1
149.1
165.1
177.1
179.1
192.1
193.1
253.3
254.3
267.4
282.3
283.3
284.3
355.6
474.8

C.

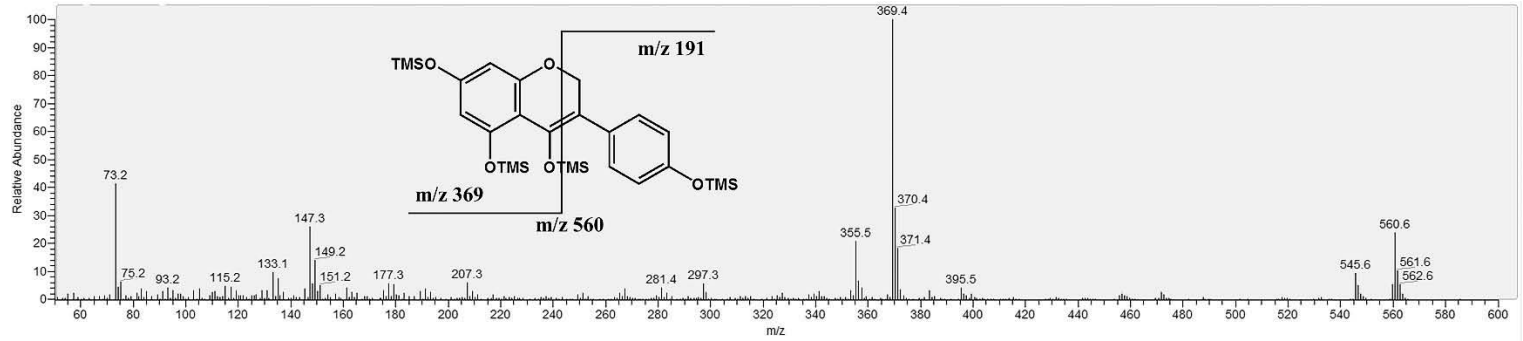

D.

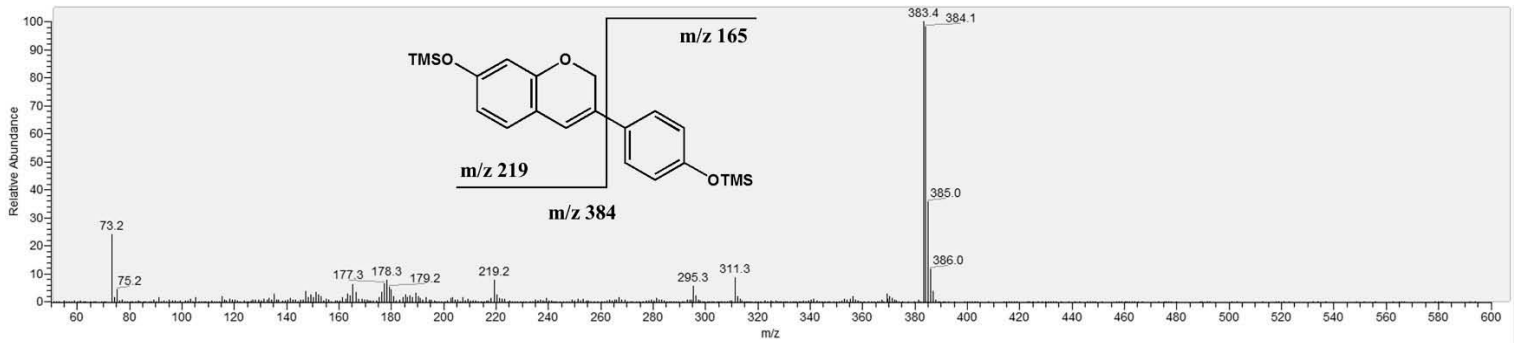

Figure 3.3 EI mass spectra of genistein metabolites and phenoxodiol.

(A) DHG (enol), (B) 5-hydroxy-equol (*peak 1*), (C) 5-hydroxy-dehydroequol (*peak 2*) and (D) phenoxodiol (dehydroequol), which were indicated on **Fig. 3.2**.

3.3.2 Determination of absolute configuration of biosynthesized 5-hydroxy-equol

In order to determine absolute configuration of biosynthesized 5-hydroxy-equol, circular dichroism (CD) analysis was performed. Biosynthesized 5-hydroxy-equol displayed a high-amplitude negative cotton at 243 nm and a positive cotton effect (CE) at 270 nm (**Fig. 3.4**). In contrast, (*S*)-equol shows a high-amplitude positive peak near 238 nm and a negative peak near 285 nm (Wang et al. 2005a; Yokoyama and Suzuki 2008). In general, (3*S*)-isoflavans have negative CEs in the 260-320 nm transition region and positive CEs in the 220-260 nm (Slade et al. 2005), suggesting that the biosynthesized 5-hydroxy-equol has R-configuration at C3. However, based on the optical rotation result, another physical property of this compound, the biosynthesized 5-hydroxy-equol seems to have S-configuration at C3. Biosynthesized (*S*)-equol was reported to have a negative [α] value ([α] = - 23.0° in ethanol) (Wang et al. 2005a), whereas the specific rotation of biosynthesized 5-hydroxy equol in this study was - 4.1° in ethanol. Both showed a negative rotation of plane-polarized light at 589 nm.

In addition, there is an evidence that supports the absolute configuration of the biosynthesized (-)-5-hydroxy-equol as 3S, which is the same absolute configuration as the equol formed by this pathway (Wang et al. 2005a). Such evidence is inferred from the inability of (3*R*)-DHG to yield the product 5-hydroxy-equol. A recombinant strain expressing the three reductases (DZNR, DHDR and THDR) hardly produced the 5-hydroxy-equol (data not shown). The first reductase,

DZNR, converts genistein into (3*R*)-dihydrogenistein (DHG) (Schroder et al. 2013). In the absence of the racemase DDRC, two reductases DHDR and THDR cannot further reduce (3*R*)-DHG to (3*R*,4*R*)-cis-tetrahydrogensitein (THG) or 5-hydroxy-equol. Even though (3*R*)-DHG is known to be isomerized into (3*S*)-DHG by tautomerization, chiral HPLC result showed that only 13% and 28% of (3*R*)-DHG was isomerized into (3*S*)-DHG during 5 h and 10 h of DZNR reaction (genistein into DHG), respectively (**Fig. 3.5**). When the racemase is added, (3*R*)-DHG can be rapidly converted to (3*S*)-DHG, which can be reduced by DHDR to (3*S*,4*R*)-trans-THG. Under these conditions, 5-hydroxy-equol is formed, indicating that it has 3S-configuration. However, the absolute configuration of (-)-5-hydroxy-equol could not be clearly determined in this study due to the disputable evidences and the lack of previous data.

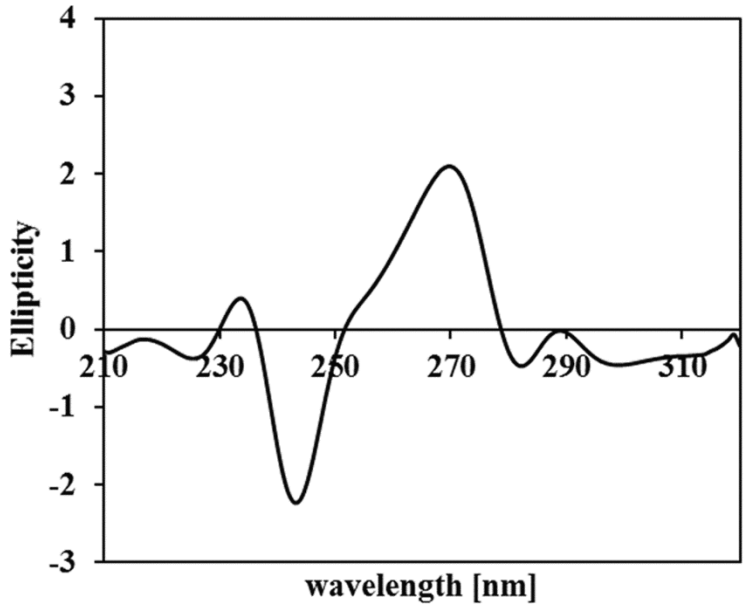

Figure 3.4 Circular dichroism spectrum of 5-hydroxy equol.

5-hydroxy-equol (*peak 1*) biosynthesized from genistein by recombinant *E. coli* was measured. The spectrum displays a high-amplitude negative cotton at 243 nm and a positive cotton effect at 270 nm. This manner of cotton effect is an inversion of the CD spectrum of (*S*)-equol, which suggests that the biosynthesized 5-hydroxy-equol has R-configuration, however, biotransformation evidence supports S-configuration at C3 of 5-hydroxy-equol.

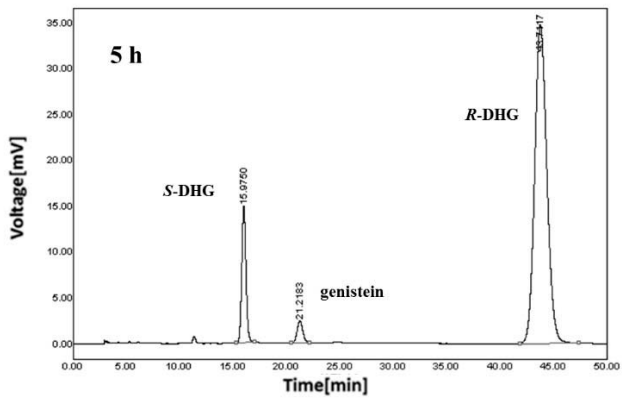

A.

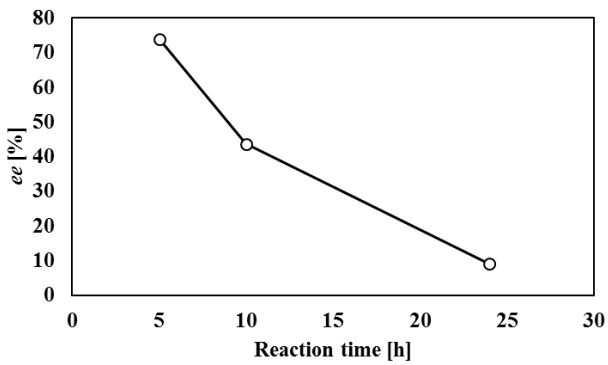

B.

Figure 3.5 Measurement of enantioselectivity of DZNR for genistein conversion and isomerization of dihydrogenistein by tautomerization.

A. HPLC spectrum of genistein into dihydrogenistein (DHG) reaction sample. 5 h reaction sample of DZNR expressing whole cell reaction system was analyzed by HPLC equipped with CHIRALCEL OJ-H column. >99% of 1 mM of genistein was converted into (*R*)-DHG enantioselectively by DZNR and some amount of (*R*)-DHG was isomerized into (*S*)-DHG by tautomerization mechanism. **B.** Enantiomeric excess (*ee = (R-S)/(R+S) X 100(%)*) was measured along reaction time. After 24 h, most of DHG was racemized in the reaction condition (0.2 M KPB, pH 8.0, 30ºC).

3.3.3 Compartmentalization strategy to produce 5-hydroxy-equol with high selectivity over 5-hydroxy-dehydroequol

Whole cell biotransformation with two times higher concentration of genistein (1 mM) similarly yielded (-)-5-hydroxy-equol and 5-hydroxy-dehydroequol with 199 mg/L and 63 mg/L yields, respectively (**Fig. 3.6A**).

Another engineered strain, tDDDT-PA (containing DHDR P212A mutant) yielded less 5-hydroxy-equol and 5-hydroxy-dehydroequol than tDDDT-WT (data not shown). This PA strain yielded more (*S*)-equol from daidzein than tDDDT-WT (13% higher yield; 18% higher productivity) (Lee et al. 2016a), but this improvement did not extend to the reduction of genistein. The PA strain converted more than 99% of genistein into DHG, but subsequent reduction to (-)-5-hydroxy-equol and 5-hydroxy-dehydroequol was not detected, indicating lower activity of the DHDR P212A.

For efficient production of (-)-5-hydroxy-equol, DZNR/DDRC and DHDR/THDR were expressed separately in two different *E. coli* strains, as overexpression of four recombinant enzymes (i.e. DZNR, DDRC, DHDR and THDR) in a single strain might burden the host cells (Jones et al. 2016). This enzyme compartmentalization strategy was expected to increase the catalytic activity, or even alleviate competition for cofactor (i.e. NADPH) usage by both DZNR and DHDR. In general, protein expression in two separate organisms may restrict substrates accessibility to enzymes, then supportive transport systems are often necessary. But in the case of isoflavonoids, their permeability through cell membrane seemed not

to be restricted. Previous study suggested uncharged hydrophobic steroid could diffuse to gram-negative bacterial cytoplasm through the lipid bilayers of the membrane (Plesiat and Nikaido 1992). Similarly, molecular structures of isoflavones are planar and they are very hydrophobic similar to steroids. To verify their permeability through the *E. coli* membrane, concentrations of genistein, DHG and final reduced products were measured both in the reaction sample and centrifuged the reaction mixture, then the transport issue was not a rate-limiting step (data not shown). Therefore, the permeability of isoflavonoids through cell membrane does not appear to be a critical problem in the compartmentalized expression system.

To construct the compartmentalized expression system, tDD and tDT were separately grown, induced and prepared, then the normalized cell mass, tDD (o.d. = 10) and the tDT (OD_{600} = 10), were mixed and used as the sources of whole cell catalyst. Under the same reaction condition, the mixed cell reaction showed 230 mg/L yield for (-)-5-hydroxy-equol and 12 mg/L for 5-hydroxy-dehydroequol, which were 16% increase in (-)-5-hydroxy-equol final yield and 81% decrease in 5-hydroxy-dehydroequol, a byproduct final yield, respectively (**Fig. 3.6B**). Interestingly, productivity of (-)-5-hydroxy-equol by tDD +tDT was significantly increased (38 mg/L/h), which was 1.6-fold higher than that by tDDDT (23 mg/L/h), whereas that of 5-hydroxy-dehydroequol was decreased. The improved productivity seemed to be caused by increased expression level of the four recombinant enzymes, especially THDR (**Fig. 3.6C**). In addition, separated utilization of NADPH by DZNR and DHDR in the two individual cells could be another reason for the improved productivity. Because DZNR and DHDR have a cofactor preference of NADPH over

NADH, cofactor imbalance of NADPH/NADH might also interrupt the whole cell viability, which could be alleviated by compartmentalization of the two reductases (Shimada et al. 2011; Shimada et al. 2010).

In the reaction by tDD + tDT, the selectivity toward (-)-5-hydroxy-equol to 5-hydroxy-dehydroequol was significantly enhanced. The concentration ratio of (-)-5-hydroxy-equol/5-hydroxy-dehydroequol of tDD + tDT (i.e. ~18) was about 6 fold higher than that of tDDDT (i.e. ~3). The higher selectivity might result from dramatically enhanced expression level of THDR in tDD + tDT system, thereby increasing metabolic flux into (-)-5-hydroxy-equol. When THDR was overexpressed in the compartmentalized system, the main conversion pathway (genistein to (-)-5-hydroxy-equol) could be accelerated, while the side reaction to 5-hydroxy-dehydroequol was relatively reduced. This means that 5-hydroxy-dehydroequol is metabolized from one of the competitive precursors of (-)-5-hydroxy-equol, not directly from (-)-5-hydroxy-equol. So far, no biosynthetic pathways to 5-hydroxy-dehydroequol were reported, and this is the first report showing direct experimental evidence of biosynthesis of 5-hydroxy-dehydroequol, as far as we know. Likewise, it was suggested that dehydroequol could be formed by dehydration of tetrahydrodaidzein (THD) (Wang et al. 2005a).

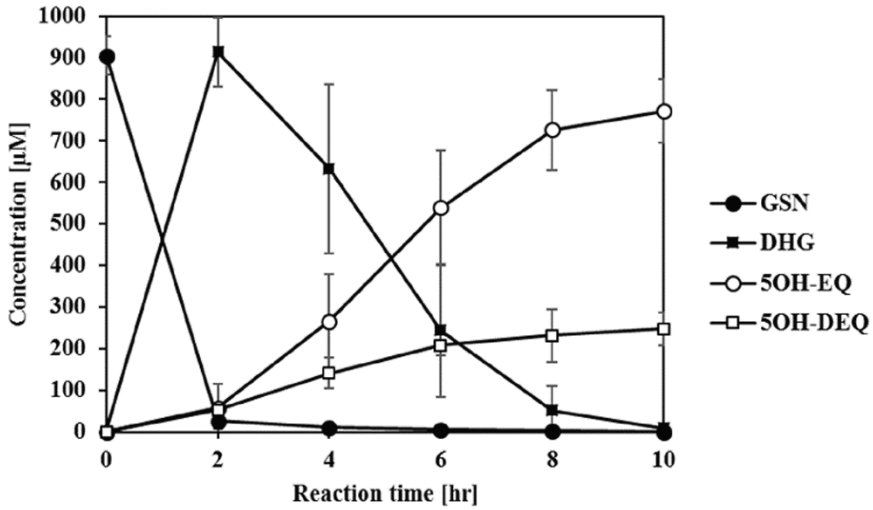
Concentration [μM]
1000
900
800
700
600
500
400
300
200
100
0
0
2
4
6
8
10
Reaction time [hr]
GSN
DHG
5OH-EQ
5OH-DEQ

A.

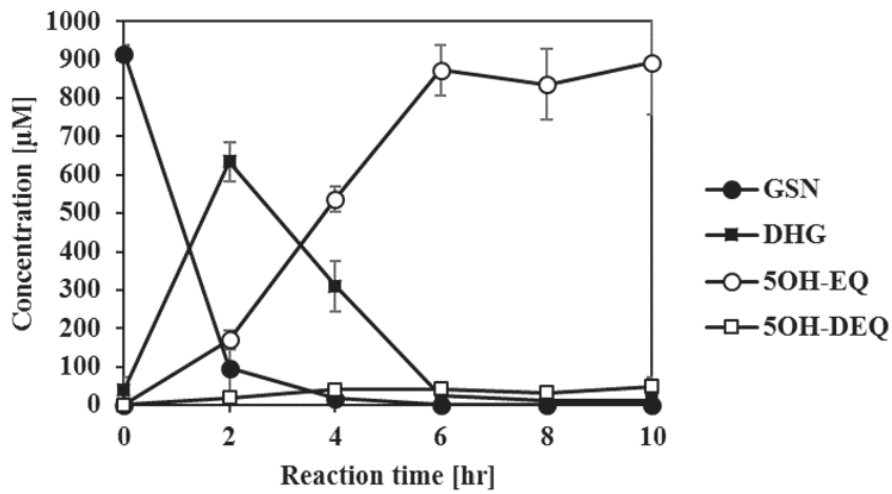
Concentration [μM]
1000
900
800
700
600
500
400
300
200
100
0
0
2
4
6
8
10
Reaction time [hr]
GSN
DHG
5OH-EQ
5OH-DEQ

B.

C.

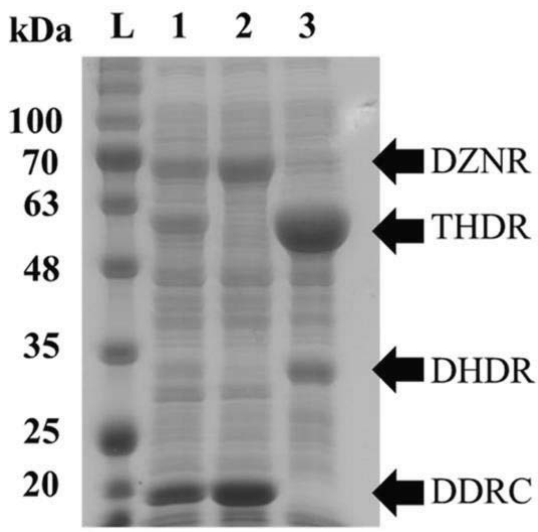

Figure 3.6 Effect of enzyme compartmentalization to production of (-)-5-hydroxy-equol.

Time profiles of metabolite concentrations of (**A**) tDDDT and (**B**) tDD + tDT strains (GSN: genistein, DHG: dihydrogenistein, 5OH-EQ: 5-hydroxy-equol, 5OH-DEQ: 5-hydroxy-dehydroequol). (**C**) SDS PAGE of the cell extracts of each transformant after electrophoresis. L: protein marker, Line 1: cell extract of transformant DDDT (20 μg), Line 2: cell extract of transformant DD (20 μg), Line 3: cell extract of transformant DT (20 μg).

3.3.4 Selective production of 5-hydroxy-dehydroequol in the absence of THDR

Inspired by the previous observation of the synthesis of a novel isoflavene, 5-hydroxy-dehydroequol, the selective production of 5-hydroxy-dehydroequol was attempted as the second biotransformation goal. Because dehydroequol, which is also known as a phenoxodiol, is a promising anti-cancer synthetic isoflavene against prostate and ovarian cancer cells (Gamble et al. 2006; Gibney et al. 2010; Kelly et al. 2011), 5-hydroxy-dehydroequol, a firstly reported novel isoflavene in this study, would be developed as a potent anti-cancer drug. Based on the idea that 5-hydroxy-dehydroequol is derived from THG, the strain without THDR was expected to be able to transform genistein to 5-hydroxy-dehydroequol without formation of (-)-5-hydroxy-equol. To verify this assumption, two THDR-less recombinant strains, tDDD and tDZDH, were constructed (**Table 3.1**). If *trans*-THG is a direct precursor of 5-hydroxy-dehydroequol, tDDD would produce the final product. If *cis*-THG is the precursor, on the other hand, tDZDH would mainly produce the 5-hydroxy-dehydroequol. In results, 5-hydroxy-dehydroequol was produced only by the tDDD without (-)-5-hydroxy-equol formation when 1 mM of genistein was fed into both of the strain cultures (**Fig. 3.7**, in the case of tDZDH, data not shown). The final yield of genistein into 5-hydroxy-dehydroequol by tDDD strain was the highest up to 0.39 mM (i.e. 99 mg/L) when 1.0 mM of initial genistein was used. Interestingly, the final conversion yield of genistein to 5-hydroxy-dehydroequol was about 40% regardless initial genistein concentration, which suggested that the dehydration should be

reversible and reverse hydration reaction of 5-hydroxy-dehydroequol into trans-THG would occur as well.

Therefore, it is proposed that 5-hydroxy-dehydroequol is converted from *trans*-THG as a direct precursor through unknown dehydration mechanism. This finding suggests the following reductive metabolic pathways of genistein into (-)-5-hydroxy-equol and 5-hydroxy-dehydroequol by the gut microbial enzymes shown in **Fig. 3.1**. Because the whole reaction was catalyzed by recombinant *E. coli*, the dehydration was facilitated by either certain native dehydratases of *E. coli* or spontaneous chemical dehydration. In this study, we could not isolate *trans*-THG, then the dehydration mechanism or any dehydrating catalyst were still under investigation. In future, it is expected that this novel reaction (i.e. isoflavene synthesis or isoflavon-4-ol dehydration) would offer novel methods to prepare diverse isoflavenes poorly studied.

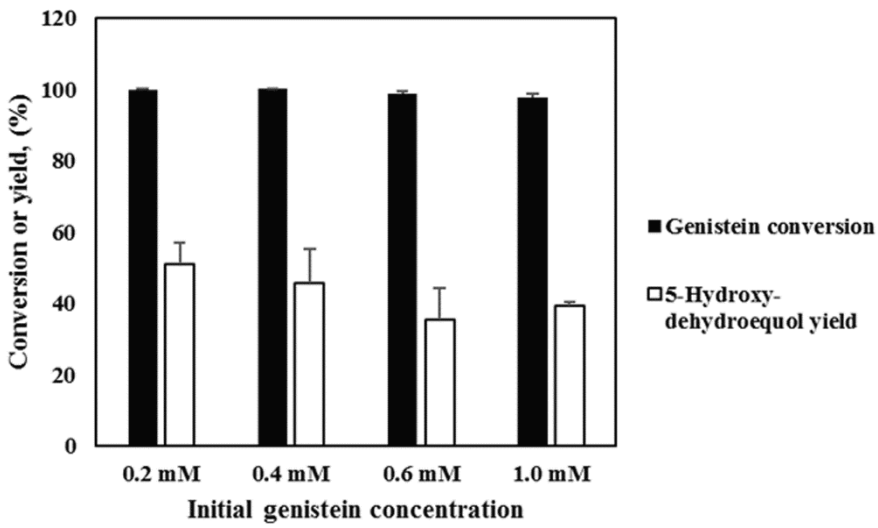

Figure 3.7 Selective production of 5-hydroxy-dehydroequol using THDR-lacking recombinant *E. coli* tDDD strain.

Genistein conversion and 5-hydroxy-dehydroequol conversion yield (%) profiles were recorded along different initial genistein concentrations.

3.3.5 Phytoestrogenic property of (-)-5-hydroxy-equol

The efficacy of (-)-5-hydroxy-equol as an effective potent phytoestrogen was examined through competitive human estrogen receptor (hER) binding assay (**Table 3.2**). It showed 0.13% relative binding affinity (RBA) of 17β-estradiol for hERα and 0.15% RBA for hERβ in competitive antagonism assay. Its RBA for hERα were relatively higher than that of genistein or (*S*)-equol, while the RBA for hERβ was about 50 times lower than that of genistein and 20 times lower than that of (*S*)-equol (Muthyala et al. 2004). The calculated β/α selectivity based on Ki of (-)-5-hydroxy-equol was 0.4, indicating its ERα preferred property. Its thoroughly studied analogue, (*S*)-equol has 13 β/α selectivity (Muthyala et al. 2004) and another reference also showed ERβ-selective property of (*S*)-equol (9 β/α selectivity, calculated from Ki values of 6.4 for ERα and 0.7 for ERβ) (Setchell et al. 2005). Daidzein and genistein, the most abundant soy isoflavones, also have preferred β/α selectivity, i.e. 1.5 and 180, respectively. This data suggests that (-)-5-hydroxy-equol is more similar to the natural estrogen in terms of its β/α selectivity, 17β-estradiol than other phytoestrogens (Muthyala et al. 2004). Because most of plant or microbial-derived phytoestrogens such as genistein, (*S*)-equol, coumestrol are rather ERβ-selective (Kuiper et al. 1998), its ERα preferred property, which was often found at estrogenic chemicals such as tamoxifen and raloxifen, is very unique among other phytoestrogens (Barkhem et al. 1998; Kuiper et al. 1998). Thus, this study suggests that (-)-5-hydroxy-equol appears to resemble traditional chemical estrogens rather than general phytoestrogens, despite its relatively lower binding affinity. Further

studies of microbial derived (-)-5-hydroxy-equol would reveal its potent estrogenic characters as an ER agonist or a selective estrogen receptor modulator (SERM).

Additionally, anti-oxidant property of 5-hydroxy-equol is worthy of attention. It is well-known that equol has greater antioxidant activity than daidzein (Arora et al. 1998; Choi and Kim 2014). The significant antioxidant activity of equol was suggested to result from the loss of 2,3-double bond coupled with the absence of 4-oxo group in isoflavone structure (Arora et al. 1998). 5-hydroxy-equol has better antioxidant activity than (*S*)-equol. As it has one more hydroxyl group at C5 on the equol backbone, which was known to contribute to its better antioxidant activity than equol (Arora et al. 1998). Despite the outstanding character of 5-hydroxy-equol, no reports about its *in vivo* or *in vitro* biological functions for human cells or health have been reported yet due to its low availability. It was recently known to increase the lifespan of *Caenorhabditis elegans*, and enhance its resistance against thermal and oxidative stress through DAF-2/DAF-16 Insulin/IGF-1 signaling pathway (Zhang and Wang 2014).

Table 3.2 hER binding assay of (-)-5-hydroxy-equol.

	RBA[a](%)		β/α[c]	K_i[b] (nM)		β/α[c]	Ref.
Ligand	**hERα**	**hERβ**		**hERα**	**hERβ**		
Estradiol	100	100	1	0.2	0.5	0.4	(Muthyala et al. 2004)
Daidzein	0.010	0.040	4	2000	1300	1.5	(Muthyala et al. 2004)
Genistein	0.017	7.4	440	1200	6.7	180	(Muthyala et al. 2004)
(*S*)-equol	0.10	3.20	32	200	16	13	(Muthyala et al. 2004)
(-)-5-hydroxy-equol	0.13	0.15	1.2	150	340	0.4	This study

[a] RBA = Relative binding affinity (%) measured in a competitive binding assay. The K_d values of estradiol for ERα and ERβ are 0.2 nM and 0.5 nM, respectively (Muthyala et al. 2004).
[b] K_i = inhibition constant, calculated from the IC_{50} of 5-hydroxy-equol using Cheng Prussof competitive equation: $IC_{50}/(([L]/K_d)+1)$ (Wells 1992)
[c] For RBA, the β/α ratio is calculated from $RBA_{hER\beta}/RBA_{hER\alpha}$, whereas for K_i, the β/α ratio is calculated from $K_{ihER\alpha}/K_{ihER\beta}$.

In the case of 5-hydroxy-dehydroequol, it is firstly observed and synthesized in this study. There have been no reports of this compound among several natural isoflav-3-enes of *Leguminosae* (Veitch 2007; Veitch 2013). Thus, the novel isoflav-3-ene has no revealed biological roles and known beneficial effects to human health yet. Only its analogue, dehydroequol (phenoxodiol), which lacks a hydroxyl group at C5, has been proved to inhibit prostate or ovarian cancer cell growth and subjected to clinical phase II (Gamble et al. 2006; Kelly et al. 2011). There has been no clinical test for 5-hydroxy-dehydroequol yet due to the difficulties of preparation method. Its bioavailability or safety or any adverse effects on human body should be evaluated in future.

3.4 Conclusion

In conclusion, quantitative preparation of (-)-5-hydroxy-equol and 5-hydroxy-dehydroequol was successfully achieved using the same series of enzymes as that for the biosynthesis of (*S*)-equol. The previously constructed recombinant strain was verified as a versatile whole cell catalyst producing not only (*S*)-equol, but also (-)-5-hydroxy-equol and 5-hydroxy-dehydroequol in this study. It is also expected that this recombinant system would also convert glycitein, another isoflavone component in soybean extract, into its corresponding equol derivative, 6-methoxy-equol, which was previously detected in glycitein-treated human feces (Simons et al. 2005). Furthermore, the recombinant *E. coli* strain could be utilized as a versatile catalytic tool for the preparation of other equol derivatives such as 3'-hydroxy-equol, 6-hydroxy-equol, other mono- or dihydroxy-equols and isoflavan glycosides, which have not been synthesized in quantity, so that no physiological roles could be ever reported (Rufer et al. 2006). Another interesting finding through this study was that using two separate strains for the synthesis of (-)-5-hydroxy-equol, which was quite effective and advantageous to improve its selective production and yield, so that such enzyme compartmentalization strategy will be quite useful to synthesize other equol derivatives and to expedite understanding of their new biological roles in human health. Along the same line, their potent benefits and/or risks for human health would explain the ambiguous positive effect of soybean diets to human health.

Chapter 4.

Protein engineering and isoflavone solubilization strategy for g/L scale production of equol and 5-hydroxy-equol

4.1 Introduction

Bioprocess, which mainly comprises biotransformation and fermentation offers the opportunity to prepare versatile bio-derived chemicals. Differently from chemical synthesis, the bioprocess requires aqueous conditions that are compatible with most of biocatalysts including microbial cells and enzymes. The water-based reaction system enabled efficient production of water-soluble cellular metabolites such as organic acids, amino acids and short-chain alcohols over 100 g/L level (Alfenore et al. 2004; Becker et al. 2011; Ji et al. 2010; Okino et al. 2008). However, the titers of hydrophobic chemical species including free fatty acids, short-chain alkanes and flavonoids produced in bioprocess reached only below 10 g/L (less than 1 g/L in most cases) (Choi and Lee 2013; Leonard et al. 2008; Xu et al. 2013). Since hydrophobic chemicals generally require higher cellular energy in production for their highly ordered molecular structure, and their low solubility limits efficient mass transfer or flux of substrate/products, relatively low titers may occur.

(*S*)-equol is a reductive isoflavone derivative that is more hydrophobic than its precursor, daidzein. During the last decade, (*S*)-equol has attracted nutritional scientists owing to its moderate estrogenic properties. This potent phytoestrogen is formed by some of gut bacteria which convert soy isoflavone, daidzein into (*S*)-equol (Matthies et al. 2009; Minamida et al. 2006; Wang et al. 2005a). Because (*S*)-equol binds selectively to estrogen receptor ERβ over α, it can escape general adverse effects prompted by ERα activation (Setchell et al. 2005). The selective ERβ activation has been exploited for reducing menopausal symptoms, osteoporosis, cardiovascular risk, prostate or breast cancer incidence rates, skin aging, and even

preventing hair loss (Jackson et al. 2011; Jenks et al. 2012). Therefore, (*S*)-equol was developed as a dietary supplement for postmenopausal women, and racemic equols were used as additives for anti-aging cosmeceuticals. Its market has been expanding in USA and Japan, substituting for the market of traditional hormone supplement and cosmetic ingredients. On the other hand, 5-hydroxy-equol, a kind of equol derivative derived from genistein, has lower ER binding affinity than equol, but it is the most potent antioxidant among other isoflavone derivatives and its anticancer activity against hematocellular carcinoma has been recently proved (Arora et al. 1998; Gao et al. 2018; Lee et al. 2017). Despite no practical applications reported yet, 5-hydroxy-equol could be a novel candidate as cosmetic ingredient or pharmaceuticals.

To meet the burgeoning demands for (*S*)-equol, various chemical and biological synthetic methods have been examined by several research groups (Wang et al. 2005a; Yang et al. 2012). However, previous biotransformation methods only showed μg/L or mg/L production scales of (*S*)-equol, and the requirement of anaerobic condition for equol-producing bacteria was proved as one of the major drawbacks to replace undesirable, but high-productive organic synthetic methods. To overcome the bottleneck, we recently developed oxygen-tolerant recombinant bacteria and introduced an engineered enzyme with better efficiency for aerobic production of (*S*)-equol (Lee et al. 2016a), however the strain still showed sub g/L yields that are not economically sufficient.

In this study (Lee et al. 2018b), we postulated that poor solubility of isoflavonoid would be a major obstacle to prevent a high yield production of (*S*)-

equol in the whole-cell biotransformation system. Based on the postulation, several commercial hydrophilic polymer (HP)s were screened to increase the solubility of isoflavone in the aqueous medium. HPs such as polyethylene glycol (PEG) and polyvinylpyrrolidone (PVP) have been traditionally used in food chemistry to solubilize water-insoluble ingredients and are known to be generally and biologically safe (Khare 2005). However, use of HPs in whole-cell biotransformation was not investigated enough to support their validity. Here, dramatic increase of daidzein solubility was observed by the addition of HPs, and their potent application to enhance the final (*S*)-equol yield was shown in whole-cell biotransformation of daidzein (**Fig. 4.1A**).

Moreover, the abovementioned HPs were applied to enhance the bioconversion performance for 5-hydroxy-equol. Because simple HP supplementation did not increase the production level of 5-hydroxy-equol, rate-determining enzyme was explored and the identified enzyme (i.e. tetrahydrodaidzein reductase: THDR) was engineered using the computationally predicted information comprising homology modeling and substrate docking simulation, which led to high yield production of 5-hydroxy-equol comparable to that of (*S*)-equol.

A.

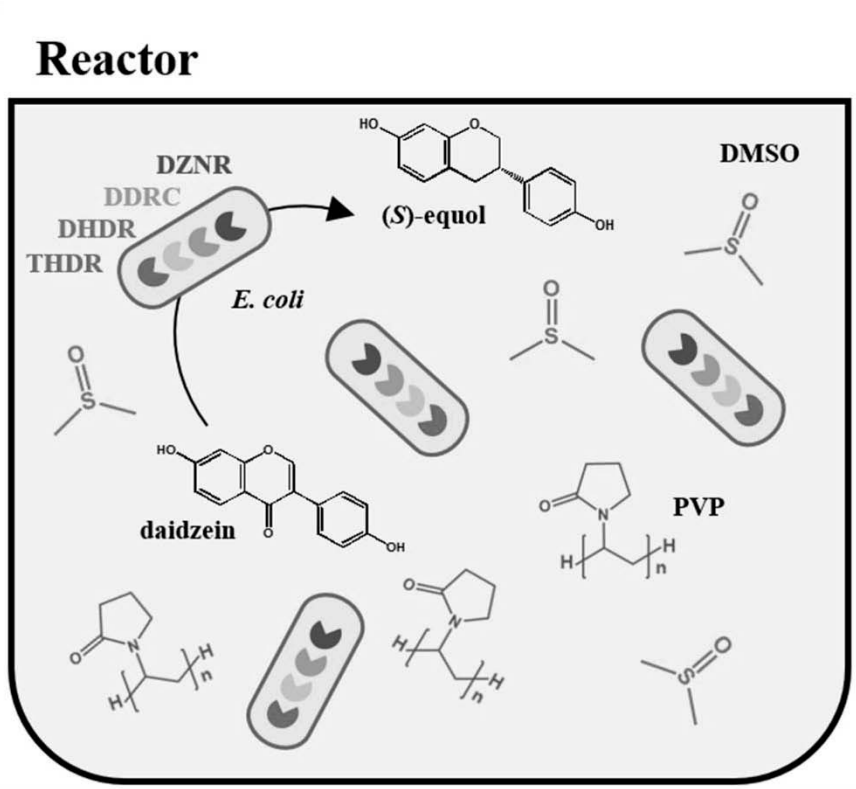
Reactor
DZNR
DDRC
DHDR
THDR
E. coli
(S)-equol
DMSO
daidzein
PVP

B.

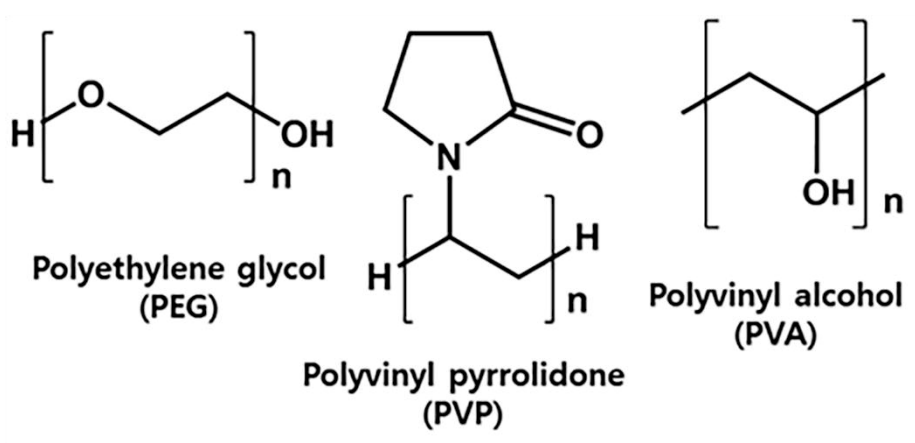
Polyethylene glycol
(PEG)
Polyvinyl pyrrolidone
(PVP)
Polyvinyl alcohol
(PVA)

C.

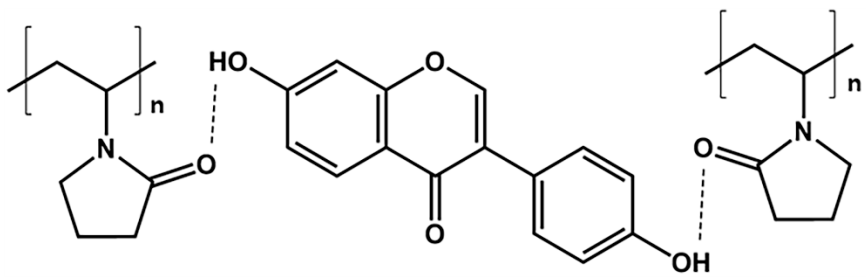

Figure 4.1 Schemes of hydrophilic polymer supplemented whole-cell biotransformation

A. Schematic representation of whole-cell catalytic reaction system for daidzein to (*S*)-equol bioconversion in the engineered solvent. *E. coli* whole cell catalyst containing four heterologously expressed enzymes including DZNR: daidzein reductase, DDRC: dihydrodaidzein racemase, DHDR: dihydrodaidzein reductase and THDR: tetrahydrodaidzein reductase, substrate (daidzein), product ((*S*)-equol), and solvent components (PVP and DMSO) are shown in notation. **B.** Commercial HPs examined in this study. **C.** Proposed hydrogen bonding interactions between daidzein (H-donor) and PVP (H-acceptor).

4.2 Materials and Methods

4.2.1 Chemicals

Daidzein, genistein, hydrophilic polymers and other chemicals were purchased from Sigma Aldrich. (*S*)-equol was purchased from Cayman Chemical (Ann Arbor, MI) and dihydrogenistein was purchased from Toronto Research Chemicals Inc. (North York, Ontario, Canada) and 5-hydroxy-equol and 5-hydroxy dehydroequol were biosynthesized using whole cell catalysts.

4.2.2 Solubility test

For solubility study, 2 mg of daidzein powder was dissolved into 0.4 mL of 0.2 M potassium phosphate buffer (KPB) (pH 8.0) with or without specified amounts (i.e. weight or volume %) of HP and dimethyl sulfoxide (DMSO), and the mixture solution was incubated under vigorous shaking over 24 h at 37ºC. After the incubation, the mixture solution was kept at room temperature for 3 h to prevent supersaturation. Subsequently, the solution was centrifuged at 13000 rpm for 15 min. The supernatant was centrifuged once again under the same condition to completely exclude undissolved isoflavone or other polyphenols. Each sample solution was then diluted with 50% (v/v) methanol solution by 2~10 fold. To determine solubility of daidzein and other polyphenols, the diluted samples were analyzed by HPLC (YoungLin, South Korea) equipped with the COMOSIL $5C_{18}$-AR-II column (5 μm particle size, 4.6 mm I.D. x 150 mm; Nacalai tesque, Japan). The mobile phase was composed of 40% acetonitrile and 60% water containing 0.1% trifluoroacetic acid, and 0.7 ml/min isocratic flow rate was applied for 10 min. Daidzein was detected at

280 nm in UV spectrometer, and the concentration was calculated using standard curves. Other polyphenols were detected at 288 nm with the same elution method. All experiments were performed more than three times and standard deviation was denoted as error bars.

4.2.3 Whole-cell biotransformation study

A previously constructed *E. coli* strain (tDDDT-WT) harboring two plasmids (i.e. pRSFDuet-1 carrying *dzr*: daidzein reductase and *ifcA*: dihydrodaidzein racemase, and pCDFDuet-1 carrying *ddr*: dihydrodaidzein reductase and *tdr*: tetrahydrodaidzein reductase or its variants) was used as a whole cell biocatalyst, and the protocol of daidzein to (*S*)-equol bioconversion reaction followed the previous reference with slight modification (Lee et al. 2016a; Lee et al. 2017). In brief, 6.8 g of dry cell weight (DCW)/L was suspended in 0.2 M KPB (pH 8.0) containing 2% (w/v) glucose, 1% (v/v) glycerol, 10 mM L-ascorbic acid and a specified amount of HPs. Biotransformation was initiated by the addition of daidzein or genistein (from 100 mM DMSO stock). The unbaffled vials were used for the reaction, and they were gently agitated in a shaker at 150 rpm and 30ºC. At each sampling point, 50 μl of the reaction solution was sampled and mixed with 150 μl of distilled water and 800 μl of ethyl acetate (EA). After vigorous shaking, the extracted EA layer was evaporated, and subsequently redissolved into pure methanol for HPLC analysis. The average concentrations of isoflavone derivatives were quantified using respective standard curves.

4.2.4 Homology modeling and docking simulation

THDR (tetrahydrodaidzein reductase) from *Slackia isoflavoniconvertens* DSM22006 had 25% identity and 38% similarity with 3-ketosteroid Δ^1-dehydrogenase from *Rhodococcus erythropolis* SQ1 (PDB ID: 4c3x) in their amino acid sequences. Five THDR model structures was generated using 4c3x as a template with Modeller9.18 (Webb and Sali 2014) and the model with the lowest DOPE score was selected for following docking simulation study. AutoDock Vina 1.1.2 (Trott and Olson 2010) and MGLTools 1.5.6 were used for predicting binding mode of (3*S*,4*R*)-tetrahydrodaidzein (or tetrahydrogenistein) to the THDR homology model. Prior to docking simulation, polar hydrogens were added to THDR by Python Molecular Viewer 1.5.6. The center of the grid box (40 Å x 40 Å x 40 Å) was fixed at the *re*-face of flavin adenine dinucleotide (FAD) embedded in THDR active site. Exhaustiveness was set to 8 with an energy range of 5. 20 docking results with minimum energy were obtained and visualized using Chimera 1.11.2 (Pettersen et al. 2004).

4.2.5 Site-directed mutagenesis of THDR

Nine residues of THDR predicted to interact with (3*S*,4*R*)-tetrahydrodaidzein were substituted with alanine or phenylalanine using a previously-established protocol (Zheng 2004). Proline 464 was further mutated by several other amino acids using the specific mutagenesis primers (**Table 4.1**), and all constructs were confirmed by sequencing.

Table 4.1 Transformants and primers information for site-directed mutagenesis of THDR.

Transformant notation	
Name	**Plasmid description**
tDDDT-WT	pRSFDuet-1(*dzr/ifcA*) + pCDFDuet-1(*ddr/tdr*)
tDDDT-TPA	pRSF Duet-1(*dzr/ifcA*) + pCDF Duet-1(*ddr/thdr P464A*)

Site-directed mutagenesis of THDR

Primer	**Primer sequences (5' to 3')**
E50A_F	GTTCGCCGCGGGCACGGCTG
E50A_B	CCGTGCCCGCGGCGAACACC
T52A_F	CCGAGGGCGCGGCTGCATTTG
T52A_B	ATGCAGCCGCGCCCTCGGCG
F99A_F	CCCGCGCAGCTGTGGAGAACTCC
F99A_B	GTTCTCCACAGCTGCGCGGGCAAC
L252A_F	CTGCCCGGCGCTCGCTGCGG
L252A_B	CAGCGAGCGCCGGGCAGGTG
E291A_F	CGGTCGCTGCTAACCTCGGCG
E291A_B	CCGAGGTTAGCAGCGACCGATTC
N292A_F	CGCTGAAGCTCTCGGCGATATCG
N292A_B	CGCCGAGAGCTTCAGCGACC
M419A_F	CTGGCACCGCTGGTTCTGCCG
M419A_B	GCAGAACCAGCGGTGCCAGTTG
Y459F_F	GGCGATTCCTTTAACATGGAAATTC
Y459F_B	TTCCATGTTAAAGGAATCGCCATAC
P464A_F	GGAAATTGCTGGTTGCGCGAATG
P464A_B	GCGCAACCAGCAATTTCCATG
P464R_F	GGAAATTCGTGGTTGCGCGAATG
P464R_B	GCGCAACCACGAATTTCCATG
P464D_F	GGAAATTGATGGTTGCGCGAATG
P464D_B	GCGCAACCATCAATTTCCATG
P464T_F	GGAAATTACTGGTTGCGCGAATG
P464T_B	GCGCAACCAGTAATTTCCATG
P464N_F	GGAAATTAATGGTTGCGCGAATG
P464N_B	GCGCAACCATTAATTTCCATG
P464F_F	GGAAATTTTTGGTTGCGCGAATG
P464F_B	GCGCAACCAAAAATTTCCATG
P464L_F	GGAAATTCTGGGTTGCGCGAATG
P464L_B	GCGCAACCCAGAATTTCCATG

4.3 Results

4.3.1 Isoflavone solubility in HP supplemented solution

As a proof-of-concept study, we examined seven species of commercially available HPs including polyethylene glycol (PEG) (0.6k, 2k and 6k), polyvinyl pyrrolidone (PVP) (10k and 40k) and polyvinyl alcohol (PVA) (27k and 61k) to solubilize one of major soy isoflavones, daidzein with 5% (w/v) final HP concentration (**Fig. 4.1B and C**). Daidzein solubility (2.4 mg/L in 0.2 M KPB, pH 8.0) was remarkably increased by addition of PEG (4~7-fold), PVP (30~40-fold) and PVA (5~6-fold) (**Fig. 4.2**). Based on the results, we could understand that the solubility of daidzein was strongly affected by the type of HP, rather than the molecular weight of HP. The most improvement was achieved by 5% PVP-40k containing solution that showed 104.2 (44-fold) mg/L of daidzein solubility.

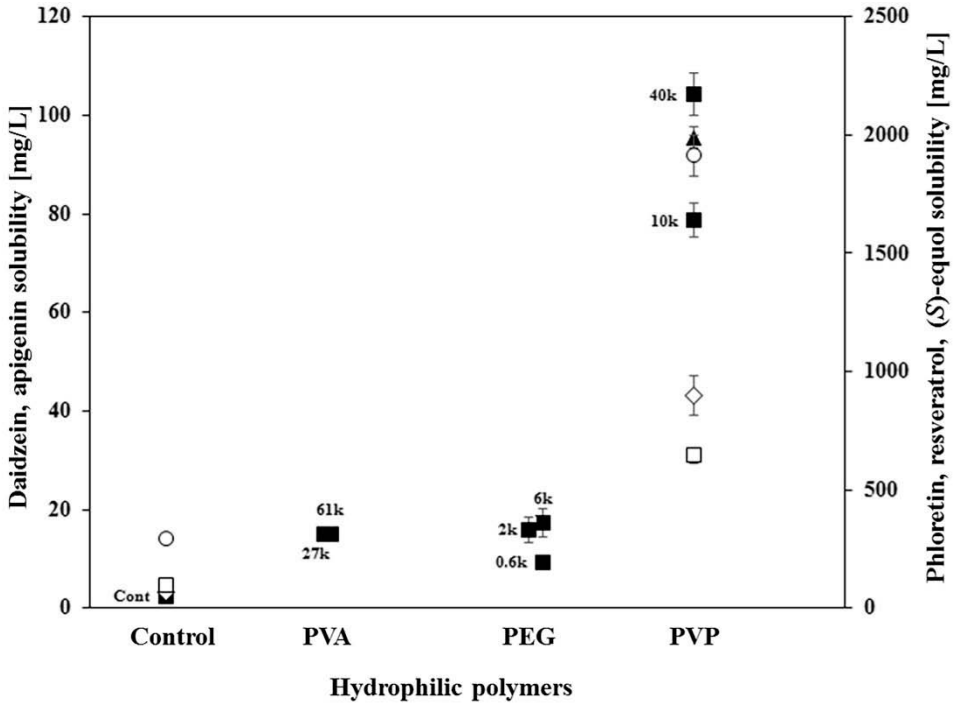

Figure 4.2 Polyphenol solubility in 0.2 M KPB (pH 8.0) solution containing 5% (w/v) HP.

In the case of daidzein (black square), seven commercial HPs including three PEGs (0.6k, 2k and 6k), two PVPs (10k and 40k) and two PVAs (27k and 61k) were examined, otherwise only PVP (40k) was examined for the other natural polyphenols including apigenin (black triangle), phloretin (white circle), resveratrol (white diamond) and (*S*)-equol (white square). The control contained no HP.

To investigate the change of its solubility according to the concentration of the HP and co-utilization of water-miscible organic solvents, daidzein solubility was measured by varying the HP contents from 0 to 10% (w/v) (**Fig. 4.3A**). PVP-40k and PEG-6k increased daidzein solubility linearly within the examined ranges. The slopes of the increase were 20.7 mg/L/% PVP-40k and 3.7 mg/L/% PEG-6k, respectively. In addition, dimethyl sulfoxide (DMSO), a widely used polar aprotic water miscible organic solvent showed a slight synergistic effect on daidzein solubility in 5% (w/v) PVP-40k and PEG-6k solution (**Fig. 4.3B**). The positive effect, which was defined by a slope in 'DMSO content vs. daidzein solubility' plot, was about 3.5-fold larger in PVP-40k (i.e. 6.0 mg/L/% DMSO) than in PEG-6k (i.e. 1.7 mg/L/% DMSO). This result shows that PVP-40k is the most promising HP for increasing isoflavone solubility, and the addition of polar aprotic co-solvent, i.e. DMSO synergistically increase the isoflavone solubility. Therefore, PVP-40k was selected for subsequent solubility and bioconversion studies.

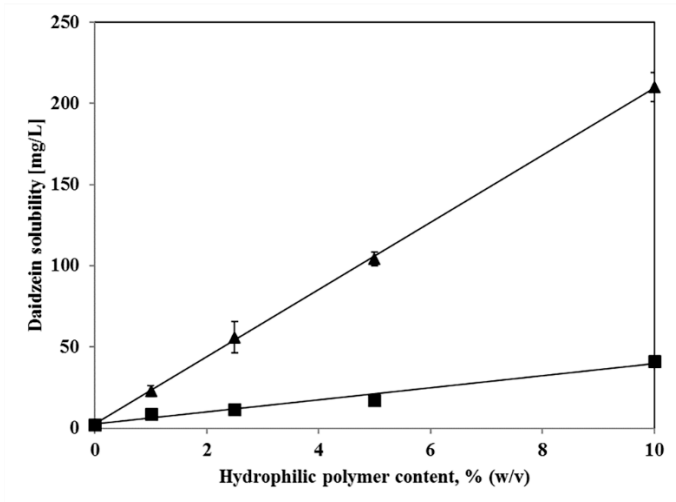

A.

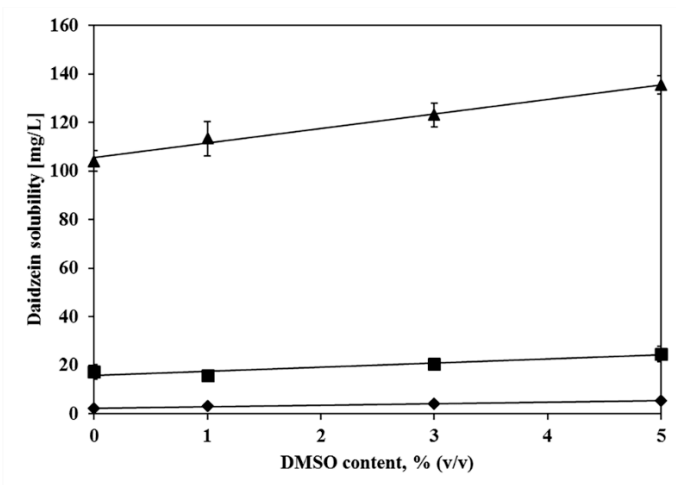

B.

Figure 4.3 Solubility increase by addition of HP and DMSO.

A. Daidzein solubility in 0.2 M KPB (pH 8.0) solution with 0 to 10% (w/v) of PEG-6k (square) or PVP-40k (triangle). **B.** Daidzein solubility in 0.2 M KPB (pH 8.0) solution with a fixed 5% (w/v) PEG-6k (square) or PVP-40k (triangle) and specified amounts (i.e. from 0 to 5% (v/v)) DMSO. The control (diamond) contained no HP, but varied concentration of DMSO.

4.3.2 HP addition effect on (*S*)-equol bioconversion system

We postulated HP and polar aprotic co-solvent would enable the usage of whole-cell biocatalyst to work for biotransformation of hydrophobic chemicals by increasing solubility of the hydrophobic substrates without severe toxicity to cell. To verify the postulation, bioconversion of daidzein into (*S*)-equol was performed using recombinant *E. coli* as a whole cell biocatalyst in the previously mentioned 5% (w/v) HPs and 3% (v/v) DMSO. After 12 h reaction, conversion yields of (*S*)-equol from 0.76 g/L of daidzein were recorded (**Fig. 4.4**). In the case of control reaction without any HP, the final yield of (*S*)-equol (i.e. 0.28 g/L) was achieved in 3 h, and further biotransformation did not increase the final equol formation. Interestingly, quite significant increases in conversion yields were achieved by the addition of PVP and PEG, whereas PVA addition was not so significant. The most improved result was found with PVP-40k, which increased (*S*)-equol yield up to 0.68 g/L (94% conversion yield). The final yield was further pulled up by 5% (w/v) PVP-40k and 5% (v/v) DMSO as co-solvents, which gave 1.22 g/L of (*S*)-equol from 1.27 g/L of daidzein (almost 100% conversion yield) within 24 h reaction time (**Fig. 4.5**). This is the best record ever reported for enantiopure (*S*)-equol biosynthesis. Plotting daidzein solubility in different HP solutions versus final bioconversion yield (**Fig.4. 6**) revealed a linear relationship with some errors: [yield, mg/L] = 6.42 x [daidzein solubility, mg/L] + 265 with R^2= 0.87, which showed that (*S*)-equol bioconversion yield in this reaction system seems to be highly correlated with daidzein solubility. In detail, PEGs might have positive impact on the bioconversion yield, while PVP negatively affected the yield of (*S*)-equol relative to the average linearity. Therefore,

the solubility increase of hydrophobic substrate (daidzein) raised by HP addition enhanced the conversion yield up to g/L level, which indicates the high biocompatibility of HP in whole-cell biotransformation.

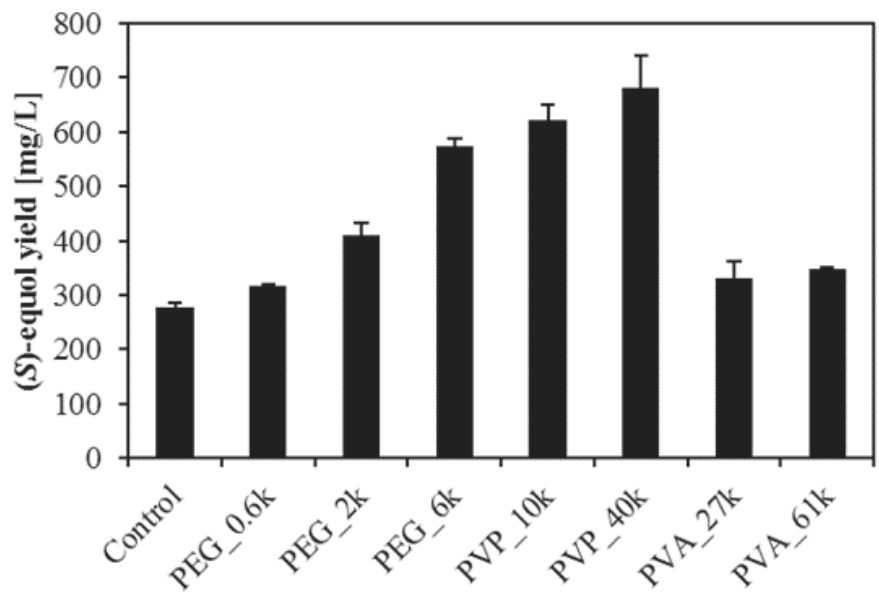

Figure 4.4 Final (*S*)-equol yields in whole-cell biotransformation in HP added reactions.

The average yield was calculated from the individual two samples collected after 12 h reaction, where 3 mM (0.76 g/L) of daidzein (from 100 mM DMSO stock solution, i.e. 3% (v/v) final DMSO) was fed as an initial substrate. 0.2 M KPB (pH 8.0) with 5% (w/v) each HP was used for reaction solution.

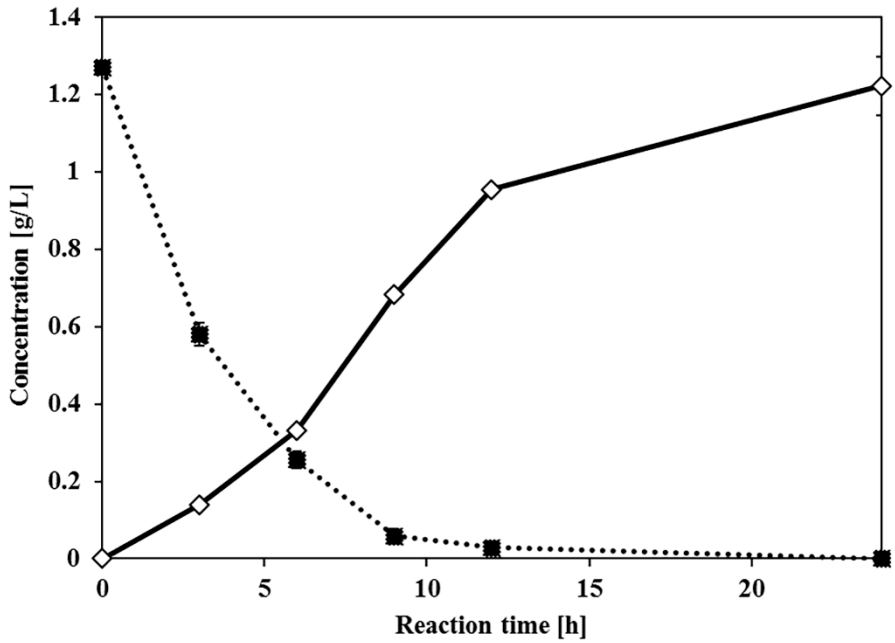

Figure 4.5 Time course concentration profile of daidzein to (*S*)-equol biotransformation.

0.2 M KPB (pH 8.0) solution with 5% (w/v) PVP-40k and 5% (v/v) DMSO was used as co-solvents. 1.27 g/L of daidzein (black square) was fed as an initial substrate and 1.22 g/L of (*S*)-equol (white diamond) was produced in average of three individual trials. The biotransformation was catalyzed by a *E. coli* whole-cell catalyst (6.8 gDCW/L) expressing four equol-forming enzymes (i.e. daidzein reductase, dihydrodaidzein reductase, tetrahydrodaidzein reductase and dihydrodaidzein racemase).

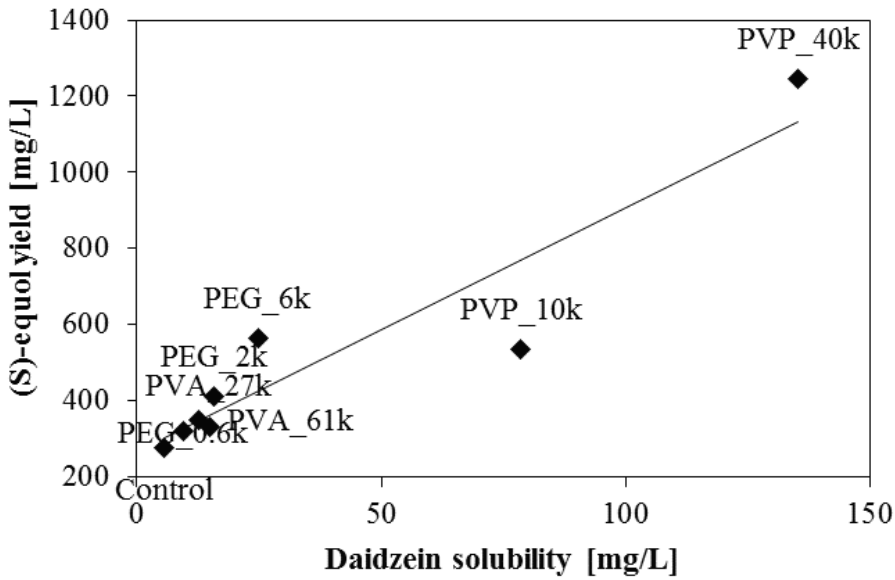

Figure 4.6 Correlation plot between daidzein solubility vs. (*S*)-equol yield.

Linear plotting between two parameters: daidzein solubility and (*S*)-equol biotransformation yield, represents the following equation: [yield, mg/L] = 6.42 x [daidzein solubility, mg/L] + 265 with R^2= 0.87. It strongly suggests that daidzein solubility is a major determinant (or bottleneck) for (*S*)-equol yield in the biotransformation.

4.3.3 Application of HP into other polyphenols solubilization

To generalize the positive solubilization effect of PVP for other polyphenols, three noteworthy polyphenols including phloretin (dihydrochalcone), resveratrol (stilbene) and apigenin (flavone) were examined as well (**Fig. 4.2**). All the three polyphenols attracted great attention by their potential use and unique biological functions for human health such as antioxidant and antitumor activities (Galati et al. 2002; Yao et al. 2004). The solubilities of the three polyphenols with/without 5% (w/v) PVP-40k were compared. For all the three polyphenols, PVP addition generally increased solubility, but the degree of the enhancement varied depending on the compounds. Among the three polyphenols, phloretin showed the highest solubility in buffer solution with (i.e. 293 to 1914 mg/L = 650% increase). Solubility of resveratrol and apigenin were also significantly enhanced by PVP addition (i.e. 66 to 901 mg/L = 1365%, and 4 to 95 mg/L = 2375% increase, respectively). This result demonstrates that the solubility increase of polyphenols by PVP addition is a general phenomenon.

4.3.4 Homology modeling of THDR and docking simulation

Even though genistein is different only in a hydroxyl group at C5 compared to daidzein, bioconversion of genistein to 5-hydroxy-equol was not so much influenced by hydrophilic polymer addition. Actually genistein is more soluble than daidzein that solubility would not be the major bottleneck to inhibit the biocatalytic performance. Comparing the previous studies, 5-hydroxy-equol formation was more reluctant to equol formation in the same whole-cell biotransformation system (Lee et al. 2016a; Lee et al. 2017). We noted that previous better expression of

tetrahydrodaidzein reductase (THDR) displayed selective production of 5-hydroxy-equol with improved productivity, which guided us to explore THDR for high yield production of 5-hydroxy-equol.

Due to the lack of structural information, we performed computational prediction to get homology model of THDR using the 3-ketosteroid Δ^1-dehydrogenase (Δ^1-KSTD1) from *Rhodococcus erythropolis* SQ1 (PDB ID: 4c3x) as a template. A homology model with minimum DOPE score was structurally aligned with the template, and the prosthetic group, flavin-adenine dinucleotide (FAD) was well conserved in the model as in the template (**Fig. 4.7**). A Walker A motif (or dinucleotide-binding motif) observed in THDR sequence, 14-GGGASGKS-21, indicates phosphate binding region, and the loop was truly associated with phosphate groups of FAD in the model. The *re*-face of FAD was predicted as the active site of THDR, because its catalytic reaction involved oxido-reduction with putative hydride transfer (Kim et al. 2010a). The predicted active site had open form with possible substrate binding space and corresponded to active site of Δ^1-KSTD1. However, two catalytic tyrosines, Tyr119 and Tyr318 conserved in Δ^1-KSTD1 was not found in THDR, which indicated that different hydride transfer mechanism might be engaged (**Fig. 4.8**) (Rohman et al. 2013). Only THDR Tyr459 corresponding to Δ^1-KSTD1 Y487 that was known to interact with substrate by a hydrogen bond was structurally aligned. Moreover, THDR Phe99 was also aligned to Δ^1-KSTD1 Phe116 that was in a position for hydrophobic stacking interactions with the B-ring of the 3-ketosteroid (Rohman et al. 2013).

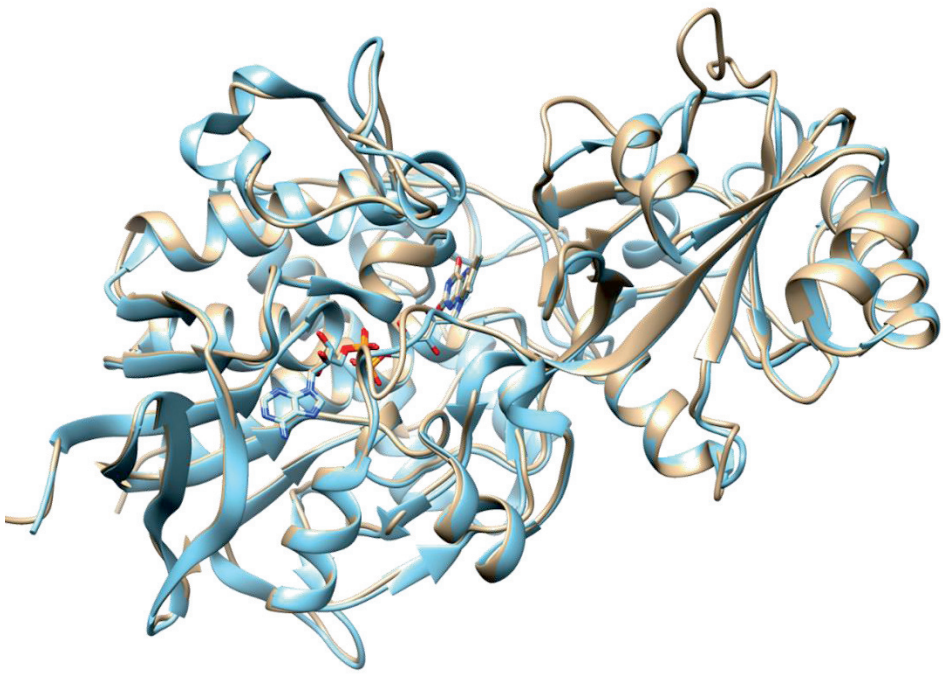

Figure 4.7 Structural alignment of two proteins: Δ^1-KSTD1 and THDR.

Δ^1-KSTD1 from *Rhodococcus erythropolis* SQ1 (PDB ID: 4c3x) (cyan), and THDR from *Slackia isoflavoniconvertens* DSM22006 (model, constructed in this study) (brown). FAD molecules were shown by distinct atom/bonds representation. The image was generated with UCSF Chimera 1.11.2.

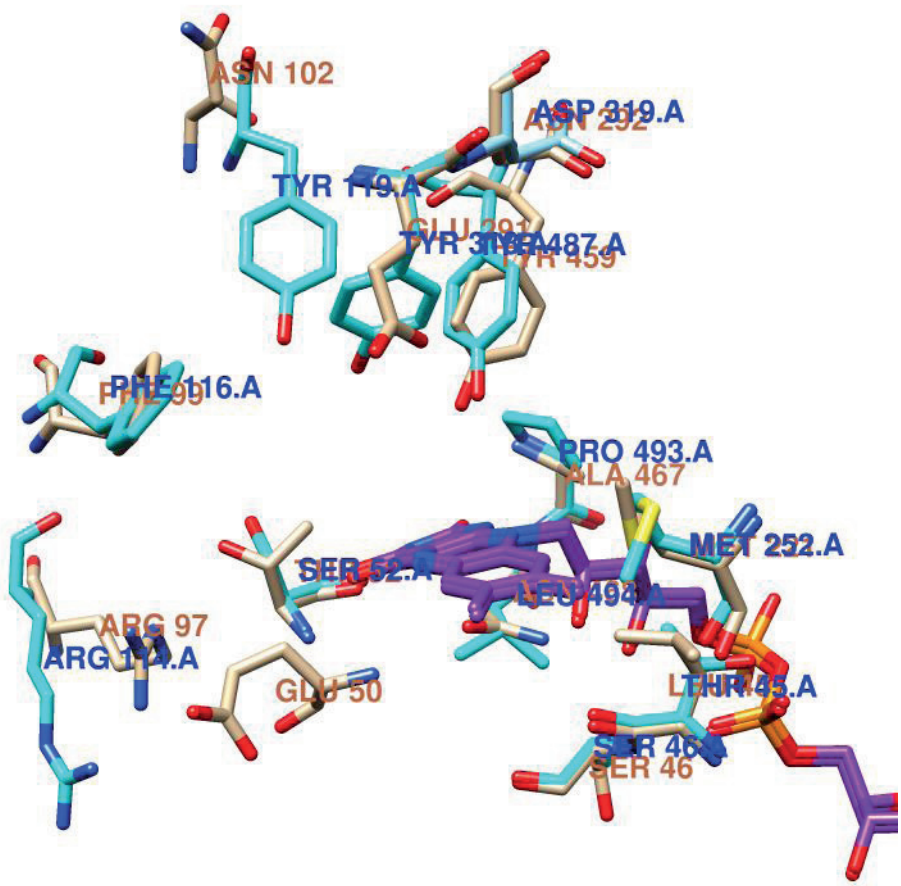

Figure 4.8 Structural alignment of active sites of the Δ^1-KSTD1 and THDR.

Active site residues of Δ^1-KSTD1 and THDR were shown with cyan and brown, respectively, with residue labels. FAD molecules were shown with purple with distinct color notation of hetero atoms. The image was generated with UCSF Chimera 1.11.2.

Next, docking simulation was performed to predict what residues in the predicted active site of THDR are important to bind its substrate, (3*S*,4*R*)-tetrahydrodaidzein (THD). Then, the most plausible binding mode with minimum binding energy could be obtained (**Fig. 4.9**). In the binding mode, Tyr459 is in a good position for hydrophobic stacking interactions with the B-ring of the (3*S*,4*R*)-THD and at the same time, hydrogen interactions with the hydroxyl group of the C-ring. Phe116 might also have van der Waals interactions with the A-ring of substrate. A couple of hydrogen interactions between substrate and Thr52, Met419 were also observed. However, similar docking result was not observed for (3*S*,4*R*)-THG.

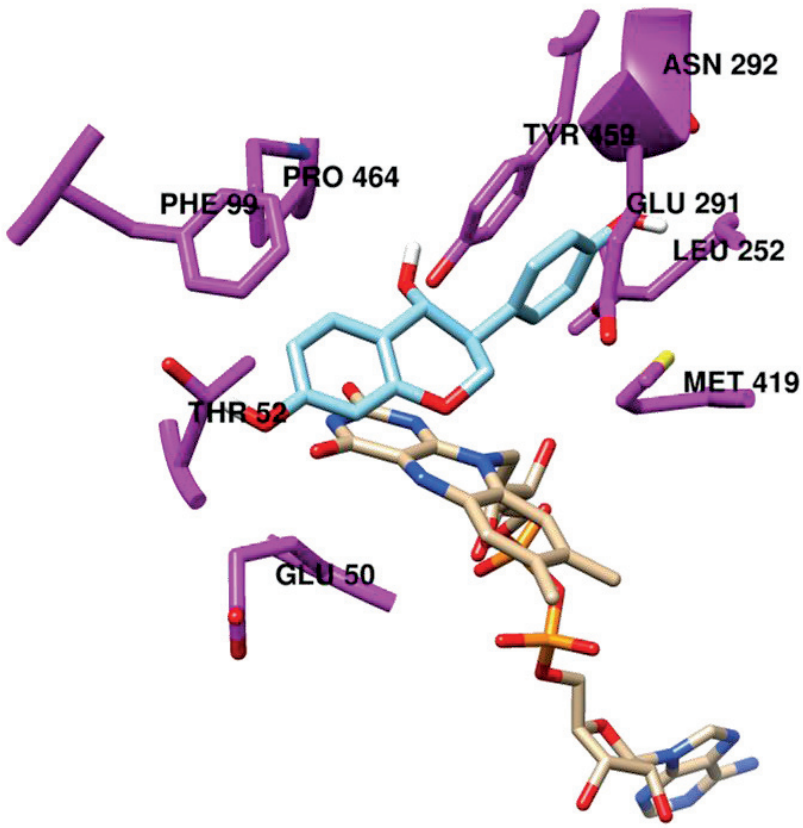

Figure 4.9 Computational docking simulation result.

(3*S*,4*R*)-THD was virtually docked into THDR model. Nine purple residues interact with the THD in the model. The image was generated with UCSF Chimera 1.11.2.

4.3.5 Site-directed mutagenesis of THDR and biotransformation using the mutants

To verify the importance of the interacting residues including Glu50, Thr52, Phe99, Leu252, Glu291, Asn292, Met419, Y459 and P464 were substituted with alanine or phenylalanine. Then, the mutants were introduced into daidzein-to-equol (or genistein-to-5-hydroxy-equol) production system and initial equol forming rate (at 2 h reaction time) was recorded (**Fig. 4.10A**). As a result, four mutants including E50A, F99A, L252A and M419A showed severe defects in equol or 5-hydroxy-equol production, while E291A and P464A displayed increased production rate. Three mutants including T52A, N292A and Y459F showed relatively modest decrease in equol production. Interestingly, P464A mutation improved 5-hydroxy-equol production rate by more than 5-fold, while substitutions to other residues including R, D, N, T, L and F did not show significant increase (**Fig. 4.10B**). Taken together, we regarded that THDR P464A would be a positive variant for equol production, especially on 5-hydroxy-equol. The interesting improvement attracted us to examine the variant for high yield production of 5-hydroxy-equol. When the recombinant strain harboring THDR P464A was fed with 1.35 g/L genistein with 5% (w/v) PVP_40k, most of genistein was converted into 5-hydroxy-equol in 24 h, yielding 1.3 g/L titer (**Fig. 4.11B**). Interestingly, 5-hydroxy-dehydroequol was rarely formed, while control strain harboring THDR wild-type represented 0.43 g/L of 5-hydroxy-equol and 0.26 g/L of 5-hydroxy-dehydroequol (**Fig. 4.11A**).

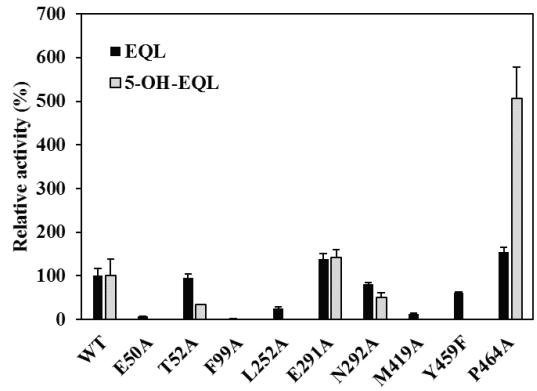

A.

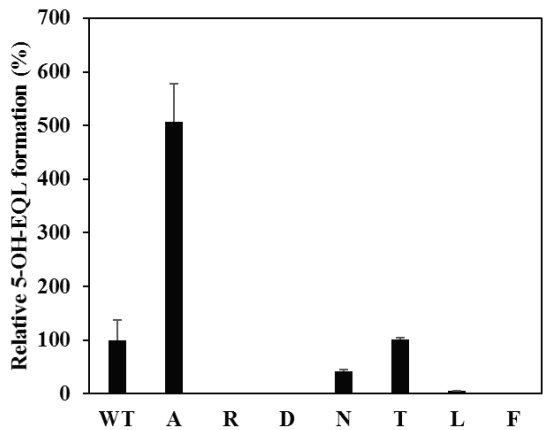

B.

Figure 4.10 Whole-cell biotransformation assay for the nine site-directed THDR mutants.

Recombinant *E. coli* harboring the mutants were used as whole-cell catalysts for daidein or genistein (1mM). (**A**) Initial equol (EQL, 2 h) or 5-hydroxy-equol (5-OH-EQL, 3 h) formation rates were relatively recorded for the recombinant strains containing THDR mutation. (**B**) 5-Hydroxy-equol formation rate was also compared between THDR Pro464 mutants. 1% (w/v) PVP and 1% (v/v) DMSO were supplemented for the bioconversion not to be interfered by low solubility of substrate. Average yield was obtained from more than two independent experiments and normalized by average values of control (tDDDT-WT).

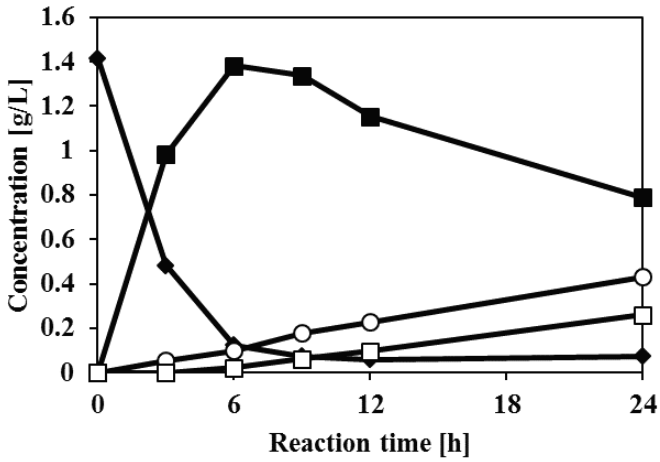

A.

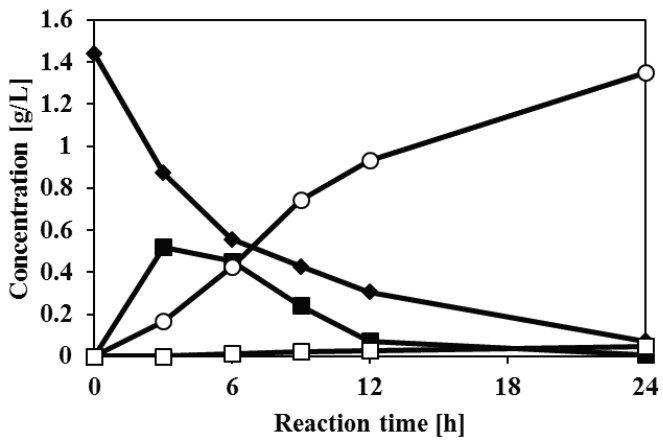

B.

Figure 4.11 Time course production of 5-hydroxy-equol from 1.35 g/L (5 mM) genistein in the whole-cell biotransformation.

(A) tDDDT-WT and (**B**) tDDDT-TPA with OD_{600} = 20 were used as whole-cell catalysts in the 1.35 g/L genistein bioconversion to 5-hydroxy-equol. 5% (w/v) PVP and 5% (v/v) DMSO were supplemented as co-solvents, and isoflavone concentrations were monitored along reaction time. (genistein; closed diamond, dihydrogenistein; closed square, 5-hydroxy-equol; open circle, 5-hydroxy-dehydroequol; open square).

Since the THDR P464A mutant was also validated in the enhanced productivity of (*S*)-equol (**Fig. 4.10A**), the recombinant *E. coli* harboring the mutant was examined in a whole-cell biotransformation with serial daidzein feeding. Consecutive feeding of 3 mM (ca. 0.76 g/L) daidzein every 3 hours with total 15 mM (ca. 3.8 g/L) of substrate, gave 1.88 g/L of (*S*)-equol production in 34 h, while the control harboring wild-type THDR produced 1.72 g/L of (*S*)-equol in the duplicate experiments (**Fig. 4.12**). Notably, the initial equol forming rate (equol production level at 6 h after daidzein feeding) in the mutant-introduced system (ca. 124 mg/L/h) was three times higher than in the control (ca. 41 mg/L/h). The enhanced titer and productivity of equol could be rationalized by the resolution of DHD accumulation, which was given by faster THD to equol conversion of THDR P464A mutant. Because DHDR was esteemed to have 15 times higher enzymatic activity than THDR (Schroder et al. 2013), the low concentration level of THD in both strains was not by low activity of DHDR, but just due to low equilibrium of THD/DHD ratio in *E. coli* cytoplasm (Lee et al. 2016a). Therefore, the bottleneck of overall reaction at high load of daidzein was suggested to be THDR, not DHDR. Additionally, isoflavone solubility was still important factor for g/L titer of (*S*)-equol, since insoluble isoflavone aggregates were observed during the biotransformation. Further improvement in (*S*)-equol titer would be achieved by further increase in isoflavone solubility with whole-cell compatibility, enhanced stability of the heterologously expressed enzymes, and effective NADPH supply in whole-cells.

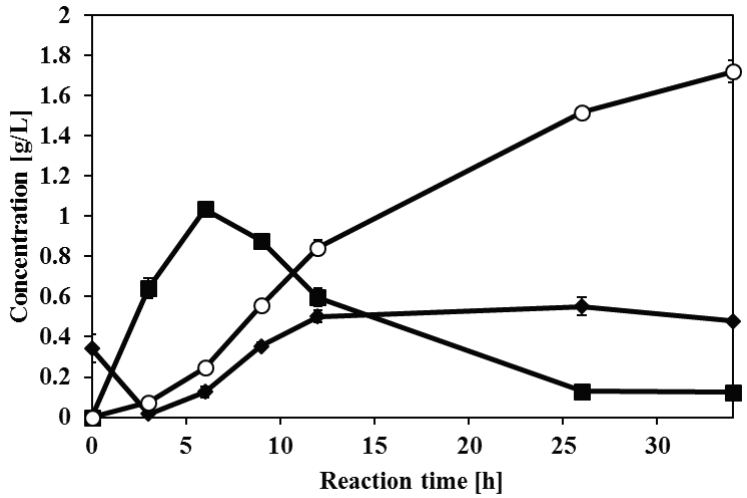

A.

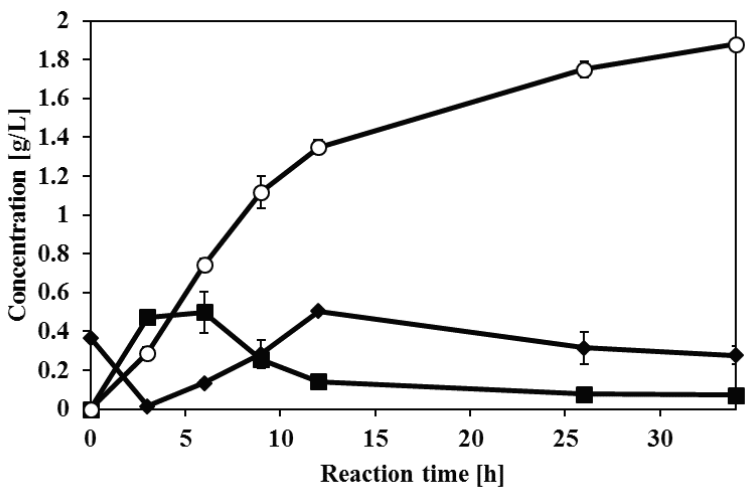

B.

Figure 4.12 Time course production of (*S*)-equol from serial daidzein feed

(A) tDDDT-WT and (**B**) tDDDT-TPA with OD_{600} = 20 were used as whole-cell catalysts in the 3.8 g/L daidzein (0.76g/L (from 76g/L DMSO stock) was fed at 0, 3, 6, 9 and 12 h right after sampling). 5% (w/v) PVP were supplemented as an isoflavone solubilizing solvent, and isoflavone concentrations were monitored along reaction time. (daidzein; closed diamond, dihydrodaidzein; closed square, (*S*)-equol; open circle).

4.4 Discussion

Whole-cell biotransformation is a fascinating and efficient reaction system to prepare versatile bio-derived chemicals (de Carvalho 2011). However, since it exploits living microbial cells as biocatalyst, direct use of organic solvent is not recommended, which limits its application to prepare water-immiscible hydrophobic chemicals. In this study, the significant increase in solubility of polyphenolic substrates by HP addition was investigated. HPs such as PEG and PVP are generally known to be safe as bio-additives, and the examined HPs in this study actually did not prevent whole-cell catalytic activity. In fact, PVP hydrogel was not known to have anti-microbial activity to *Escherichia coli* (El-Mohdy and Ghanem 2009), and PVP was rather demonstrated to protect the red blood cells against noncryogenic damage such as mechanical injury and osmotic fragility (Ben-David and Gavendo 1972). However, it is also known that 1 to 5% PVP works as a strong animal cell aggregating agent, deforming red blood cells (Nash and Meiselman 1983). Considering these facts and our results, 5% PVP may interact with microbial cells through a direct contact to cell outer membrane without lethal cytotoxic effect.

Among the examined HPs, the 5% PVP 40k supplementation solubilized daidzein and other polyphenols by 6 to 44-fold better in phosphate buffer, which led to the best production yield of (*S*)-equol ever reported. The titer has met the limitation up to ~1 g/L. To pull the titer up more, we tried loading more substrate or PVP. When two times higher load of daidzein (i.e. 2.54 g/L) or PVP-40k (i.e. 10% (w/v)) were used, they resulted poor yields, which might be caused by substrate precipitation and some negative effects by the viscosity increase of the reaction

mixture, respectively (data not shown). Actually, PVP seems to have negative impact on the isoflavone bioconversion compared to PEG or PVA, when their conversion efficiency was normalized by solubility increase (**Fig. 4.6**). However, its outstanding isoflavone-solubilizing character makes it the most promising reaction supplement among other HPs. Finally, we suggest that ~2 g/L of daidzein is the maximum capacity in the whole-cell biocatalytic reaction system with serial daidzein feed. The solubility of daidzein in the optimized reaction solution (i.e. 5% (w/v) PVP-40k and 5% (v/v) DMSO) is 135.4 mg/L according to Fig. 2. But the loaded daidzein in the optimized reaction was almost 15-fold (i.e. 2 g/L) of its original solubility. However, the excessive daidzein did not aggregate or precipitate, but it was well dispersed in the whole reaction solution. This means that not only substrate solubility, but dispersion of substrate also plays an important role in bioconversion yield in HP added reaction. And the HPs appear to have a positive effect on the isoflavone dispersion, as well.

The mechanism of the solubility increase by PVP could be understood by its adsorption character toward phenolic compounds. PVP easily adsorbs phenolic chemicals via hydrogen (H)-bonding (Loomis and Battaile 1966). The characteristics as a strong H-acceptor rather than a H-donor make PVP effective in adsorbing polyphenols, enabling it to be an outstanding supplement over other water-soluble polymers (**Fig. 4.1B and C**).

Because PVP works as an H-acceptor for the hydroxyl groups of polyphenols, the strong hydrogen bonding interactions and high water-solubility of PVP makes general enhancement in solubility of polyphenols in aqueous solution as

we showed in Fig. 2. Actually, other previous studies on using HPs to overcome encountered solubility problem of polyphenols are also found from literature, even though they did not systematically examine about that. For example, in the case of resveratrol, a lot of studies for its microbial production have been thoroughly performed and a recent paper well reviewed the previous results (Mei et al. 2015). Among them, the highest biotransformation titer of resveratrol, i.e. ~2.3 g/L, was achieved from 15 mM *p*-coumaric acid as a substrate by Mattheos A. G. Koffas group (Lim et al. 2011). The engineered *E. coli* strain yielded resveratrol with a high titer that was about 40 times of the solubility. And the initial substrate concentration also exceeded its aqueous solubility by 2.5 times. Although the researchers did not mention about the gap between the titer and solubilities, the successful production without solubility problems might be due to 10 g/L of PEG they added to the reaction medium, so that the added PEG might increase solubility of *p*-coumaric acid or resveratrol. And, it made that the solubility issue was not a major bottleneck in their study.

On the other hand, we performed computational approach to THDR protein structure and plausible substrate binding mode. Through alanine (or phenylalanine) substitution experiment, four residues including E50A, F99A, L252A and M419A were identified catalytically important. Because all the four mutants showed residual equol-forming activity at prolonged reaction time (i.e. 18 h, data not shown), they are not mechanismically essential, but may disturb catalytically relevant substrate orientation. For instance, diminished hydrophobic interaction raised by F99A and L252A, or disrupted hydrogen interaction between M419A and substrate could

explain the decrease in productivity. However, precise interpretation of the catalytic change requires exact structural information based on crystallography and biochemical evidences for unveiled catalytic mechanism of THDR.

In the case of 5-hydroxy-equol production, the high yield bioconversion was not solely achieved by HP addition, but conversion efficiency was improved when THDR P464A was introduced with PVP supplemented reaction solution. In order to understand the substitution effect on the yield increase, a homology model of THDR P464A was constructed and computational docking simulation was also performed for (3*S*,4*R*)-THG. However, no similar docking mode of (3*S*,4*R*)-THG was observed. Instead, possible steric hinderance by Pro464 was predicted at C5 in the binding of (3*S*,4*R*)-THD (**Fig. 4.13**). Therefore, it seems that P464A release the steric contacts between a hydroxyl group of genistein at C5 and Pro464 of THDR wild-type, which finally enabled g/L production of 5-hydroxy-equol.

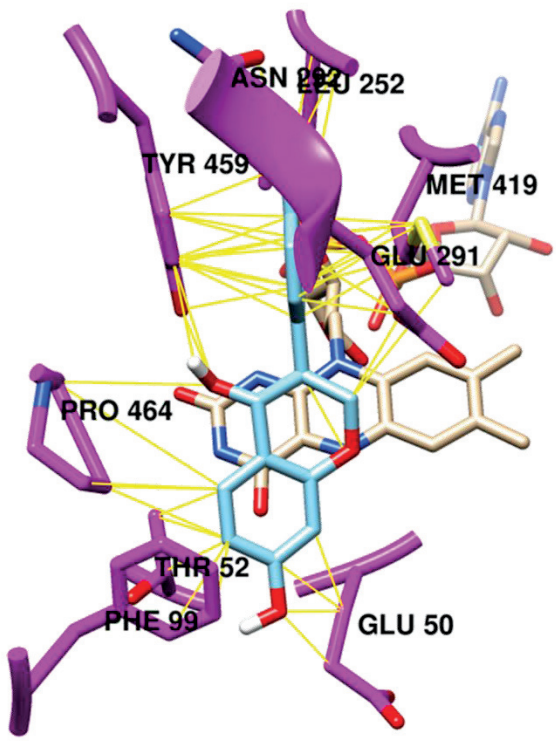

Figure 4.13 Possible contacts between THDR and (3*S*,4*R*)-THD.

Predicted contacts between THDR active site residues (magenta) and substrate (cyan) were shown with yellow line and Pro464 was recognized as the key residue hindering sterically for 5-OH of (3*S*,4*R*)-THG.

4.5 Conclusion

We found that substrate solubility was a critical bottleneck to enhance final biotransformation yield of (*S*)-equol. And, we elucidated that hydrophilic polymer (HP) is a good mean to increase solubility of polyphenols. Among the tested commercial HPs, PVP showed the utmost enhancement for the solubility of isoflavone, flavone, dihydrochalcone and stilbene. Through exploiting the great solubilizing characters of PVP for isoflavones and synergistic effect of a polar aprotic solvent (i.e. DMSO) on their solubility, a potent phytoestrogen (*S*)-equol was successfully synthesized up to 1.9 g/L from 3.8 g/L of daidzein in the fed-batch whole-cell biotransformation system, which is the highest titer ever reported. In addition, 1.3 g/L of 5-hydroxy-equol was also achieved by THDR engineering. One arising problem in the HP-added reaction process would be purification of highly produced products from the reaction medium. We extracted (*S*)-equol from diluted reaction solution using ethyl acetate, but residual PVP was detected in ^{1}H-NMR analysis (data not shown). One possible solution could be consecutive extractions with organic solvents that solubilize isoflavones, but not HPs. For example, ethers could be the candidates for PVP exclusion, since PVP is insoluble in ethers and some other organic solvents (Jirgensons 1952). Our study offers quantitative information of HPs to efficiently solubilize polyphenols and evidence of their applicability in whole-cell biocatalysis. At the same time, structural clues for catalytic activity of THDR and a catalytically enhanced variant was also provided in this study. This kind of solvent or protein engineering would be potent and economic ways to enhance the biotransformation yield of equol derivatives furthermore.

Chapter 5.

Regioselective *ortho*-hydroxylation of isoflavones and equols using engineered tyrosinase

5.1 Introduction

Ortho-dihydroxyisoflavones (ODIs) was firstly isolated in various fermented soy pastes such as Doenjang (from Korea), Miso (from Japan), and Tempeh (from Indonesia) (GYöRGY et al. 1964; Hirota et al. 2004; Park et al. 2008). The hydroxylation is mainly performed by several microorganisms during fermentation, and the hydroxylated isoflavones can function as beneficial components for human health with superior bioactivity to original isoflavones without fermentation. They were verified to show anti-inflammatory, anti-cancer and anti-oxidant activities through various biological mechanisms (Lee et al. 2011; Park et al. 2008). For example, 6-hydroxydaidzein and 8-hydroxydaidzein have been validated to show preventive effects on adipogenesis (anti-diabetic effect) and atopic dermatitis symptoms (skin anti-inflammatory effect), respectively (Kim et al. 2014; Seo et al. 2013b). In a recent study, 8-hydroxydaidzein has been also validated to show preventive effect on atherosclerosis via attenuating adhesion of THP-1 monocytes to human vein endothelial cells (Lee et al. 2018).

The *ortho*-dihydroxylation could be also found in equol metabolites converted by human liver metabolism (Rufer et al. 2006). Various *ortho*-hydroxyequols (OHEs) including 3'-hydroxyequol, 6-hydroxyequol and 8-hydroxyequol have been identified in the equol reaction by isolated human microsome. However, no biological functions of them have not been elucidated yet. To utilize the benefits of ODIs or possible effects of OHEs, sufficient production method should be secured with acceptable costs and

available large quantity. However, most isoflavone derivatives have restrictions in commercialization due to lack of natural sources, efficient bio-catalysts and production/purification methods. In this study, the *ortho*-dihydroxylation of isoflavones with regioselective control was thoroughly investigated using tyrosinase as a potent biocatalyst.

Tyrosinase is a type 3 copper protein that catalyzes monophenols into *o*-diphenols, and subsequently to *o*-quinones (Solomon et al. 1996). This oxygenation does not require any reducing cofactors such as NAD(P)H unlike most oxygenases including cytochrome P450 oxidase and flavin-dependent monooxygenase (Hannemann et al. 2007; Huijbers et al. 2014). Instead, its unique enzyme mechanism mediated by incorporated di-copper ions enables substrate to be oxidized by molecular oxygen directly (**Fig. 5.1**). Two copper ions are coordinated by six conserved histidine residues in the tyrosinase's active site. The di-copper-6-His complex has high affinity toward molecular oxygen, then easily binds it, forming [Cu^{II}-O_2^{2-}-Cu^{II}] complex, which is denoted as an '*oxy*-tyrosinase'. *oxy*-tyrosinase oxidizes both monophenols (cresolase activity) or diphenols (catecholase activity) (**Fig. 5.1**). In the cresolase cycle, one monophenol is oxidized into an *o*-diphenol and subsequently to an *o*-quinone, regenerating *deoxy*-tyrosinase. Otherwise, the substrate of both *oxy*-tyrosinase and *met*-tyrosinase is only diphenolic compounds in the catecholase cycle. During the subsequent oxidation, two individual catechols are converted into quinones which are spontaneously oxidized to quinone polymerized products and finally into dark pigment, melanin. Since most tyrosinases show a

higher catalytic activity to *o*-diphenols than monophenols, the catecholase cycle proceeds more favorable over the cresolase cycle.

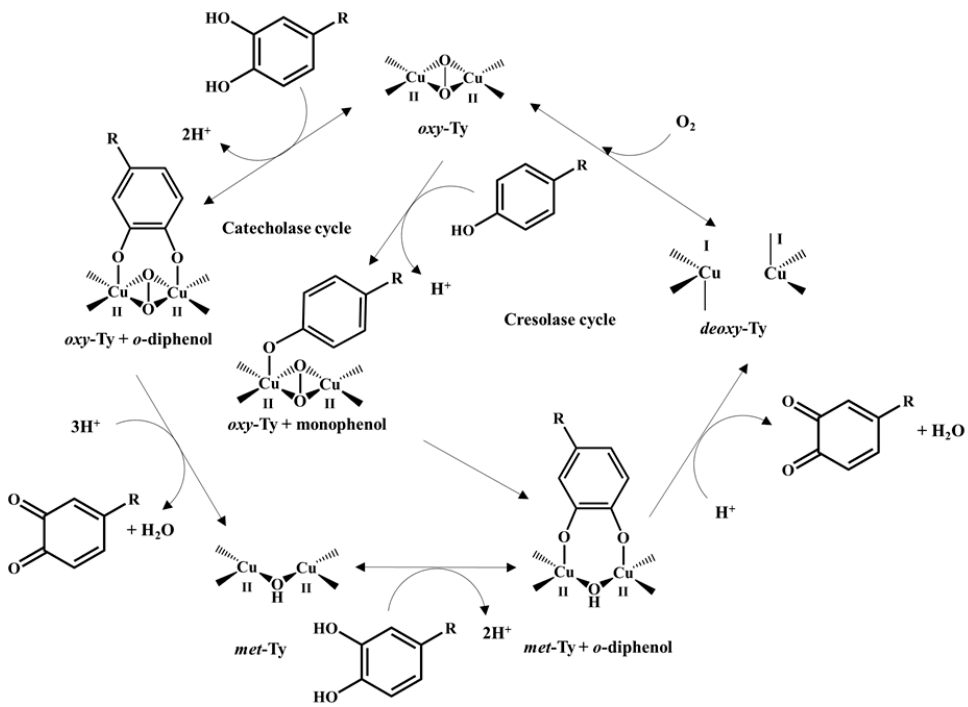

Figure 5.1 Catalytic cycle of tyrosinase.

The oxidation of monophenol and *o*-diphenol by Ty was represented with oxidation state of copper ions (Halaouli et al. 2006; Solomon et al. 1996).

In this study, we performed circular permutation (CP) protein engineering on a well-characterized bacterial tyrosinase from *Bacillus megaterium* (*Bm*Ty) to screen any mutants with broadened substrate specificity and high specific activity to polyphenolic substrate including isoflavones. CP is the protein engineering technique that covalently links a protein's native termini and inserts new artificial termini elsewhere in the polypeptide sequence. Several studies applied the method to some functional proteins or enzymes including flavin-dependent Old Yellow Enzyme (OYE1) (Daugherty et al. 2013), *Candida antarctica* lipase B (CALB) (Qian and Lutz 2005), green fluorescent protein (GFP) (Baird et al. 1999), and a shrimp luciferase (Hiblot et al. 2017). These studies generated structurally intact proteins and catalytically active enzyme variants with some showing interesting new functional features and improved activity. Most recently, Yu et al. also reported the successful CP of azurin, one of type 1 copper proteins with important roles in electron transfer in diverse biological systems (Yu et al. 2017). However, there has been no reports of circular permutation of tyrosinases such as *Bm*Ty which have a binuclear type 3 copper center located at the core of a four-helical bundle (Sendovski et al. 2011).

Herein, we investigated the impact of CP on substrate specificity, monophenolase and diphenolase activities, and kinetic characters of *Bm*Ty. Moreover, we explore novel applications of an engineered CP variant to synthesis of 3'-hydroxygenistein (orobol) in quantitative manner. Because wild-type and the mutant generated only 3'-hydroxylation, formononetin (4'-O-methyl-daidzein) was hydroxylated with other tyrosinase mutants engineered by site-directed mutagenesis

that endowed enhancement in regioselectivity. *Ortho*-hydroxyequols (OHEs) are also prepared using combinatorial reaction of oxidation based on tyrosinase and reduction by equol-producing bacteria.

5.2 Materials and Methods

5.2.1 Chemicals

All chemicals including L-tyrosine and 3,4-dihydroxy-L-phenylalanine (L-DOPA), gelatin (from porcine skin), daidzein, daidzin (daidzein 7-O-glycoside), genistein, glycitein, 3-methyl-2-benzothiazolone hydrazone (MBTH) hydrate and unmentioned chemicals were purchased from Sigma Aldrich (Yongin, Korea). (*S*)-equol was purchased from Cayman Chemical (Ann Arbor, MI), formononetin was purchased from Samjung Trading Co., Ltd (Korea), and 3'-hydroxydaidzein, 6-hydroxydaidzein and 8-hydroxydaidzein were obtained from the previous study (Choi et al. 2009).

5.2.2 Construction of CP library

In order to construct tyrosinase CP variants, the previous developed PCR method was used (Fischereder et al. 2014). Previous constructed tyrosinase (originated from *Bacillus megaterium,* ATCC 10778) genes cloned in pET28a was used for a PCR template (Lee et al. 2016b). In brief, the truncated tyrosinase (4Lys to 289Glu) gene was linearly duplicated in pRSFduet-1 vector with a linker (-ACTAGTGGC-) using the following primers, forward: 5'-GGCCACTAGTGGCAAGTACAGAGTTAG AAAAAACG-3' and reverse: 5'-GGCCACTAGTTTCTATATCGTATACG-3'. The constructed plasmid was used as a template for construction of each CP variants with respective primers (**Table 5.1**). Each construction of CP variant was verified with DNA sequencing. The nine loop regions in the tyrosinase protein structure

(PDB ID: 3nm8) were identified and visualized by UCSF Chimera (http://www.rbvi.ucsf.edu/chimera).

Table 5.1 Used primers for construction of CP variants.

Position	CP variants	Primers
Truncated WT (4Lys ~ 289Glu)	tWT	for: 5'-GCCCCATGGGCAAGTACAGAGTTAGAAAAAAC -3' rev: 5'-CGCGAGCTCTTATTCTATATCGTATACGTAC -3'
Loop1 N-terminus	cp(F48)	for: 5'-GCCCCATGGGCTTTCATACTCCTCCGGGC -3' rev: 5'-CGCGAGCTCTTATTTACCTGCTGCACCATG -3'
Loop1 C-terminus	cp(S63)	for: 5'-GCCCCATGGGCTCTGCTTTTTTACCGTGG -3' rev: 5'-CGCGAGCTCTTAACTCATATGTGCTGCATTTC -3'
Loop2 N-terminus	cp(N84)	for: 5'-GCCCCATGGGCAATCCAGAAGTAACCCTTC -3' rev: 5'-CGCGAGCTCTTAGATTGACTGAAGGTCACG -3'
Loop2 C-terminus	cp(E93)	for: 5'-GCCCCATGGGCGAATGGGAAACGGACGCAC -3' rev: 5'-CGCGAGCTCTTACCAATAAGGAAGGGTTAC -3'
Loop3 N-terminus	cp(A98)	for: 5'-GCCCCATGGGCGCACAGATGCAGGATCCC -3' rev: 5'-CGCGAGCTCTTAGTCCGTTTCCCATTCCC -3'
Loop3 C-terminus	cp(D102)	for: 5'-GCCCCATGGGCGATCCCTCACAATCAC -3' rev: 5'-CGCGAGCTCTTACTGCATCTGTGCGTCCG -3'
Loop4 N-terminus	cp(S110)	for: 5'-GCCCCATGGGCAGTGCAGATTTTATGGG -3' rev: 5'-CGCGAGCTCTTACCAAATTTGTGATTGTG -3'
Loop4 C-terminus	cp(N119)	for: 5'-GCCCCATGGGCAATCCCATAAAAGATTTTATC -3' rev: 5'-CGCGAGCTCTTATCCGTTTCCTCCCATAAAATC -3'
Loop5 N-terminus	cp(D123)	for: 5'-GCCCCATGGGCGATTTTATCGTCGATACC -3' rev: 5'-CGCGAGCTCTTATTTTATGGGATTTCCGTTTC -3'
Loop5 C-terminus	cp(T164)	for: 5'-GCCCCATGGGCACTCGAGATGATGTCCTC -3' rev: 5'-CGCGAGCTCTTAAGGGAGTGTAGGTGCCTC -3'
Loop6 N-terminus	cp(K173)	for: 5'-GCCCCATGGGCAAAATAACTCAGTATGATAC -3' rev: 5'-CGCGAGCTCTTATAAAGCATTGAGGACATC -3'
Loop6 C-terminus	cp(S189)	for: 5'-GCCCCATGGGCAGCTTTCGTAATCAGCTTG -3' rev: 5'-CGCGAGCTCTTAGTTTTGGCTGGTCATATC -3'
Loop7 N-terminus	cp(G196)	for: 5'-GCCCCATGGGCGGATTTATTAACGGGCCAC -3' rev: 5'-CGCGAGCTCTTATTCAAGCTGATTACGAAAG -3'
Loop7 C-terminus	cp(Q202)	for: 5'-GCCCCATGGGCCAGCTTCACAATCGCGTAC -3' rev: 5'-CGCGAGCTCTTATGGCCCGTTAATAAATCC -3'
Loop8 N-terminus	cp(V217)	for: 5'-GCCCCATGGGCGTTGTGCCTACTGCTCCG -3' rev: 5'-CGCGAGCTCTTAGCCCATCTGTCCGCCAAC -3'
Loop8 C-terminus	cp(T220)	for: 5'-GCCCCATGGGCACTGCTCCGAATGATCCTG -3' rev: 5'-CGCGAGCTCTTAAGGCACAACGCCCATCTG -3'
Loop9 N-terminus	cp(H245)	for: 5'-GCCCCATGGGCCATCGTAATCAAAACTATC -3' rev: 5'-CGCGAGCTCTTAAACAATTTGCCATACAGC -3'
Loop9 C-terminus	cp(P273)	for: 5'-GCCCCATGGGCCCTGAAGACGTTATG -3' rev: 5'-CGCGAGCTCTTAGGTTGTATTCCAAGGG -3'

5.2.3 Tyrosinase activity assay

The activity of purified enzymes or crude extract (10 μl) for L-tyrosine and L-DOPA was determined by dopachrome formation measurement at 475 nm (ε = 3600 M^{-1} cm^{-1}). The enzyme source was diluted in 50 mM Tris-HCl buffer (pH 8.0) with 10 μM $CuSO_4$, which was incubated for 10 min at 37 ºC before activity assay. Each reaction was started by addition and subsequent resuspension of 100 x concentrated substrate stock. For determination of kinetic parameters, 0.1 to 1.0 mM of substrate were introduced, then the obtained data was fitted to the Michaelis-Menten equation by non-linear regression analysis.

To investigate tyrosinase activity toward other bulkier substrates (i.e. daidzin, daidzein and gelatin), 3-methyl-2-benzothiazolone hydrazone (MBTH) hydrate, a quinone adductor, was supplemented by 0.22 mg/L concentration in reaction buffer (Winder and Harris 1991). The formation rates of quinone adducts by 100 nM of purified enzymes were observed at 505 nm, which was relatively compared with the activity of tWT that was normalized to 1.

5.2.4 Enzyme expression and purification

A single colony harboring a pET28a plasmid that contains each variant of tyrosinase genes was inoculated to 3 mL LB with kanamycin (50 μg/mL) and cultured overnight at 37 ºC. The overnight 1 mL cultured cells were transferred into 50 mL of LB with selection markers and cultured up to OD_{600} ~ 0.6-0.8. Then, tyrosinase variants were expressed by addition of 0.1 mM isopropyl-thio-β-D-galactopyranoside (IPTG) and

0.5 mM $CuSO_4$. After 18 h culture at 18 ºC, the tyrosinase expressing cells were harvested by centrifugation (4000 rpm, 10 min) and were subsequently washed with phosphate buffer saline (PBS) at 4 ºC. The prepared cells were resuspended in 50 mM Tris-HCl buffer (pH 8.0) containing 1 mM phenylmethylsulfonyl fluoride (PMSF), 1 mM dithiothreitol, 1 mM ethylenediaminetetraacetic acid (EDTA), 2.5 mM $MgCl_2$ and 0.1 mM $CaCl_2$, then disrupted by 5 min sonication (3 sec pulse, 8 sec pause) under the ice-cooled water. The cell lysates were centrifuged in 15,000 rpm for 30 min at 4 °C, and supernatant samples were prepared for enzyme purification or crude extracts assay. Ammonium sulfate precipitation (30 to 50% (w/v)) and subsequent Mono Q™ 5/50 GL (GE Healthcare Life sciences, Seoul, Korea) anion exchange chromatography were exploited for purification of the selected CP variants. Or for biocatalysis experiments, 6xHis tag was introduced at the C-terminal of tWT and cp48, respectively, and they were purified using Ni-NTA agarose resin (Qiagen Korea Ltd., Seoul, Korea). If necessary, purified protein solution was dialyzed and concentrated by ultrafiltration (Amicon® Ultra-15, Merck Millipore, Ltd., Seoul, Korea). The final purity of tyrosinase variants was confirmed by SDS-PAGE analysis. The purified enzyme concentrations were determined by Bradford assay (Bradford 1976).

For chaperone co-expression, pGro7 (Takara Bio Inc., Japan) that contains groES and groEL genes was co-transformed with the pET28a-tyrosinase vector and a colony was selected by kanamycin (50 μg/mL) + chloramphenicol (20 μg/mL) contained LB agar. GroEL/ES expression was induced by 0.1 mM of L-arabinose addition in the 50 mL culture.

5.2.5 *Ortho*-hydroxylation using tyrosinase variants

The biocatalysis basically followed the method previously set-up which exploited borate-catechol chelation and reducing agents for preventing over-oxidation of desired products (Lee et al. 2016b). In this experiment, 0.5 μM of purified tWT and cp48 tyrosinase performed biocatalysis converting 4 mg of genistein under 0.5 M borate buffer (pH 9.0) containing 10% DMSO, 10 μM of $CuSO_4$ and 100 mM of L-ascorbic acid. For the hydroxylation of formononetin and (*S*)-equol, crude cell extracts were used as enzyme sources with appropriate amounts. Reaction samples were prepared by mixing with 1 N HCl and extracted by ethyl acetate, which subsequently were evaporated and redissolved into methanol for HPLC analysis. Analysis condition of HPLC followed the previously mentioned (Lee et al. 2016b). Orobol standard curve, ^{1}H-NMR and GC-MS data were also obtained from the previous study. cp48 showed same region-selectivity of tWT (i.e. 3'-hydroxylation).

5.2.6 Computational analysis and site-directed mutagenesis

The computational docking simulation and site-directed mutagenesis of tyrosinase followed the descripted methods in **Chapter 4.3.4** and **4.3.5**, respectively. An online-uploaded tyrosinase structure (PDB ID: 3nm8) was used for docking simulation and structural interpretation of functional circular permutants. Energy-optimized 3D molecular structures of formononetin or (3*S*)-equol were generated using ChemOffice™ Chem3D (PerkinElmer Inc.). The primers used for site-directed mutagenesis were listed in **Table 5.2**.

Table 5.2 Primers used for random mutation of *Bm*Ty at R209 and V218.

Primer	Primer sequences (5' to 3')
R209_ndtF	TCGCGTACAC**NDT**TGGGTTGGCGGAC
R209_ndtR	GCCAACCCA**AHN**GTGTACGCGATTGTG
V218_ndtF	GATGGGCGTT**NDT**CCTACTGCTCCGAATG
V218_ndtR	GAGCAGTAGG**AHN**AACGCCCATCTGTC

N = A, T, G, C

D = A, T, G

H = A, T, C

5.2.7 Whole-cell biotransformation

The previously developed *E. coli* strain (tDDDT-WT) expressing four equol forming enzymes (DZNR, DDRC, DHDR and THDR) was used as a whole cell biocatalyst for production of *ortho*-hydroxyequols (OHEs) from 0.5 mM *ortho*-dihydroxyisoflavones (ODIs). The biotransformation and analysis protocol followed the abovementioned method in **Chapter 2.3.4**. The reaction products were identified with following HPLC and GC-MS analysis.

For the reaction of whole cells expressing cytochrome P450 (CYP102D1 F96V or CYP102G4)) and HpaBC, the baffled flasks containing the whole cells (OD_{600} = 10), buffer (0.1M KPB, pH 7), carbon sources (2% (w/v) glucose and 1% (v/v) glycerol) were agitated in a shaker at 37ºC by 200 rpm. All the recombinant strains were obtained from the previous studies (Choi et al. 2015; Kim et al. 2018a).

5.3 Results and Discussion

5.3.1 Construction of smart CP library of *Bm*Ty

*Bm*Ty has several advantages as a target protein for circular permutation (CP). The microbial tyrosinase has a close distance (ca. 12Å) between its N and C termini (PDB ID: 3nm8) (Sendovski et al. 2011), which could be further reduced to 4.5Å by removing 4 and 5 amino acids from its N and C termini, respectively, generating truncated wild-type (tWT). The shortened distance between the native termini could be easily bridged by an artificial flexible linker composed of three amino acids (—Thr-Ser-Gly—) to generate functional CP variants in this study. Moreover, the native enzyme has high tolerance against a variety of organic solvents and high thermostability (Shuster and Fishman 2009). Because CP tended to destabilize protein scaffolds and prevent catalytically active folding in some cases (Qian et al. 2007; Zhang and Schachman 1996), the high stability and tolerance of *Bm*Ty against organic solvents could compensate the detrimental effects of CP by maintaining the native protein structure. These characters of *Bm*Ty were recognized to make this tyrosinase as a proper target for CP.

The maximum theoretical library size for CP variants of *Bm*Ty is about 300, the number of its total amino acids. In order to optimize library design and to increase the number of functional CP variants, our library generation was limited to flexible loop regions in the tyrosinase structure. In several previous studies, these regions were shown to be most amendable to CP (Daugherty et al. 2013; Li et al. 2016). Guided by the *Bm*Ty crystal structure, we therefore targeted each of the enzyme's

nine surface loops (**Fig. 5.2**). This strategy resulted in a total of 18 cp*Bm*Ty variants that were generated by using site-specific DNA primers in combination with PCR methods previously reported (Fischereder et al. 2014).

Among these 18 variants, seven library members (cp48, 63, 98, 102, 202, 220 and 245) showed catalytic activity toward L-tyrosine, L-3,4-dihydroxy-phenylalanine (DOPA), and daidzein (**Fig. 5.3**). Variant cp273 exhibited only residual activity for daidzein (**Figure S1B**). The results demonstrated that the loop-specific design yielded ~40% of active cp*Bm*Ty variants, roughly twice the frequency of random designs (Daugherty et al. 2013; Li et al. 2016).

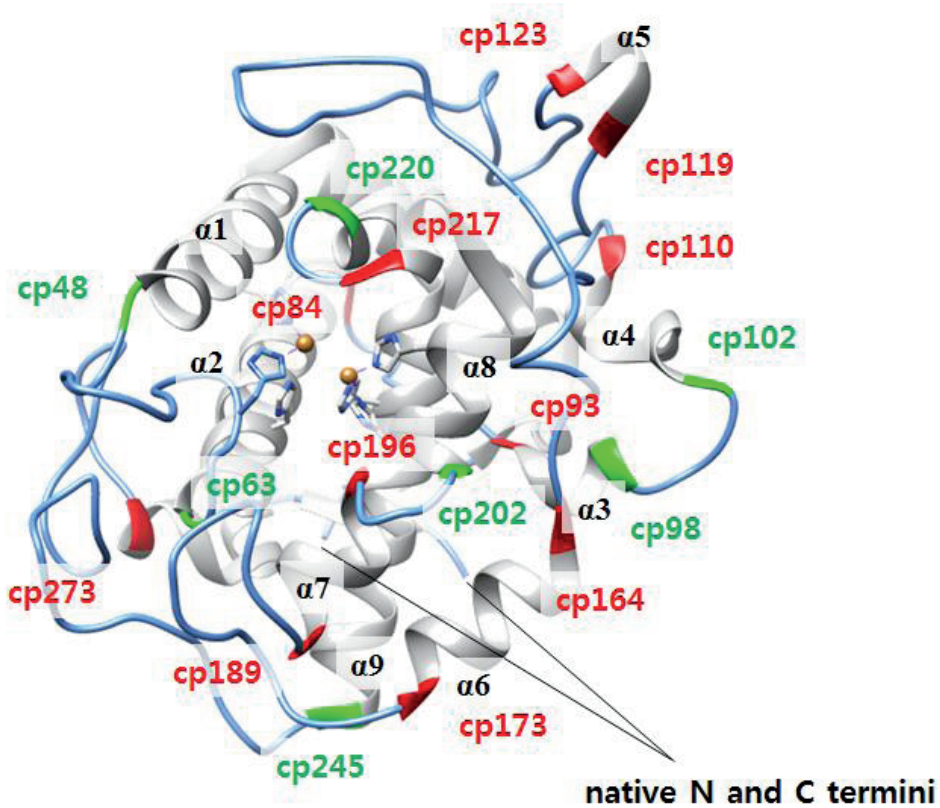

Figure 5.2 Protein crystal structure of wild-type *Bm*Ty.

The crystal structure (PDB ID: 3nm8) (Sendovski et al. 2011) is presented with indication of nine loops (blue), helical regions (gray) and 18 circular permuted points (green for active variants and red for inactive variants) at both terminal sites of each loop. Di-copper ions in the center of enzyme are shown as brown spheres coordinated by six histidines of tyrosinase.

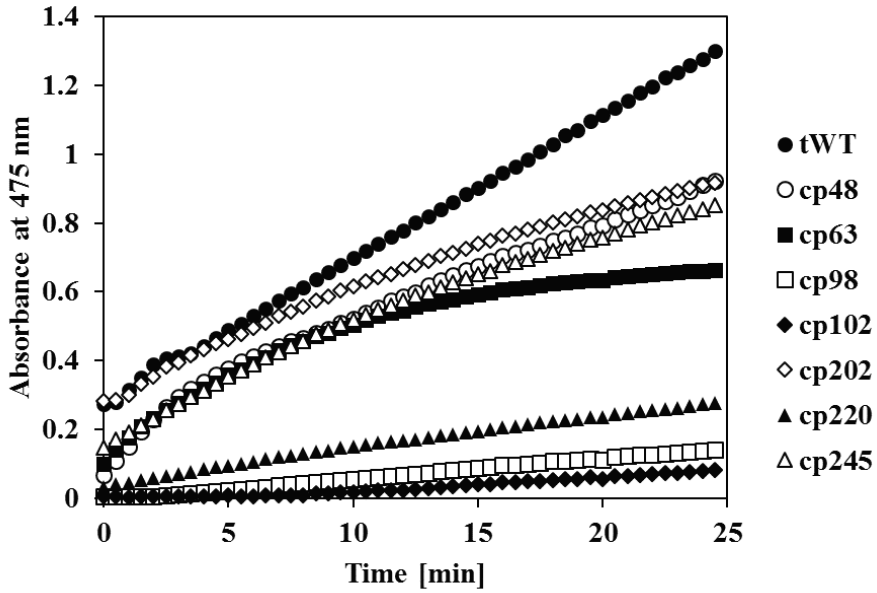
Absorbance at 475 nm
1.4
1.2
1
0.8
0.6
0.4
0.2
0
0
5
10
15
20
25
Time [min]
tWT
cp48
cp63
cp98
cp102
cp202
cp220
cp245

A.

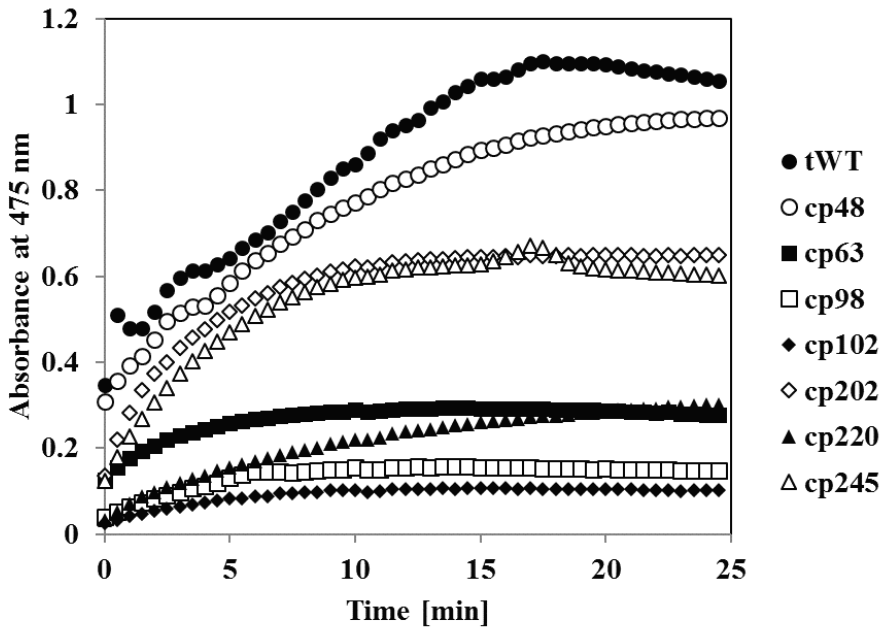
Absorbance at 475 nm
1.2
1
0.8
0.6
0.4
0.2
0
0
5
10
15
20
25
Time [min]
tWT
cp48
cp63
cp98
cp102
cp202
cp220
cp245

B.

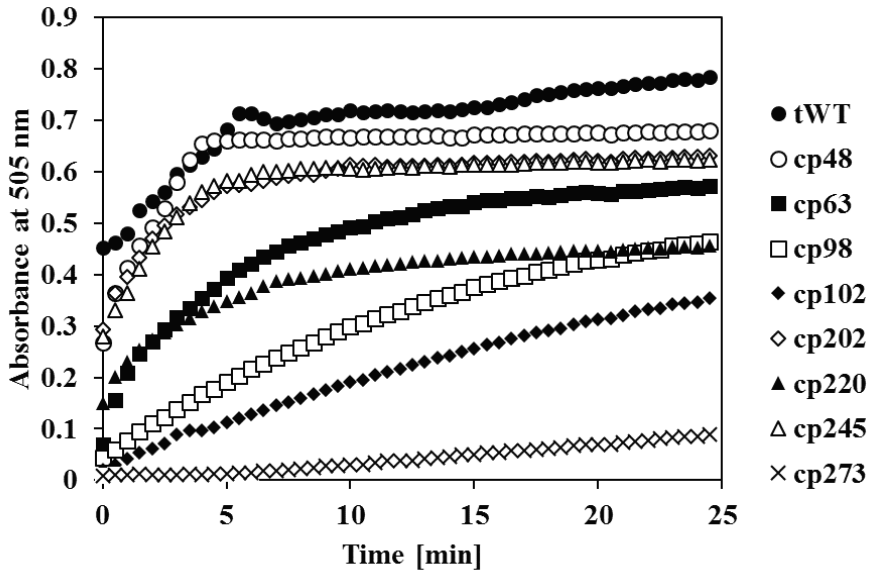

C.

Figure 5.3 Crude extract assay of rationally designed CP variant library.

tWT and 7 active CP variants were measured for (**A**) L-tyrosine (1 mM), (**B**) L-DOPA (1 mM) and (**C**) daidzein (200 μM). Dopachrome formation was monitored at 475 nm for A and B, and quinone adduct formation rate was recorded for C at 505 nm. Only tWT (control) and variants with detectable levels of activity are shown.

5.3.2 Chaperone-assisted expression of CP variants

In the case of *Bm*Ty, loop1 (cp48 and 63), loop3 (cp98 and 102), loop7 (cp202), loop8 (cp220) and loop9 (cp245) tolerated the termini relocation and produced catalytically active CP variants. These active variants were expressed at moderate levels with protein sizes similar to the truncated wild-type enzyme (**Fig. 5.4 and 5.5**). In contrast, the remaining CP variants were inactive primarily due to a lack of effective folding and structural stability (data not shown). To address the problem of protein folding, we investigated possible increases in solubility (and consequently enhanced enzyme activity) upon co-expression of native *E. coli* chaperones GroEL and GroES. These chaperones are known to raise expression levels of recombinant proteins by assisting in protein folding (Mitsuda and Iwasaki 2006; Nishihara et al. 1998). Upon co-transformation of the plasmid encoding GroEL/GroES (pGro7) into *E. coli* BL21 (DE3) strain, chaperone expression was induced with L-arabinose whereas tyrosinase expression was induced with IPTG. Strains coexpressing the chaperones showed increased amounts of soluble *Bm*Ty in crude cell extracts (**Fig. 5.4**). Significantly increased solubility of cp48, 202 and 245 in the chaperone-assisted system was also detected. In functional assays using crude cell extracts, tyrosinase activity increased about 2 to 4-fold in the presence of the chaperone system. Therefore, co-expression of GroEL/GroES is a very powerful and simple strategy to increase yields of CP variants by improving effective folding of soluble protein.

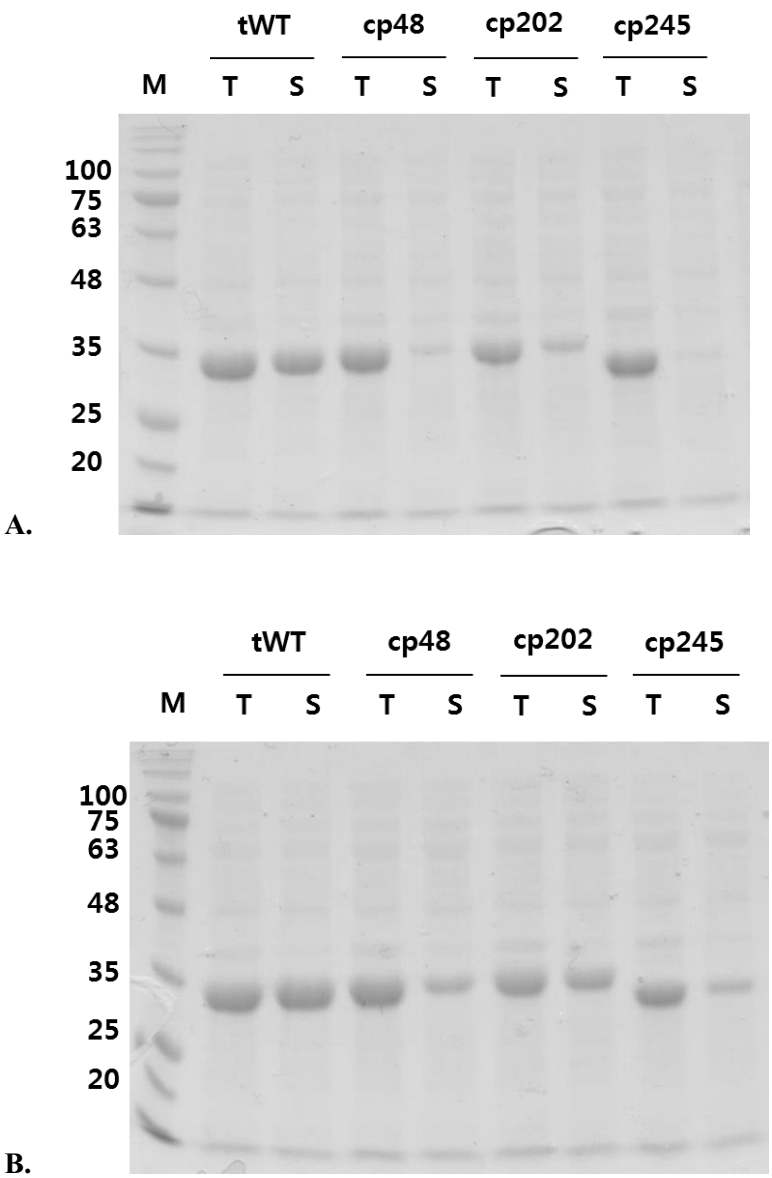

Figure 5.4 Chaperone coexpression effect in solubilization of CP tyrosinase.

SDS-PAGE results of four active CP variants and tWT (**A**) with or (**B**) without pGro7 (GroEL/ES) coexpression were shown.

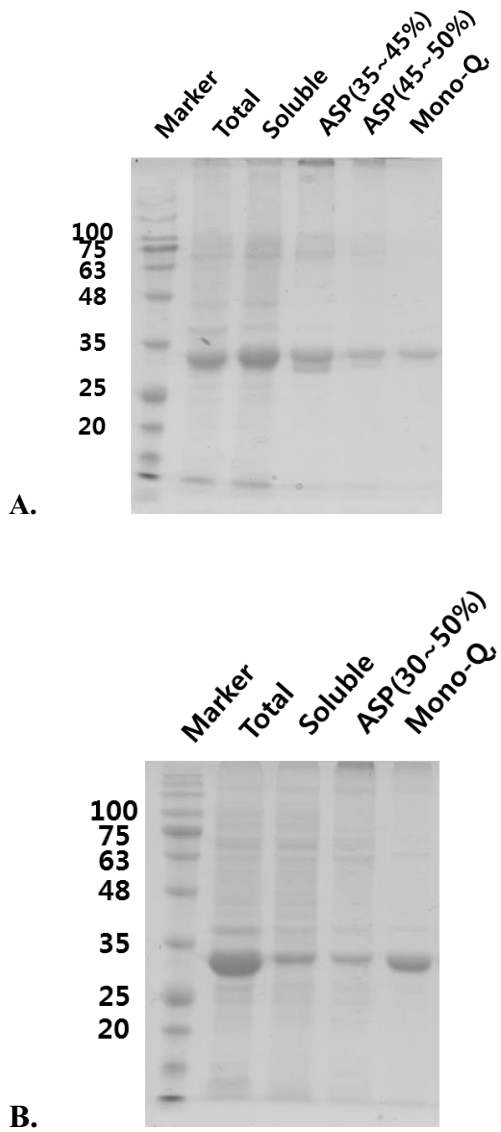

Figure 5.5 SDS-PAGE results of purification of (A) tWT and (B) cp48.

Two sequential purification techniques, ammonium sulfate precipitation and Mono-Q anion exchange chromatography, were carried out for getting pure tWT and CP variants, which were subsequently used to determine kinetic parameters and substrate specificity of the enzymes.

Further functional analysis of cp*Bm*Ty variants focused on cp48, cp63, cp202 and cp245 as they showed levels of activity comparable to tWT. Cp48 and cp63 are located in loop3 which connects the extended surface-exposed helix α1 (from Asn10 to Phe48) and core helix α2 (from Ser63 to Asn84). Loop 3 also accommodates one of the three CuA-coordinating histidines (His60). Given the functional importance of this metal-binding site, the close proximity of the new termini in cp48 and in particular cp63 is noteworthy as the increased conformational flexibility of termini regions does not seem to significantly impede on the catalytic activity of these two variants. A similar tolerance for CP was observed in cp202, the last amino acid residue in loop 7 which preceeds two adjacent CuB coordinating histidines (His204 and His208) in helix α7. To demonstrate the importance of termini location, a secondary library of CP variants including cp198, 200, 204 and 206 were prepared and examined for tyrosinase activity. In this follow-up study, only cp198, 200, and 202 had detectable catalytic activity (data not shown). These results validated our original library design focusing on loop regions and also underlined the critical functional role of the active site-forming core helix α7. The third region compatible to CP includes residues flanking helix α8. Helix α8 contains His231 which is part of the coordination sphere for CuB, yet tolerates protein backbone cleavage nearby. Two variants, cp220 at the end of loop 8 and cp245 at the beginning of loop 9, both expressed significant levels of monophenolase and diphenolase activity. In summary, we have identified a number of catalytically active CP variants by focusing on loop regions within *Bm*Ty. Interestingly, the new protein termini in these variants are all located adjacent to the secondary structures that contain

dinuclear copper-coordinating histidines. Consequently, CP could perturb substrate binding in the active site of *Bm*Ty, affecting substrate specificity and potentially resulting in activity for novel compounds.

5.3.3 Determination of kinetic characters and substrate specificity

In crude cell extract assays, the variation in protein expression levels among active CP variants complicates the assessment of their relative catalytic performances. Selected variants were therefore overexpressed and purified to homogeneity to determine their kinetic parameters and substrate specificity. Specifically, we chose four representative CP variants (cp48, 102, 202 and 245) and tWT which were purified by ammonium sulfate precipitation and Mono-Q anion exchange chromatography, followed by full kinetic characterization (**Fig. 5.5**).

Our kinetic studies of these variants and tWT concentrated on the evaluation of monophenolase and diphenolase activities (**Table 5.1**). Consistent with the previous reports, tWT showed a roughly 4-fold higher rate constant for L-DOPA over L-tyrosine (Shuster and Fishman 2009). At the same time, its K_M values for L-DOPA and L-tyrosine differ by 4 to 5-fold, resulting in similar catalytic efficiencies (k_{cat}/K_M) for monophenolase and diphenolase activity (M/D ratio: 1.1). Compared to tWT, the four CP variants showed lower catalytic efficiency for either substrate. In variants cp48, 102 and 245, activity for L-tyrosine oxidation fell below the detection limit while the catalytic efficiency for L-DOPA decreased 10 to 20-fold, the drops

attributed exclusively to lower turnover rates. These findings suggest that the three variants have become catechol oxidases instead of tyrosinases by eliminating their native monophenolase activity. However, the variants certainly retained a residual monophenolase activity, since they were actually determined to be active by a screening with L-tyrosine (**Fig. 5.3**). Therefore, the variants seemed to prefer the catecholase cyle rather than the cresolase cycle in Scheme 1. In contrast, cp202 shows the highest levels of activity among these variants and also retained both monophenolase and diphenolase activities. The effects of termini relocation did overproportionally affect the former activity, resulting in a shift of the M/D ratio to 0.32. Interestingly, the changes in catalytic efficiency for cp202 were primarly caused by dramatic increases in Michaelis binding constant (K_M).

A similar catalytic profile was observed in the tyrosinase-like protein NP_519622 which shows a clear preference for oxidizing *o*-diphenols with low monophenolase activity, behaving like a catechol oxidase (Hernández-Romero et al. 2006). Its unique preference for diphenolase activity was rationalized by controlled substrate access to the active site via a gate-keeping residue such as F261 in catechol oxidase. F261 was proposed to block the re-orientation of monophenols toward CuA, which is essential for its hydroxylation when the substrate is bound to CuB (Tepper et al. 2005). The corresponding residue in *Bm*Ty is V218 which was acutally confirmed to act as gate-keeper in a previous study (Goldfeder et al. 2013). Separately, mutations at position R209 in *Bm*Ty were suggested to modulate the enzyme's M/D ratio affecting substrate binding of L-DOPA (Ben-Yosef et al. 2010). Residues Q202 and R209 are both located on helix α7 which caps the active site. The

backbone cleavage at Q202 likely results in conformational changes that directly affect access to CuA. Moreover, the new termini are located near the two CuB-coordinating histidines on α7 (i.e. His204 and His208). Structural pertubations at these positions as a result of circular permutation are possible and interfere with the correct binding of *o*-diphenol to CuB, explaining the significant increase in the K_M value for L-DOPA (**Table 5.3**). In the other CP variants (cp48, 102, 245), the proximity of the new termini to CuA and multiple core helices could have a similar effect on that binding site, preventing proper positioning of monophenols in the CuA site and causing the dramatic loss of monophenolase activity. Further studies of these variants by X-ray crystallography will be necessary to better understand the structural consequences of CP on *Bm*Ty.

Table 5.3 Kinetic parameters of tWT and four active CP variants for L-tyrosine and L-DOPA.

	L-tyrosine			L-DOPA			
	k_{cat} s^{-1}	K_M μM	k_{cat}/K_M $M^{-1}\cdot s^{-1}$	k_{cat} s^{-1}	K_M μM	k_{cat}/K_M $M^{-1}\cdot s^{-1}$	Mono/Di†
tWT	3.56 ± 0.08	43.00 ± 9.25	8.28×10^4	14.50 ± 0.45	193.73 ± 9.15	7.49×10^4	1.11
cp48	n.d.	n.d.	n.d.	0.62 ± 0.01	174.07 ± 15.73	0.36×10^4	-
cp102	n.d.	n.d.	n.d.	1.72 ± 0.17	138.39 ± 41.08	1.24×10^4	
cp202	1.63 ± 0.25	331.95 ± 54.32	0.49×10^4	5.44 ± 0.19	350.89 ± 41.61	1.55×10^4	0.32
cp245	n.d.	n.d.	n.d.	1.24 ± 0.07	120.67 ± 21.02	1.03×10^4	-

n.d. not determined for no activity toward L-tyrosine.

† defined by k_{cat}/K_M of monophenolase activity / k_{cat}/K_M of diphenolase actvity

To determine whether CP induces any change in substrate specificity, L-tyrosine, L-DOPA, daidzein, daidzin (daidzein 7-O-glycoside), and porcine gelatin were tested against tWT and the four CP variants (**Fig. 5.6**). Overall, the substrate profile for tWT and cp202 showed similar levels of activity for all five substrates. Nevertheless, cp202 exhibited slightly increased activity toward daidzein, daidzin and gelatin; all bulkier substrates compared to L-tyrosine and L-DOPA. As discussed above, the other three CP variants (cp48, 102 and 245) did not hydroxylate L-tyrosine, yet showed catalytic conversion for L-DOPA and the bulkier substrates. Beyond this change, the substrate-activity profile for cp102 and cp245 largely reflected the parental enzyme albeit at lower activity overall. An interesting deviation of that activity profile is cp48 which showed an interesting 3 to 4-fold increase in catalytic activity for daidzein, daidzin and gelatin compared to tWT. In previous studies, *Bm*Ty was shown to possess broad substrate specificity including for *o*-diphenolic compounds, yet its catalytic activity was low for macromolecular substrates (Shuster and Fishman 2009). In contrast, the bacterial tyrosinase (MelC2) from *Streptomyces avermitilis* MA4680 exhibits very high activity for macromolecular substrates including gelatin and tyramine-conjugated hyaluronic acid. This activity was explained by the enzyme's active site surface exposure, enabling large substrates to easily reach the di-copper centers and other catalytic residues (Kim et al. 2018b). Given the location of the new protein termini in cp48 on the edge of loop1 (F48 to S63) that connects a core helix (α2) to the surface-surrounding long helix (α1), the active site defined by the di-copper complex and the surrounding residues should experience structural relaxation as a result of the

backbone cleavage. Similar effects were reported in a previous CP study of a lipase (Qian and Lutz 2005). On the other hand, polyphenol-specific oxidation by cp48 without tyrosine hydroxylase activity closely resembles a plant polyphenol oxidase (PPO) isolated from snapdragon flowers (Nakayama et al. 2001). The chalcone specificity of that PPO was rationalized by its insufficient binding affinity for tyrosine or tyramine (Molitor et al. 2016), an effect that can explain the observed shift in the M/D ratio for cp48.

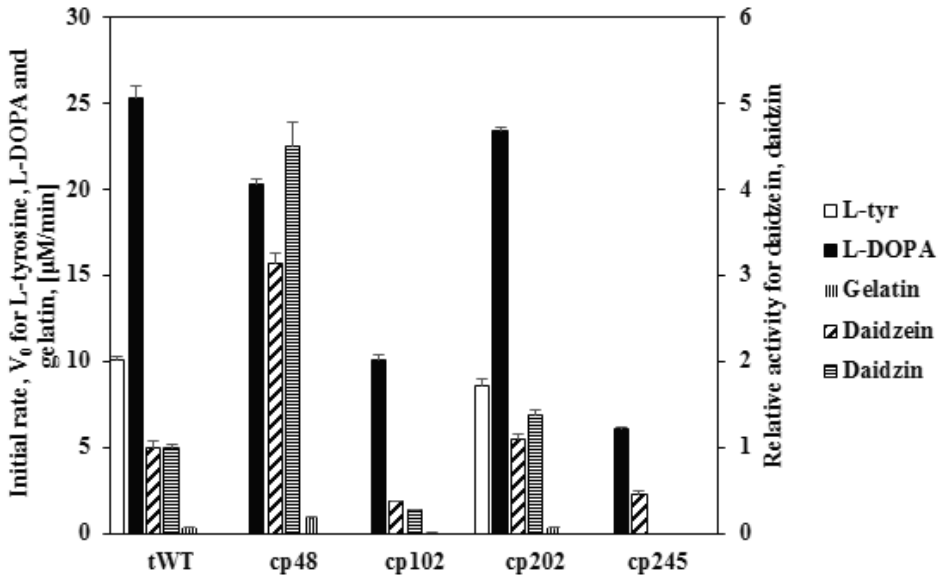

Figure 5.6 Substrate specificity of cp*Bm*Ty variants.

100 nM of purified tyrosinases were characterized by substrate specificity to L-tyrosine (1 mM), L-DOPA (1 mM), gelatin (0.3% (w/v)), daidzein (0.2 mM) and daidzin (0.2 mM). Initial conversion rate was determined by dopachrome formation rate (475 nm) for L-tyrosine and L-DOPA, whereas conversion rates for other substrates were measured at 505 nm at which MBTH-quinone adduct was detected. The tWT activities toward daidzein and daidzin were normalized to 1, respectively, and activity of variants was relatively recorded.

5.3.4 Quantitative preparation of 3'-hydroxygenistein (orobol) using cp48

To determine whether the novel tyrosinase variant is functional in preparative-scale biocatalysis, cp48 was tested as a polyphenol oxidase for the conversion of genistein (**Fig. 5.7**). Hydroxylation of genistein (2 g/L) was tested by enzyme variant cp48 or tWT (0.5 μM each) in 0.5 M borate buffer (pH 9.0) supplemented with 10% DMSO. Over the 5h, the cp48-catalyzed reaction orobol (3'-hydroxy-genistein) reached 75% completion, yielding 1.48 g/L orobol. In contrast, tWT only produced approximately 0.25 g/L (15% conversion) over the same time period. This result demonstrated that cp48 is a suitable preparative-scale biocatalyst to prepare valuable hydroxylated polyphenols in a quantitative manner.

Native *Bm*Ty is also known for its oxygenase activity in the presence of organic solvents including DMSO, methanol and ethanol (Shuster and Fishman 2009). Such solvent tolerance is unusual among this family of tyrosinases but offers great advantages in synthetic applications. As part of our preparative-scale experiments, we examined the performance of CP variants in a recently developed borate-catechol chelating system to prepare diverse versatile catechol-like polyphenols (Lee et al. 2016b). The results for cp48 clearly demonstrated that the enzyme variant retains its activity at up to 10% DMSO.

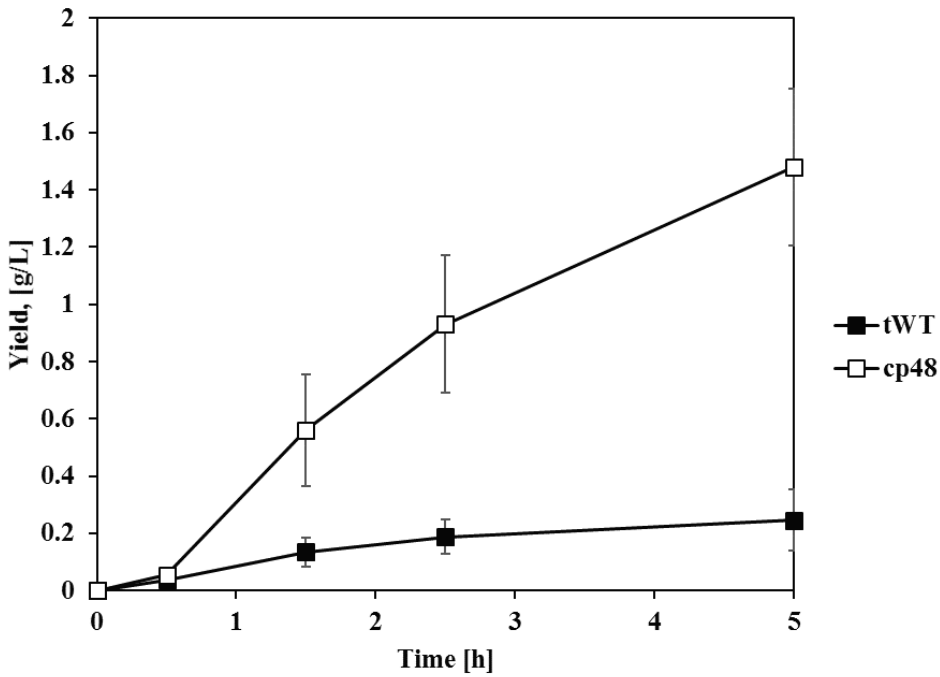

Figure 5.7 Biocatalysis of genistein to orobol by purified tWT and cp48.

The concentration of converted orobol was recorded along reaction time. 2 g/L (4 mg) of genistein was catalyzed by 0.5 μM each catalyst in 2 mL of 0.5 M borate buffer (pH 9.0) containing 10% DMSO, 10 μM of $CuSO_4$ and 100 mM of L-ascorbic acid. Reaction was performed at 37 ºC with a gentle shaking.

5.3.5 Regioselective hydroxylation of formononetin using tyrosinase mutants

B-ring specific *ortho*-hydroxylation of daidzein or genistein have been accomplished in the *Bm*Ty-borate oxido-chelating reaction system (**Fig. 5.7**) (Lee et al. 2016b). However, the tyrosinase was abandoned to produce different regiomeric ODIs rather than 3'-ODI. Its limited regioselectivity might be caused by inhibitory mechanism of the ODIs against the tyrosinase (Park et al. 2010). In fact, 6-ODI and 8-ODI are potent competitive and suicide tyrosinase inhibitors, respectively (Chang 2007; Chang et al. 2005). In addition, A-ring of isoflavone is more reluctant to hydroxylation than its B-ring owing to its structural bulkiness and higher pK_a value of the phenolic group at C7 over C4'. Therefore, the specific hydroxylation at A-ring of isoflavones using tyrosinase is a relatively unfavorable strategy.

To avoid the unfavorability and poor regioselectivity for A-ring hydroxylation, we took a detour in which a methoxy protection at daidzein C4' (using formononetin as a substrate) was adopted to completely prevent 3' hydroxylation by tyrosinase (**Fig. 5.8**). Actually, this idea has been simply verified in the previous PhD. thesis (Sang-Hyuk Lee, thesis, 2017). However, his study was focused on improvement of the tyrosinase activity toward formononetin, while regioselective hydroxylation was not fully investigation. Because the regioselective hydroxylation of formononetin was set as a goal in this study, reaction products by *Bm*Ty wild-type was firstly identified by HPLC and GC-MS analysis. Two new peaks were recognized as OHFs (**Fig. 5.9A**) and *peak1* and *2* were identified to 8-

ortho-hydroxyformononetin (8-OHF) and 6-*ortho*-hydroxyformononetin (6-OHF), respectively (**Fig. 5.9B and C**). Estimated product ratio (6-OHF/8-OHF) determined by standard 6 and 8-*ortho*-hydroxydaidzeins (OHDs) was about 4. Molecular docking simulation suggested that two binding poses of formononetin for *Bm*Ty (PDB ID: 3nm8) contribute the poor regioselectivity (**Fig. 5.10**). We attentioned to several residues interacting with formononetin in the active site. Then, two residues, Arg209 and Val218 were selected for consecutive semi-saturation mutagenesis using NDT codon. Interestingly, some variants at Arg209 represented significantly increased regioselective production manner either for 6-OHF (by R209G, ratio of 6/8 = 13.5) or for 8-OHF (by R209S, ratio of 6/8 = 0.8) (**Fig. 5.11A**). R209C also showed ratio of 6/8 even lower than R209S, but its poor conversion made us select R209S for 2nd round mutation. Subsequent saturation mutation at Val218 generated improved regioselectivity only for 8-OHF (by R209S/V218G, ratio of 6/8 = 0.16 and R209S/V218R, ratio of 6/8 = 0.12), but no further improvement was found for 6-OHF in the subsequent mutation of R209G (**Fig. 5.11B**).

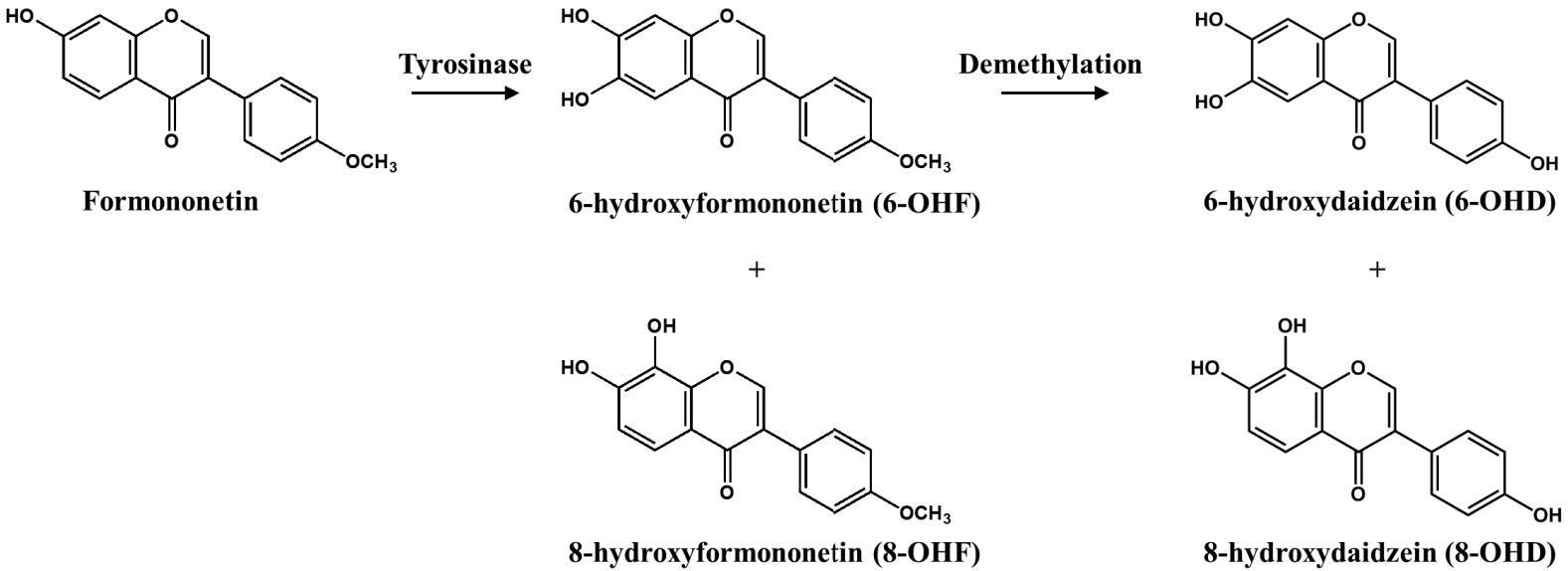

Figure 5.8 Strategy for A-ring specific hydroxylation of isoflavone.

Formononetin could be used for tyrosinase reaction only for the hydroxylation at A-ring, because 4'-O is protected by a methoxy group.

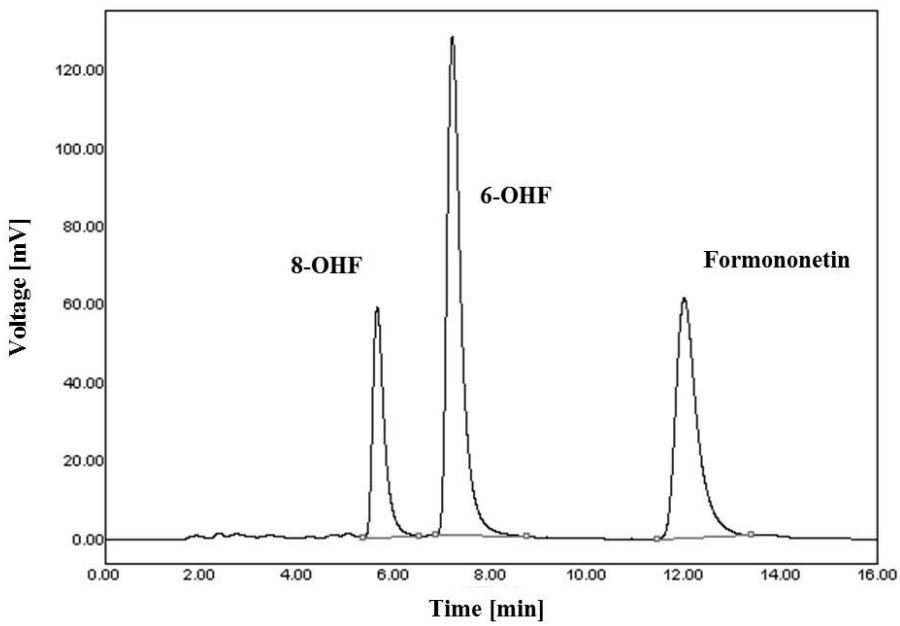

A.

Figure 5.9 Tyrosinase reaction profiles for formononetin.

Formononetin (0.5 mM) was given as a substrate of *Bm*Ty (crude cell extract; 2 mg/ml of protein) for 15 h at 37ºC. L-ascorbic acid (10 mM) and $CuSO_4$ (5 mM) were supplemented into 0.5 M boric acid buffer (pH 9.0). The reaction products were analyzed by (**A**) HPLC and (**B** and **C**) GC-MS.

B.

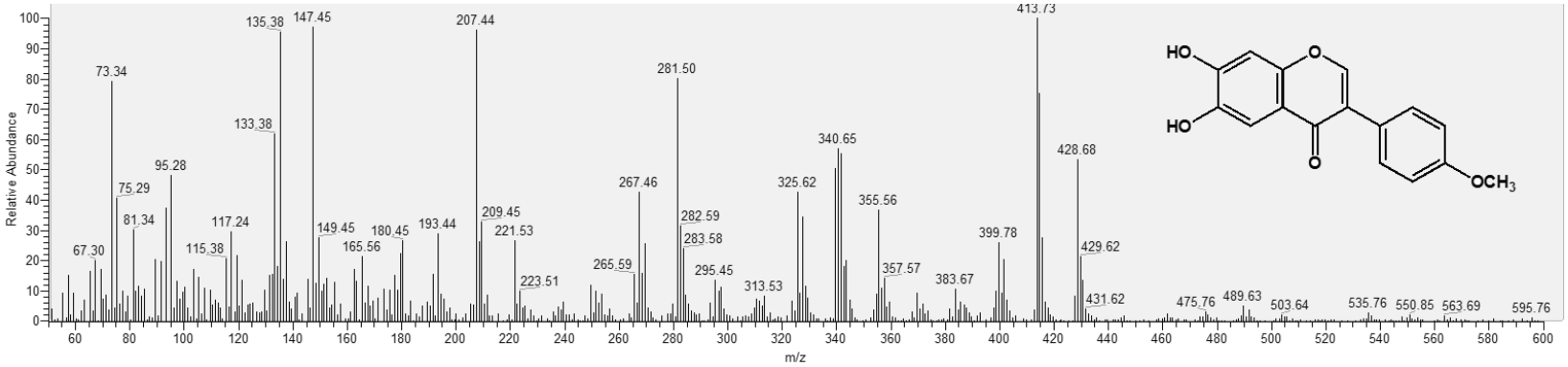
Relative Abundance
m/z
HO
HO
O
O
OCH3
135.38
147.45
207.44
73.34
281.50
133.38
340.65
428.68
95.28
267.46
325.62
75.29
355.56
81.34
209.45
117.24
149.45
180.45
193.44
221.53
399.78
67.30
115.38
165.56
265.59
282.59
283.58
429.62
357.57
295.45
223.51
313.53
383.67
431.62
475.76
489.63
503.64
535.76
550.85
563.69
595.76

C.

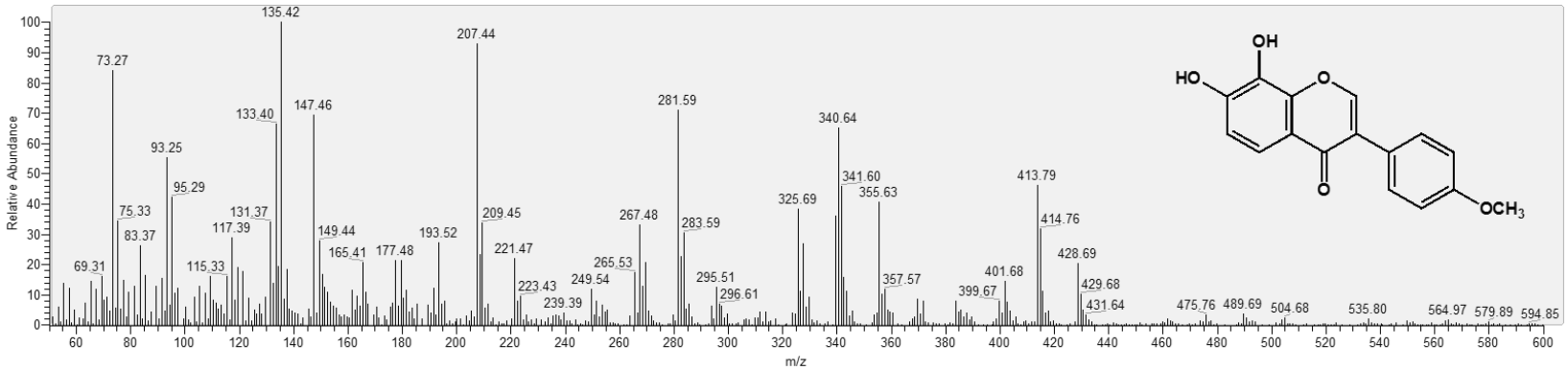
Relative Abundance
m/z
OH
HO
O
O
OCH3
135.42
207.44
73.27
281.59
133.40
147.46
340.64
93.25
341.60
413.79
95.29
355.63
325.69
75.33
131.37
209.45
267.48
414.76
83.37
117.39
149.44
193.52
283.59
428.69
165.41
177.48
221.47
401.68
69.31
115.33
265.53
357.57
429.68
249.54
223.43
295.51
399.67
239.39
296.61
431.64
475.76
489.69
504.68
535.80
564.97
579.89
594.85

A.

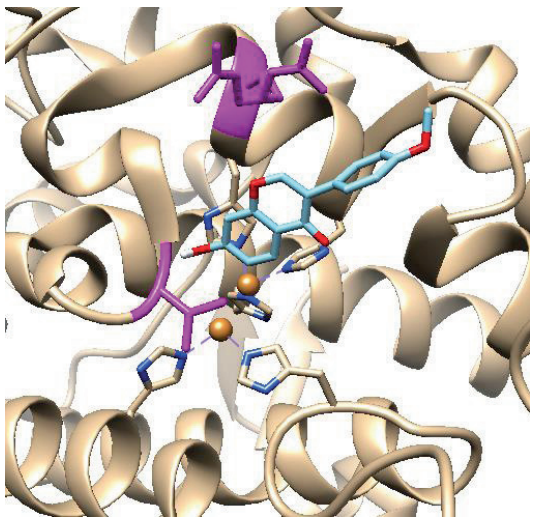

B.

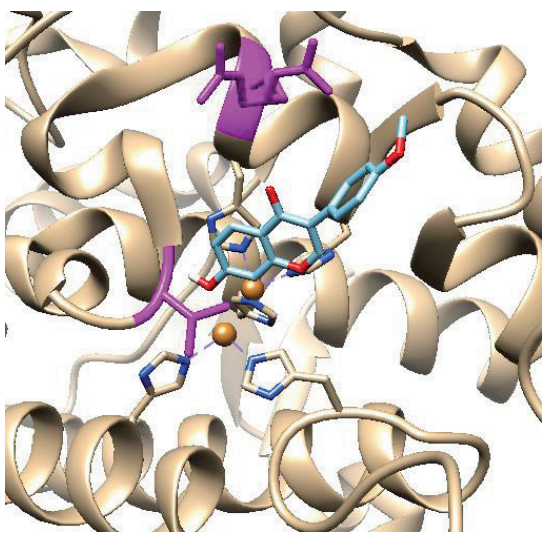

Figure 5.10 Predicted binding poses of formononetin to *Bm*Ty.

Formononetin was predicted to bind the active site of *Bm*Ty (PDB ID: 3nm8), and there were two energy-minimized binding poses: (**A**) 6-hydroxylation binding pose (and (**B**) 8-hydroxylation binding pose.

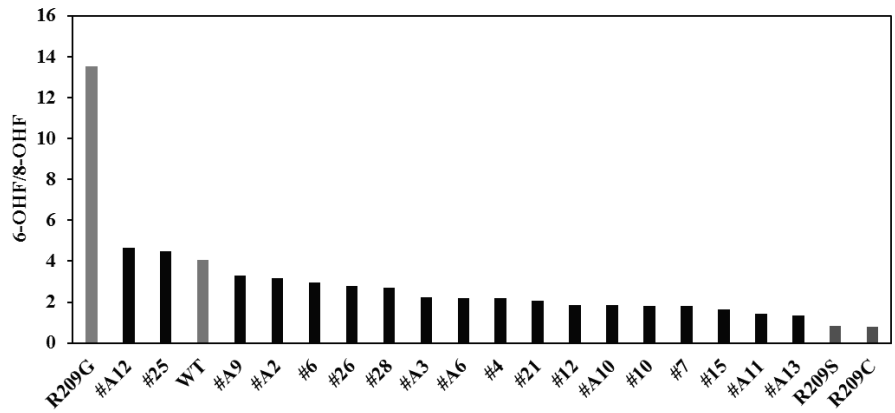

A.

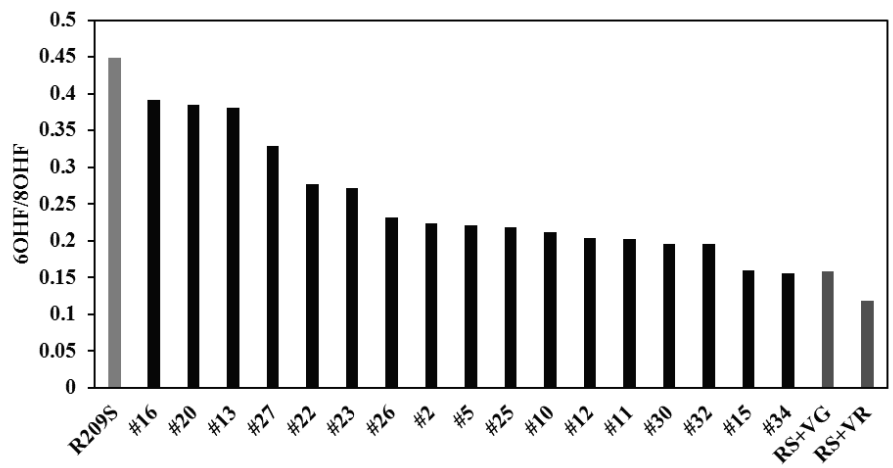

B.

Figure 5.11 Formononetin hydroxylation assay for saturated mutation library for Arg209 and Val218.

(**A**) 6-OHF/8-OHF ratio of single NDT saturated mutants at Arg209, and (**B**) NDT saturated mutants at Val218 with R209S. Selected variants with good regioselectivity were sequenced for identification of mutations.

The enhanced regioselectivity of *Bm*Ty variants was analyzed using homology models and docking simulation. Formononetin was predicted to bind to wild-type *Bm*Ty stably through cation-π interaction between Arg209 and isoflavone B-ring in either 6 or 8-hydroxylation binding pose (**Fig. 5.10**) (Caldwell and Kollman 1995). However, the same interactions were collapsed and a new proline-π interaction selectively stabilize 6-hydroxylation binding pose in R209G mutant (Zondlo 2012). Although any putative reasons to rationalize the enhanced regioselectivity of R209S/V218G toward 8-hydroxylation could not be found, certain other interactions definitely replaced the cation-π interaction, which finally reoriented formononetin binding favorably to 8-hydroxylation rather than 6-hydroxylation.

Finally, we selected two tyrosinase variants that had fine regioselectivity for the synthesis of OHF: R209G for 6-OHF and R209S/V218G for 8-OHF. For 8-OHF synthesis, R209S/V218G was selected as the more potent catalyst rather than R209S/V218R that showed poor conversion (data not shown). Then, each OHF was converted from formononetin with improved regioselectivity compared to wild-type *Bm*Ty (**Fig. 5.9A** and **5.12A**). Next, we moved to verify the possibility of enzymatic demethylation of OHF to synthesize our goal products, ODI. Because cytochrome P450 is one of the efficient O-demethylase and recently characterized CYP102G4 from *Streptomyces cattleya* has fine substrate specificity for bulky chemicals, the recombinant *E. coli* expressing CYP102G4 was exploited as a biocatalyst to demethylate 6-OHF, which actually produced 6-OHD (**Fig. 5.12B**) (Kim et al. 2018a). Even though, the catalytic efficiency was too low to be quantified, it is

meaningful result as the first report to prepare A-ring specific hydroxylated ODIs using tyrosinase and subsequent cytochrome P450. The future investigation on enhancing catalytic performance of the enzymes would enable massive production of beneficial ODIs with regioselective manner.

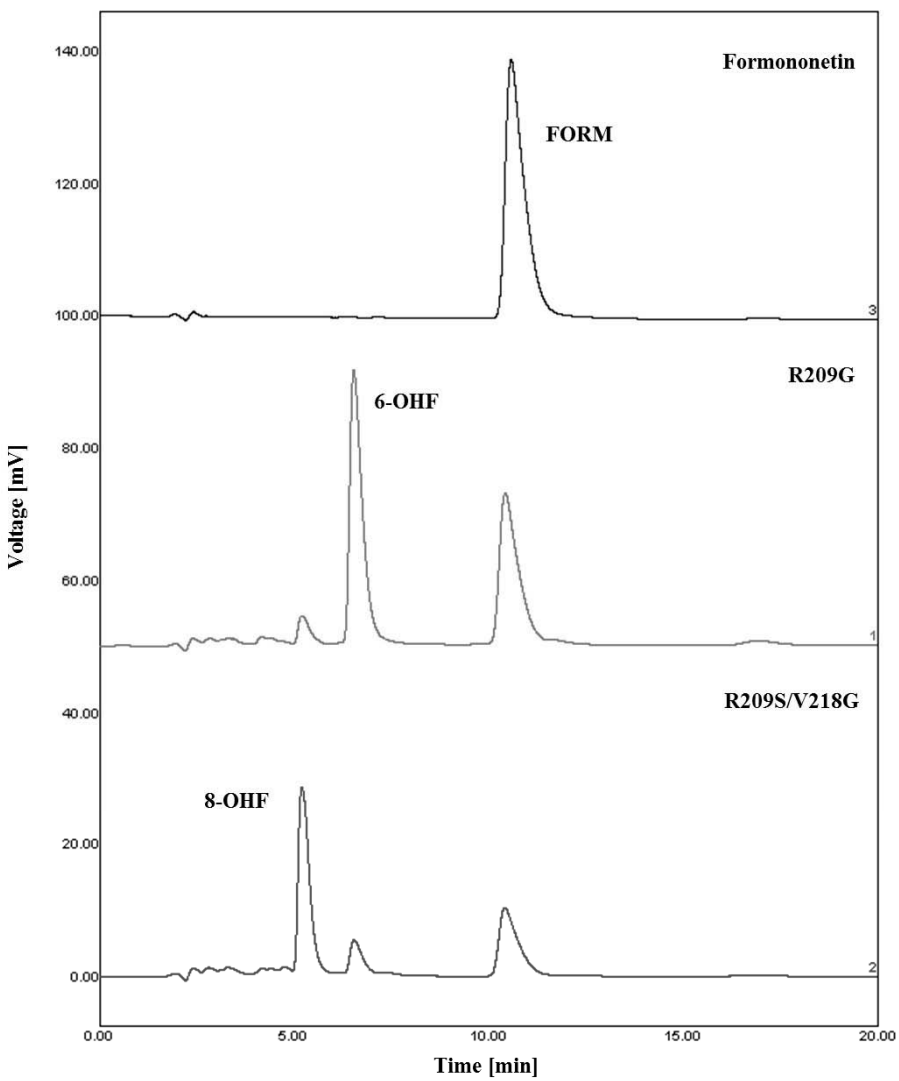

A.

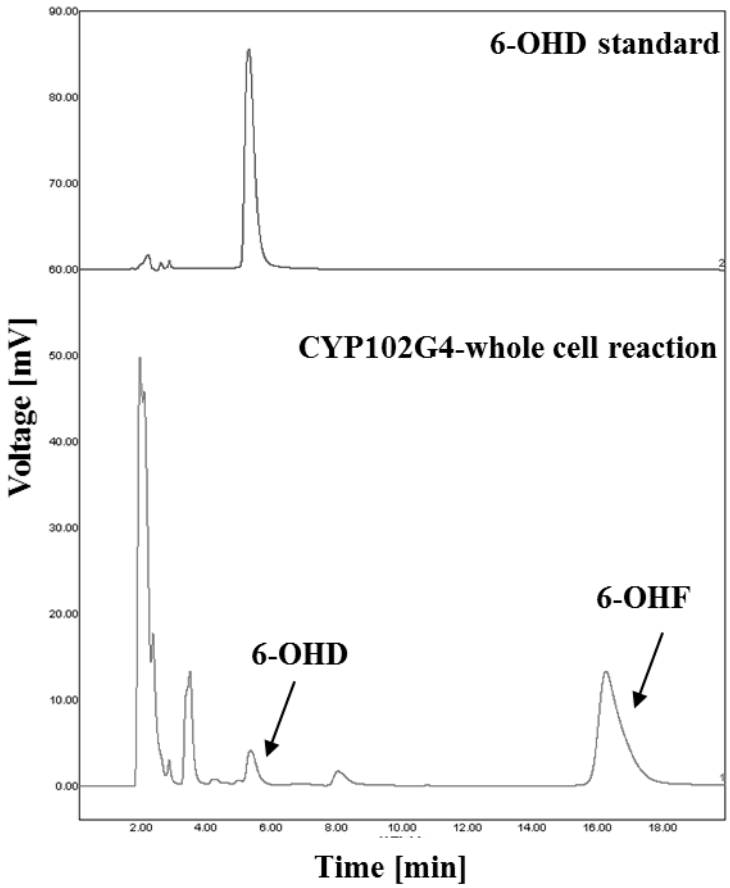

B.

Figure 5.12 Formononetin hydroxylation and demethylation using tyrosinases and CYP102G4.

(**A**) Formononetin was regioselectively hydroxylated into 6-OHF and 8-OHF by *Bm*Ty R209G and R209S/V218G variants, respectively. (**B**) Enzymatic O-demethylation of 6-OHF was confirmed by whole-cell *E. coli* expressing CYP102G4 (48 h, 37ºC).

-

5.3.6 Oxidoreductive biotransformation for regioselective preparation of *ortho*-hydroxyequols

Similar to prepare ODIs, *ortho*-hydroxyequols (OHEs) were recognized to be easily produced by exploiting hydroxylation activity of same bacterial tyrosinase. Practically, the OHE forming rate was achieved with the highest by tyrosinase among other monooxygenases including CYP102D1 (F96V) and HpaBC (**Fig. 5.13**). However, uncontrollable hydroxylation at multiple sites (i.e. mainly 3' and 6) prevented regioselective preparation of OHEs. Regioselective hydroxylation of (*S*)-equols at single site could not be achieved by site-saturation mutagenesis of *Bm*Ty at Arg209 and Val218 (data not shown). The highly reactive character of (*S*)-equol was rationalized by higher flexibility of its single-bonded C-ring than double-bonded C-ring of daidzein.

The regioselective hydroxylation of (*S*)-equol, instead, could be accomplished by change-over of isoflavone hydroxylation followed by microbial reductive pathway to equol derivatives. Indeed, versatile OHEs comprising 3'-OHE (>99%; conversion), 6-OHE (47%) and 8-OHE (81%) were synthesized from 0.5 mM of each OHD standard (**Fig. 5.14**). Although the conversion efficiency was low for 6-OHD, it could be replaced by efficient glycitein to 6-methoxy-equol conversion or subsequent demethylation (**Fig. 5.14D**). Because regioselective hydroxylation of isoflavones could be easily achieved by efficient biocatalysts previously reported (Chang et al. 2013; Lee et al. 2016b; Seo et al. 2013a), the consecutive oxido-reductive biotransformation is practically applicable strategy, expanding the

bioavailability of isoflavone derivatives. In addition, the practical preparation method would enable the nutritionists and pharmaceutical scientists to elucidate their beneficial biological functions.

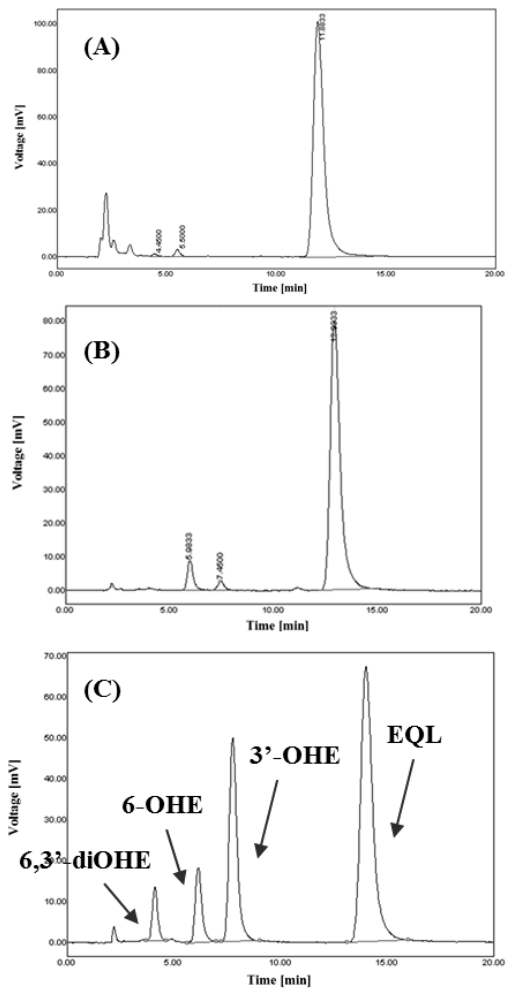

Figure 5.13 Hydroxylation of (*S*)-equol by various monooxygenases.

0.2 mM of (*S*)-equol was used as substrate for three monooxygenases: (**A**) whole cells expressing CYP102D1 (F96V), (**B**) whole cells expressing HpaBC and (**C**) crude cell extracts containing *Bm*Ty..

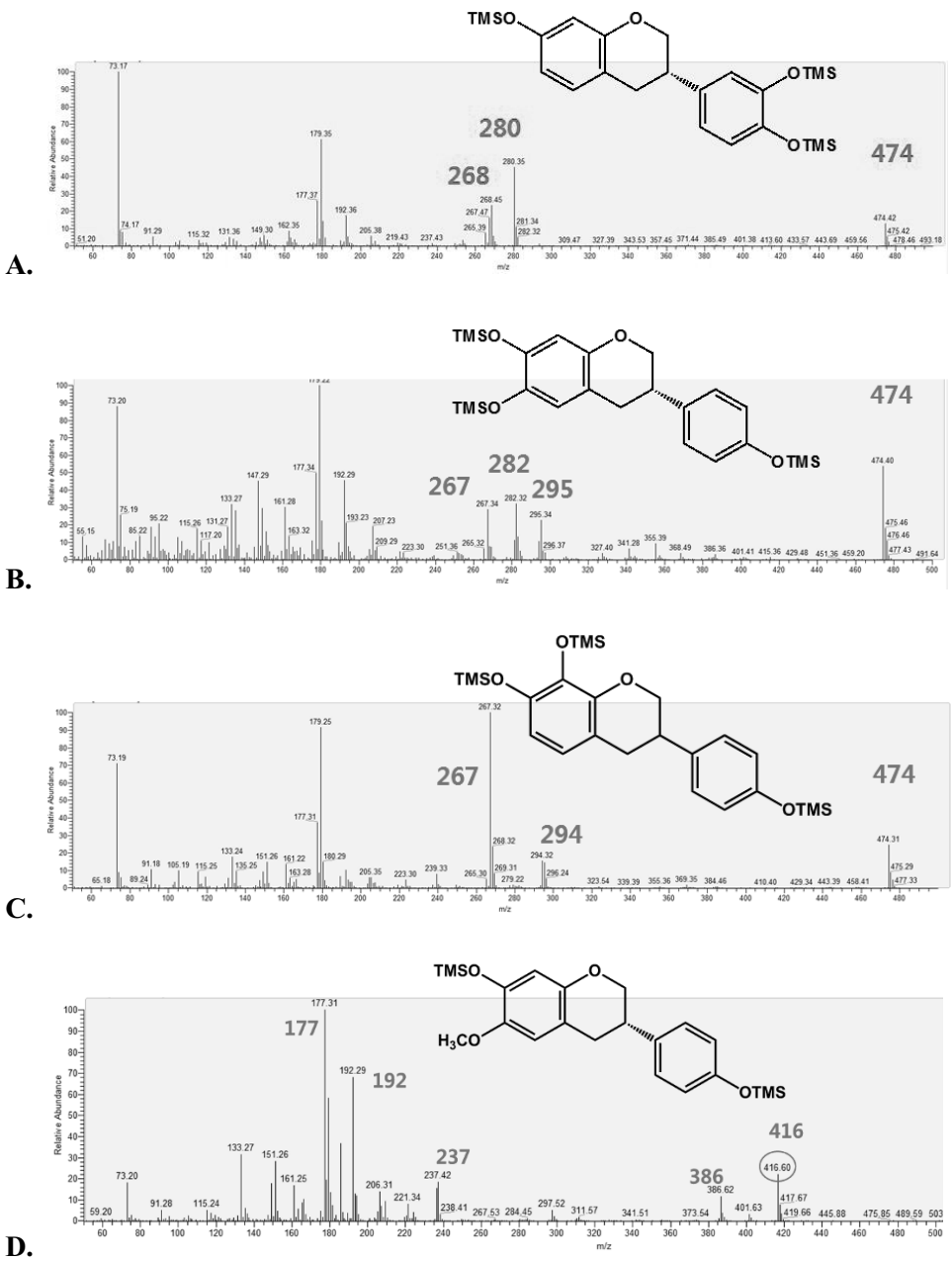

Figure 5.14 GC-MS spectra of biosynthesized OHEs and 6-methoxyequol.

All the reaction products were redissolved into ethyl acetate, then derivatized with N,O-bis(trimethylsilyl)trifluoroacetamide (BSTFA) before GC-MS analysis. (**A**) 3'-OHE, (**B**) 6-OHE, (**C**) 8-OHE and (**D**) 6-methoxyequol synthesized from glycitein.

5.4 Conclusion

In conclusion, the well-known bacterial tyrosinase *Bm*Ty was engineered using circular permutation and site-directed semi-saturation mutation. CP engineering generated several active variants, retaining correct protein folding and various levels of catalytic function. Among the active CP variants, cp48 was identified with enhanced activity for polyphenol substrates, which finally led to g scale production of 3'-OHG (orobol). To the best of our knowledge, this is the first study to apply CP on tyrosinase and to show the functional benefits of such engineering towards biocatalysts for the preparation of versatile polyphenols.

On the other hand, A-ring specific hydroxylated ODIs were also prepared using 4'-O protected substrate (formononetin) for tyrosinase reaction. Poor regioselectivity of wild-type was efficiently enhanced by sequential site-saturation mutagenesis at active site residues. Moreover, regioselective synthesis of OHEs could be achieved by consecutive *ortho*-hydroxylation of isoflavones followed by reductive pathway to equols. This study suggests that proper combination of engineered tyrosinases and the equol-producing whole cells provides a platform to prepare versatile ODIs and OHEs with fine regioselectivity.

Chapter 6.

Overall Conclusion and Further Suggestions

6.1 Production of equol derivatives using recombinant *E. coli*

Equol synthesis has been highly dependent on fermentation of naturally isolated gut bacteria and chemical methods. Because equol is mainly used as nutritional supplement and cosmetic ingredient, chemical synthesis of equol is legally refused. Biosynthetic method utilizing human gut bacteria, however, requires higher production cost by anaerobic fermentation process and low isoflavone solubility, which lead to long time culture and low purification yield per batch fermentation. These industrial problems have prevented the effective industrialization and commercialization of equol. In this study, recombinant *E. coli* harboring four heterologous equol producing enzymes has been developed for mass production of equol in aerobic process. And low solubility of isoflavone was overcome by introduction of biocompatible hydrophilic polymers. Serendipitously, all the equol producing enzymes were solubly expressed well under T7 promoter-IPTG induction system, even if *Slackia isoflavoniconvertens* (gram positive) and *E. coli* (gram negative) have different gram staining characters. The multi-expression of the enzymes was successfully achieved, which afforded daidzein to equol bioconversion up to 1 mM (~0.25 g/L) yield. The advantages of the recombinant systems are comprised of aerobic handling of the reaction process, rapid cell growth, and high equol production activities that led to high productivities.

Next, enzyme engineering and isoflavone solubilizing biocompatible polymers were utilized to pull the production titers up to g/L scale. Since isoflavone solubility was too low in aqueous reaction condition, several commercial hydrophilic polymers were supplemented to enhance the mass transfer of substrate. The simple

strategy increased equol production up to 1.9 g/L, but the same engineering strategies did not enhance the bioconversion of genistein to 5-hydroxy-equol. In the case of 5-hydroxy-equol, tetrahydrodaidzein reductase (THDR) was recognized as a key enzyme determining selectivity of products and reaction rates. Then, enhanced THDR activity by a key mutation, P464A in THDR increased 5-hydroxy-equol production up to 1.3 g/L titer in 24 h in the PVP supplemented whole-cell biotransformation, while the strain harboring wild-type THDR showed only 0.4 g/L. Overall, the production studies provide general guideline for protein/whole-cells engineering and isoflavone solubilizing strategy to prepare equol derivatives with industrially applicable production level. The production enhancement was summarized in **Fig. 6.1**.

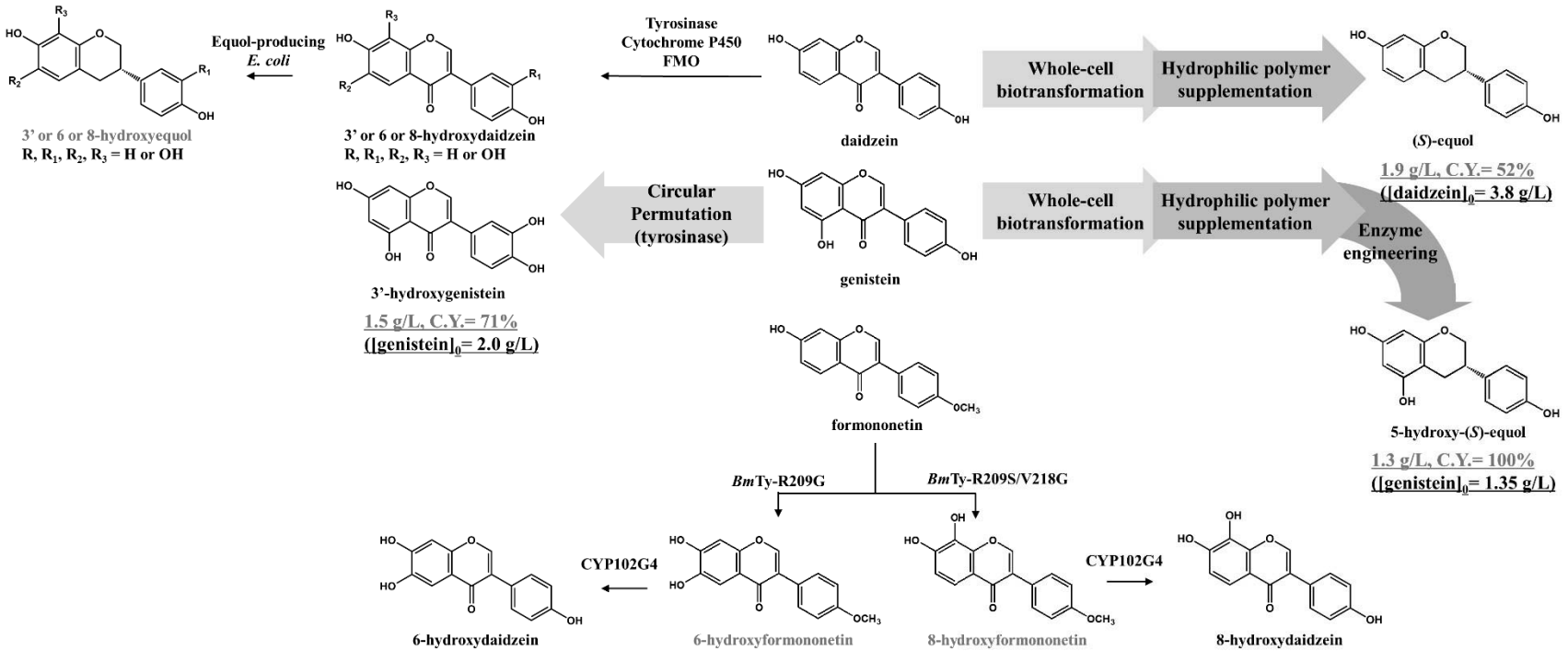

Figure 6.1 Overall biotransformation strategy and biocatalysts for preparation of ODIs and equols.

Isoflavone derivatives prepared in this thesis were summarized in the scheme with applied biotransformation strategy and biocatalysts. Significant titers of the isoflavone derivatives achieved in this studies and the novel synthesized chemicals were noted with red. (C.Y.= conversion yield)

6.2 Regioselective preparation of ODIs and OHEs using tyrosinase

Several bacterial tyrosinases have been already utilized to hydroxylate various polyphenols including isoflavones (Lee et al. 2012; Lee et al. 2015; Lee et al. 2016b). The biocatalyst enabled a dramatic breakthrough of 3'-ODI production efficiency up to g/L level. In Chapter 5 of this thesis, the bacterial tyrosinase was further engineered to overcome low polyphenol oxidation activity and poor regioselectivity for isoflavones. In order to solve the problems, two kinds of protein engineering method were exploited. First, circular permutation of a bacterial tyrosinase, *Bm*Ty enhanced polyphenol hydroxylation activity, which finally gave 1.5 g/L bioconversion of 3'-hydroxygenistein (orobol). Since circular permutation was generally introduced to increase specificity to bulkier substrates, the enhanced hydroxylation activity to polyphenols including isoflavones were expected and actually verified. On the other hand, the poor regioselectivity of the same bacterial tyrosinase for A-ring specific isoflavone hydroxylation could be overcome by iterative semi-saturation mutagenesis of amino acids in active site. Computational prediction of binding site guided a shortcut to obtain actually enhanced mutants with high regioselectivity, which indeed enabled quantitative production of 6- or 8-hydroxyformononetin. In addition, regioselective hydroxylation of equol is also firstly achieved using a novel strategy of the consecutive oxido-reductive biocatalytic system. This experimental achievement opens up the opportunity to explore their biological functions and practical utilization in cosmetic and pharmaceutical fields. Furthermore, combinatorial use of the equol producing

microbes and the engineered tyrosinases would give powerful catalytic platforms to prepare various isoflavone derivatives with oxidative or reductive modifications.

6.3 Further suggestion 1: Catalytic mechanism of tetrahydrodaidzein reductase

From the performed results above, THDR was verified as the key enzyme determining overall reaction rate. However, exact THDR catalytic mechanism has not been elucidated yet. Only, there are two speculations for the novel reduction activity. One is that the reduction includes a radical intermediate during the catalysis. The mechanism was firstly suggested by Kim *et al*., and they verified all the deuteriums on (3*S*,4*R*)-*trans*-THD-2,3,4-d_3 was conserved during the deoxygenation reaction, which excluded possible catalytic mechanisms mediating dehydration (or β–elimination) and Lewis acid-catalyzed secondary carbocation formation (Kim et al. 2010a). Instead, they propose a radical mechanism similar to ribonucleotide reductases, in which a stable benzyl radical at C-3 would be a possible intermediate. The second suggested mechanism insisted dismutation activity of THDR. The unevidenced mechanism was recently proposed by Kawada *et al* (KAWADA et al. 2016). They noted that THDR have dehydrogenation activity of THD to DHD. After the dehydrogenation, two electrons (or hydrides) derived from a sacrificed THD may be transferred to the other THD for reduction. Even though they did not provide any experimental proofs, the dismutase mechanism would explain the NAD(P)H independency of THDR. In other study, THDR had flavin-adenine dinucleotide (FAD) as a cofactor (Schroder et al. 2013) that the FAD might be potentially

concerned with the electron transfer and its catalytic activity. Because the flavin has radical generating character in many other enzymes, a similar reaction mechanism would possibly explain the novel catalytic activity of THDR (**Fig. 6.2**). In addition, the mechanismic study would provide exact understanding of THDR and other directions to design efficient catalyst to prepare various equol derivatives.

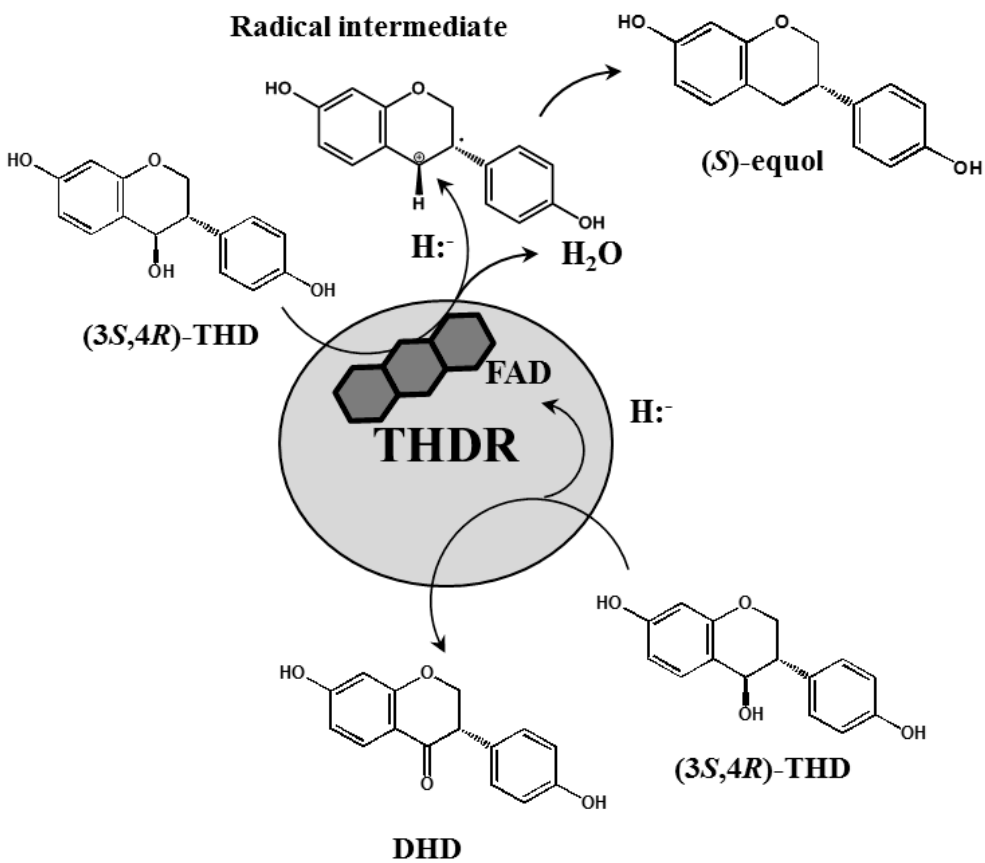

Figure 6.2 Proposed catalytic mechanism and hydride transfer of THDR.

A radical intermediate would be produced during the reduction (Kim et al. 2010a) and one THD molecule would be sacrificed to work as electron source (KAWADA et al. 2016). FAD, a prosthetic group of THDR is suggested to be the radical generating functional group.

6.4 Further suggestion 2: Equol-producing probiotics

Equol is a secondary metabolite of certain gut bacteria, which means that the natural functioning place of equol is human intestinal environment. Even though scientists only verified its clinical functions as a phytoestrogen, antitumor agent and skin anti-aging chemical, a lot of unknown biological functions of equol would be expected (Lephart 2014; Lephart 2016; Setchell et al. 2005). Especially, its effects to composition of human gut microflora and its roles in human gut health are the novel research area to be investigated in future. In that context, artificially designed probiotics retaining equol-producing capability would be a powerful tool to help the research themes and at the same time, the probiotics could be practically applied to relieve and prevent a lot of human diseases. A wide variety of synthetic biological tools that are already available will open the way for the development of the probiotics in a highly controlled manner. For example, a promising probiotic strain, *Escherichia coli* Nissle 1917 would be a potent vector for the fine-tuned equol production, since the strain is stably colonized in the human colon and good expression level of equol-producing enzymes in the recombinant *E. coli* system are already confirmed in this study (Sonnenborn and Schulze 2009). *In vitro* and *in vivo* validation of its beneficial traits should be required for the future successful application.

References

Alfenore S, Cameleyre X, Benbadis L, Bideaux C, Uribelarrea J-L, Goma G, Molina-Jouve C, Guillouet S (2004) Aeration strategy: a need for very high ethanol performance in *Saccharomyces cerevisiae* fed-batch process. Applied Microbiology and Biotechnology 63(5):537-42

Arora A, Nair MG, Strasburg GM (1998) Antioxidant activities of isoflavones and their biological metabolites in a liposomal system. Archives of Biochemistry and Biophysics 356(2):133-41

Bae JH, Park BG, Jung E, Lee P-G, Kim B-G (2014) *fadD* deletion and fadL overexpression in *Escherichia coli* increase hydroxy long-chain fatty acid productivity. Applied Microbiology and Biotechnology 98(21):8917-25

Baird GS, Zacharias DA, Tsien RY (1999) Circular permutation and receptor insertion within green fluorescent proteins. Proceedings of the National Academy of Sciences 96(20):11241-6

Barkhem T, Carlsson B, Nilsson Y, Enmark E, Gustafsson J-Å, Nilsson S (1998) Differential response of estrogen receptor α and estrogen receptor β to partial estrogen agonists/antagonists. Molecular Pharmacology 54(1):105-12

Becker J, Zelder O, Häfner S, Schröder H, Wittmann C (2011) From zero to hero—design-based systems metabolic engineering of *Corynebacterium glutamicum* for l-lysine production. Metabolic Engineering 13(2):159-68

Ben-David A, Gavendo S (1972) The protective effect of polyvinylpyrrolidone and hydroxyethyl starch on noncryogenic injury to red blood cells. Cryobiology 9(3):192-7

Ben-Yosef VS, Sendovski M, Fishman A (2010) Directed evolution of tyrosinase for

enhanced monophenolase/diphenolase activity ratio. Enzyme and Microbial Technology 47(7):372-6

Bradford MM (1976) A rapid and sensitive method for the quantitation of microgram quantities of protein utilizing the principle of protein-dye binding. Analytical Biochemistry 72(1-2):248-54

Caldwell JW, Kollman PA (1995) Cation-π interactions: Nonadditive effects are critical in their accurate representation. Journal of the American Chemical Society 117(14):4177-8

Chang T-S (2007) Two Potent Suicide Substrates of Mushroom Tyrosinase: 7, 8, 4 '-Trihydroxyisoflavone and 5, 7, 8, 4 '-Tetrahydroxyisoflavone. Journal of Agricultural and Food Chemistry 55(5):2010-5

Chang T-S, Chao S-Y, Chen Y-C (2013) Production of *ortho*-hydroxydaidzein derivatives by a recombinant strain of *Pichia pastoris* harboring a cytochrome P450 fusion gene. Process Biochemistry 48(3):426-9

Chang T-S, Ding H-Y, Lin H-C (2005) Identifying 6, 7, 4′-trihydroxyisoflavone as a potent tyrosinase inhibitor. Bioscience, Biotechnology, and Biochemistry 69(10):1999-2001

Chang Y-C, Nair MG, Nitiss JL (1995) Metabolites of daidzein and genistein and their biological activities. Journal of Natural Products 58(12):1901-5

Chemler JA, Fowler ZL, McHugh KP, Koffas MAG (2010) Improving NADPH availability for natural product biosynthesis in *Escherichia coli* by metabolic engineering. Metabolic Engineering 12(2):96-104

Cheng H, Jiang N, Shen A, Feng Y (2005) Molecular cloning and functional

expression of D-arabitol dehydrogenase gene from *Gluconobacter oxydans* in *Escherichia coli*. FEMS Microbiology Letters 252(1):35-42

Chiang C-M, Ding H-Y, Lu J-Y, Chang T-S (2016a) Biotransformation of isoflavones daidzein and genistein by recombinant *Pichia pastoris* expressing membrane-anchoring and reductase fusion chimeric CYP105D7. Journal of the Taiwan Institute of Chemical Engineers 60:26-31

Chiang C-M, Wang D-S, Chang T-S (2016b) Improving free radical scavenging activity of soy isoflavone glycosides daidzin and genistin by 3′-hydroxylation using recombinant *Escherichia coli*. Molecules 21(12):1723-31

Choi EJ, Kim GH (2014) The antioxidant activity of daidzein metabolites, O-desmethylangolensin and equol, in HepG2 cells. Molecular Medicine Reports 9(1):328-32

Choi K-Y, Jung E, Jung D-H, An B-R, Pandey BP, Yun H, Sung C, Park H-Y, Kim B-G (2012a) Engineering of daidzein 3'-hydroxylase P450 enzyme into catalytically self-sufficient cytochrome P450. Microbial Cell Factories 11(1):81-90

Choi K-Y, Jung E, Yun H, Yang Y-H, Kim B-G (2014) Engineering class I cytochrome P450 by gene fusion with NADPH-dependent reductase and *S. avermitilis* host development for daidzein biotransformation. Applied Microbiology and Biotechnology 98(19):8191-200

Choi K-Y, Park H-Y, Kim B-G (2010) Characterization of bi-functional CYP154 from *Nocardia farcinica* IFM10152 in the O-dealkylation and *ortho*-

hydroxylation of formononetin. Enzyme and Microbial Technology 47(7):327-34

Choi K-Y, Yang Y-H, Kim B-g (2015) Regioselectivity-driven evolution of CYP102D1 for improved synthesis of 3′-*ortho*-dihydroxyisoflavone. Enzyme and Microbial Technology 71:20-7

Choi KY, Jung E, Jung DH, Pandey BP, Yun H, Park Hy, Kazlauskas RJ, Kim BG (2012b) Cloning, expression and characterization of CYP102D1, a self-sufficient P450 monooxygenase from *Streptomyces avermitilis*. The FEBS Journal 279(9):1650-62

Choi KY, Jung EO, Yun H, Yang YH, Kazlauskas RJ, Kim BG (2013) Development of colorimetric HTS assay of cytochrome p450 for *ortho*-specific hydroxylation, and engineering of CYP102D1 with enhanced catalytic activity and regioselectivity. ChemBioChem 14(10):1231-8

Choi KY, Kim Tj, Koh SK, Roh CH, Pandey BP, Lee N, Kim BG (2009) A-ring ortho-specific monohydroxylation of daidzein by cytochrome P450s of *Nocardia farcinica* IFM10152. Biotechnology Journal 4(11):1586-95

Choi YJ, Lee SY (2013) Microbial production of short-chain alkanes. Nature 502(7472):571-4

Daugherty AB, Govindarajan S, Lutz S (2013) Improved biocatalysts from a synthetic circular permutation library of the flavin-dependent oxidoreductase old yellow enzyme. Journal of the American Chemical Society 135(38):14425-32

de Carvalho CC (2011) Enzymatic and whole cell catalysis: finding new strategies

for old processes. Biotechnology Advances 29(1):75-83

Ding H-Y, Chiang C-M, Tzeng W-M, Chang T-S (2015) Identification of 3′-hydroxygenistein as a potent melanogenesis inhibitor from biotransformation of genistein by recombinant *Pichia pastoris*. Process Biochemistry 50(10):1614-7

Duncan AM, Merz-Demlow BE, Xu X, Phipps WR, Kurzer MS (2000) Premenopausal equol excretors show plasma hormone profiles associated with lowered risk of breast cancer. Cancer Epidemiology Biomarkers & Prevention 9(6):581-6

El-Mohdy HA, Ghanem S (2009) Biodegradability, antimicrobial activity and properties of PVA/PVP hydrogels prepared by γ-irradiation. Journal of Polymer Research 16(1):1-10

Elghali S, Mustafa S, Amid M, Manap MYABD, Ismail A, Abas F (2012) Bioconversion of daidzein to equol by *Bifidobacterium breve* 15700 and *Bifidobacterium longum* BB536. Journal of Functional Foods 4(4):736-45

Filling C, Berndt KD, Benach J, Knapp S, Prozorovski T, Nordling E, Ladenstein R, Jörnvall H, Oppermann U (2002) Critical residues for structure and catalysis in short-chain dehydrogenases/reductases. Journal of Biological Chemistry 277(28):25677-84

Fischereder E, Pressnitz D, Kroutil W, Lutz S (2014) Engineering strictosidine synthase: Rational design of a small, focused circular permutation library of the β-propeller fold enzyme. Bioorganic & Medicinal Chemistry 22(20):5633-7

Funayama S, Anraku Y, Mita A, Komiyama K, Omura S (1989) Structural study of isoflavonoids possessing antioxidant activity isolated from the fermentation broth of *Streptomyces sp*. The Journal of Antibiotics 42(9):1350-5

Galati G, Sabzevari O, Wilson JX, O'Brien PJ (2002) Prooxidant activity and cellular effects of the phenoxyl radicals of dietary flavonoids and other polyphenolics. Toxicology 177(1):91-104

Gamble JR, Xia P, Hahn CN, Drew JJ, Drogemuller CJ, Brown D, Vadas MA (2006) Phenoxodiol, an experimental anticancer drug, shows potent antiangiogenic properties in addition to its antitumour effects. International Journal of Cancer 118(10):2412-20

Gao L, Wang K-x, Zhang N-n, Li J-q, Qin X-m, Wang X-l (2018) 1H-NMR-based metabolomics approach reveals metabolic mechanism of (-)-5-hydroxy-equol against hepatocellular carcinoma cells *in vitro*. Journal of Proteome Research 17(5):1833-43

Gibney G, Elfiky A, Bussom S, Hoimes C, Burns A, McDonough J, Rowen E, Cheng Y, Kelly W A phase II study of oral phenoxodiol in castrate and noncastrate prostate cancer patients with associated cytokine changes. In: ASCO Annual Meeting Proceedings, 2010. vol 28. p 4661

Goldfeder M, Kanteev M, Adir N, Fishman A (2013) Influencing the monophenolase/diphenolase activity ratio in tyrosinase. Biochimica et Biophysica Acta (BBA)-Proteins and Proteomics 1834(3):629-33

György P, Murata K, Ikehata H (1964) Antioxidants isolated from fermented soybeans (tempeh). Nature 203(4947):870-2

Halaouli S, Asther M, Sigoillot JC, Hamdi M, Lomascolo A (2006) Fungal tyrosinases: new prospects in molecular characteristics, bioengineering and biotechnological applications. Journal of Applied Microbiology 100(2):219-32

Hannemann F, Bichet A, Ewen KM, Bernhardt R (2007) Cytochrome P450 systems—biological variations of electron transport chains. Biochimica et Biophysica Acta (BBA)-General Subjects 1770(3):330-44

Hatakeyama M, Kitaoka T, Ichinose H (2017) Impacts of amino acid substitutions in fungal cytochrome P450 monooxygenase (CYP57B3) on the effective production of 3′-hydroxygenistein. FEMS Microbiology Letters 364(11)

Hernández-Romero D, Sanchez-Amat A, Solano F (2006) A tyrosinase with an abnormally high tyrosine hydroxylase/dopa oxidase ratio. The FEBS Journal 273(2):257-70

Hiblot J, Yu Q, Sabbadini MD, Reymond L, Xue L, Schena A, Sallin O, Hill N, Griss R, Johnsson K (2017) Luciferases with Tunable Emission Wavelengths. Angewandte Chemie 129:14748-52

Hirota A, Inaba M, Chen Y-C, Abe N, Taki S, Yano M, Kawaii S (2004) Isolation of 8-hydroxyglycitein and 6-hydroxydaidzein from soybean miso. Bioscience, Biotechnology, and Biochemistry 68(6):1372-4

Huijbers MM, Montersino S, Westphal AH, Tischler D, van Berkel WJ (2014) Flavin dependent monooxygenases. Archives of Biochemistry and Biophysics 544:2-17

Hwang CC, Chang YH, Lee HJ, Wang TP, Su YM, Chen HW, Liang PH (2013) The

catalytic roles of P185 and T188 and substrate-binding loop flexibility in 3alpha-hydroxysteroid dehydrogenase/carbonyl reductase from *Comamonas testosteroni*. PLoS One 8(5):e63594

Hwang CS, Kwak HS, Lim HJ, Lee SH, Kang YS, Choe TB, Hur HG, Han KO (2006) Isoflavone metabolites and their in vitro dual functions: they can act as an estrogenic agonist or antagonist depending on the estrogen concentration. The Journal of Steroid Biochemistry and Molecular Biology 101(4-5):246-53

Itsumi M, Shiota M, Takeuchi A, Kashiwagi E, Inokuchi J, Tatsugami K, Kajioka S, Uchiumi T, Naito S, Eto M (2016) Equol inhibits prostate cancer growth through degradation of androgen receptor by S-phase kinase-associated protein 2. Cancer science 107(7):1022-8

Jackson RL, Greiwe JS, Schwen RJ (2011a) Emerging evidence of the health benefits of S-equol, an estrogen receptor beta agonist. Nutrition Reviews 69(8):432-48

Jenks BH, Iwashita S, Nakagawa Y, Ragland K, Lee J, Carson WH, Ueno T, Uchiyama S (2012) A pilot study on the effects of S-equol compared to soy isoflavones on menopausal hot flash frequency. Journal of Women's Health 21(6):674-82

Ji X-J, Huang H, Zhu J-G, Ren L-J, Nie Z-K, Du J, Li S (2010) Engineering *Klebsiella oxytoca* for efficient 2, 3-butanediol production through insertional inactivation of acetaldehyde dehydrogenase gene. Applied Microbiology and Biotechnology 85(6):1751-8

Jin J-S, Nishihata T, Kakiuchi N, Hattori M (2008) Biotransformation of C-glucosylisoflavone puerarin to estrogenic (3*S*)-equol in co-culture of two human intestinal bacteria. Biological and Pharmaceutical Bulletin 31(8):1621-25

Jirgensons B (1952) Solubility and fractionation of polyvinylpyrrolidone. Journal of Polymer Science Part A: Polymer Chemistry 8(5):519-27

Joannou GE, Kelly GE, Reeder AY, Waring M, Nelson C (1995) A urinary profile study of dietary phytoestrogens. The identification and mode of metabolism of new isoflavonoids. The Journal of Steroid Biochemistry and Molecular Biology 54(3-4):167-84

Jokela T (2011) Synthesis of Reduced Metabolites of Isoflavonoids, and their Enantiomeric Forms. Academic Dissertation, University of Helsinki

Jones JA, Vernacchio VR, Sinkoe AL, Collins SM, Ibrahim MH, Lachance DM, Hahn J, Koffas MA (2016) Experimental and computational optimization of an *Escherichia coli* co-culture for the efficient production of flavonoids. Metabolic Engineering 35:55-63

Jou H-J, Tsai P-J, Tu J-H, Wu W-H (2013) Stinky tofu as a rich source of bioavailable *S*-equol in Asian diets. Journal of Functional Foods 5(2):651-9

Kanellakis P, Nestel P, Bobik A (2004) Angioplasty-induced superoxide anions and neointimal hyperplasia in the rabbit carotid artery: suppression by the isoflavone *trans*-tetrahydrodaidzein. Atherosclerosis 176(1):63-72

Kataoka M, Sri Rohani LP, Wada M, Kita K, Yanase H, Urabe I, Shimizu S (1998) *Escherichia coli* transformant expressing the glucose dehydrogenase gene

from *Bacillus megaterium* as a cofactor regenerator in a chiral alcohol production system. Bioscience, Biotechnology, and Biochemistry 62(1):167-9

Kawada Y, Yokoyama S, Yanase E, Niwa T, Suzuki T (2016) The production of *S*-equol from daidzein is associated with a cluster of three genes in *Eggerthella* sp. YY7918. Bioscience of Microbiota, Food and Health 35(3):113-21

Kelly MG, Mor G, Husband A, O'Malley DM, Baker L, Azodi M, Schwartz PE, Rutherford TJ (2011) Phase II evaluation of phenoxodiol in combination with cisplatin or paclitaxel in women with platinum/taxane-refractory/resistant epithelial ovarian, fallopian tube, or primary peritoneal cancers. International Journal of Gynecological Cancer 21(4):633-639

Khare AB (2005) Soluble isoflavone compositions. US6855359B2

Kim H, Kim JR, Kang H, Choi J, Yang H, Lee P, Kim J, Lee KW (2014) 7, 8, 4′-Trihydroxyisoflavone attenuates DNCB-induced atopic dermatitis-like symptoms in NC/Nga mice. PloS one 9(8):e104938

Kim J, Lee P-G, Jung E-o, Kim B-G (2018a) In vitro characterization of CYP102G4 from *Streptomyces cattleya*: A self-sufficient P450 naturally producing indigo. Biochimica et Biophysica Acta (BBA)-Proteins and Proteomics 1866(1):60-67

Kim M, Kim SI, Han J, Wang XL, Song DG, Kim SU (2009) Stereospecific Biotransformation of Dihydrodaidzein into (3*S*)-Equol by the Human Intestinal Bacterium *Eggerthella* Strain Julong 732. Applied and Environmental Microbiology 75(10):3062-8

Kim M, Marsh EN, Kim SU, Han J (2010a) Conversion of (3*S*,4*R*)-tetrahydrodaidzein to (3*S*)-equol by THD reductase: proposed mechanism involving a radical intermediate. Biochemistry 49(26):5582-7

Kim M, Won D, Han J (2010b) Absolute configuration determination of isoflavan-4-ol stereoisomers. Bioorganic & Medicinal Chemistry Letters 20(15):4337-41

Kim S-H, Lee S-H, Lee J-E, Park SJ, Kim K, Kim IS, Lee Y-S, Hwang NS, Kim B-G (2018b) Tissue adhesive, rapid forming, and sprayable ECM hydrogel via recombinant tyrosinase crosslinking. Biomaterials. In press

Klus K, Barz W (1995) Formation of polyhydroxylated isoflavones from the soybean seed isoflavones daidzein and glycitein by bacteria isolated from tempe. Archives of Microbiology 164(6):428-434

Ko S, Yang Y-H, Choi K-Y, Kim B-G (2015) rational design and directed evolution of CYP102A1 (BM3) for regio-specific hydroxylation of isoflavone. Biotechnology and Bioprocess Engineering 20(2):225-233

Komiyama K, Funayama S, Anraku Y, Mita A, Takahashi Y, Omura S, Shimasaki H (1989) Isolation of isoflavonoids possessing antioxidant activity from the fermentation broth of *Streptomyces* sp. The Journal of antibiotics 42(9):1344-9

Kuiper GG, Lemmen JG, Carlsson B, Corton JC, Safe SH, Van Der Saag PT, Van Der Burg B, Gustafsson J-Ak (1998) Interaction of estrogenic chemicals and phytoestrogens with estrogen receptor β. Endocrinology 139(10):4252-63

Kwon JE, Lim J, Kim I, Kim D, Kang SC (2018) Isolation and identification of new

bacterial stains producing equol from *Pueraria lobata* extract fermentation. PloS one 13(2): e0192490

Lee CC, Dudonné S, Kim JH, Kim JS, Dubé P, Kim J-E, Desjardins Y, Park JHY, Lee KW, Lee CY (2018a) A major daidzin metabolite 7, 8, 4′-trihydroxyisoflavone found in the plasma of soybean extract-fed rats attenuates monocyte-endothelial cell adhesion. Food Chemistry 240:607-14

Lee DE, Lee KW, Jung SK, Lee EJ, Hwang JA, Lim T-G, Kim BY, Bode AM, Lee HJ, Dong Z (2011) 6, 7, 4′-trihydroxyisoflavone inhibits HCT-116 human colon cancer cell proliferation by targeting CDK1 and CDK2. Carcinogenesis 32(4):629-35

Lee H, Kim B-G, Ahn J-H (2014) Production of bioactive hydroxyflavones by using monooxygenase from *Saccharothrix espanaensis*. Journal of Biotechnology 176:11-7

Lee J-K, Koo B-S, Kim S-Y, Hyun H-H (2003) Purification and characterization of a novel mannitol dehydrogenase from a newly isolated strain of *Candida magnoliae*. Applied and Environmental Microbiology 69(8):4438-47

Lee N, Kim EJ, Kim B-G (2012) Regioselective hydroxylation of trans-resveratrol via inhibition of tyrosinase from *Streptomyces avermitilis* MA4680. ACS Chemical Biology 7(10):1687-92

Lee N, Lee S-H, Baek K, Kim B-G (2015) Heterologous expression of tyrosinase (MelC2) from *Streptomyces avermitilis* MA4680 in *E. coli* and its application for ortho-hydroxylation of resveratrol to produce piceatannol. Applied Microbiology and Biotechnology 99(19):7915-24

Lee P-G, Kim J, Kim E-J, Jung E, Pandey BP, Kim B-G (2016a) P212A Mutant of Dihydrodaidzein Reductase Enhances (*S*)-Equol Production and Enantioselectivity in a Recombinant *Escherichia coli* Whole-Cell Reaction System. Applied and Environmental Microbiology 82(7):1992-2002

Lee P-G, Kim J, Kim E-J, Lee S-H, Choi K-Y, Kazlauskas RJ, Kim B-G (2017) Biosynthesis of (-)-5-hydroxy-equol and 5-hydroxy-dehydroequol from soy isoflavone, genistein using microbial whole cell bioconversion. ACS Chemical Biology 12:2883-90

Lee P-G, Lee S-H, Kim J, Kim E-J, Choi K-Y, Kim B-G (2018b) Polymeric solvent engineering for g/L scale production of a water-insoluble isoflavone derivative, (*S*)-equol. Applied Microbiology and Biotechnology, https://doi.org/10.1007/s00253-018-9137-8

Lee SH, Baek K, Lee JE, Kim BG (2016b) Using tyrosinase as a monophenol monooxygenase: A combined strategy for effective inhibition of melanin formation. Biotechnology and Bioengineering 113(4):735-43

Leonard E, Yan Y, Fowler ZL, Li Z, Lim C-G, Lim K-H, Koffas MA (2008) Strain improvement of recombinant *Escherichia coli* for efficient production of plant flavonoids. Molecular Pharmaceutics 5(2):257-65

Lephart ED (2013) Protective effects of equol and their polyphenolic isomers against dermal aging: microarray/protein evidence with clinical implications and unique delivery into human skin. Pharmaceutical Biology 51(11):1393-400

Lephart ED (2014) Review: Anti-oxidant and anti-aging properties of equol in prostate health (BPH). Open Journal of Endocrine and Metabolic Diseases

04(01):1-12

Lephart ED (2016) Skin aging and oxidative stress: Equol's anti-aging effects via biochemical and molecular mechanisms. Ageing Research Reviews 31:36-54

Li F, Luan Z, Chen Q, Xu J, Yu H (2016) Rational selection of circular permutation sites in characteristic regions of the α/β-hydrolase fold enzyme RhEst1. Journal of Molecular Catalysis B: Enzymatic 125:75-80

Li M, Li H, Zhang C, Wang XL, Chen BH, Hao QH, Wang SY (2015) Enhanced biosynthesis of O-desmethylangolensin from daidzein by a novel oxygen-tolerant cock intestinal bacterium in the presence of atmospheric oxygen. Journal of Applied Microbiology 118(3):619-28

Lim CG, Fowler ZL, Hueller T, Schaffer S, Koffas MA (2011) High-yield resveratrol production in engineered *Escherichia coli*. Applied and Environmental Microbiology 77(10):3451-60

Ling S, Dai A, Williams MR, Husband AJ, Nestel PJ, Komesaroff PA, Sudhir K (2004) The isoflavone metabolite cis-tetrahydrodaidzein inhibits ERK-1 activation and proliferation in human vascular smooth muscle cells. Journal of Cardiovascular Pharmacology 43(5):622-8

Loomis WD, Battaile J (1966) Plant phenolic compounds and the isolation of plant enzymes. Phytochemistry 5(3):423-38

Lund TD, Munson DJ, Haldy ME, Setchell KD, Lephart ED, Handa RJ (2004) Equol is a novel anti-androgen that inhibits prostate growth and hormone feedback. Biology of Reproduction 70(4):1188-95

Matthies A, Blaut M, Braune A (2009) Isolation of a human intestinal bacterium capable of daidzein and genistein conversion. Applied and Environmental Microbiology 75(6):1740-4

Matthies A, Clavel T, Gütschow M, Engst W, Haller D, Blaut M, Braune A (2008) Conversion of daidzein and genistein by an anaerobic bacterium newly isolated from the mouse intestine. Applied and Environmental Microbiology 74(15):4847-52

Matthies A, Loh G, Blaut M, Braune A (2011) Daidzein and genistein are converted to equol and 5-hydroxy-equol by human intestinal *Slackia isoflavoniconvertens* in gnotobiotic rats. Journal of Nutrition 142(1):40-6

Mei Y-Z, Liu R-X, Wang D-P, Wang X, Dai C-C (2015) Biocatalysis and biotransformation of resveratrol in microorganisms. Biotechnology Letters 37(1):9-18

Minamida K, Ota K, Nishimukai M, Tanaka M, Abe A, Sone T, Tomita F, Hara H, Asano K (2008) *Asaccharobacter celatus* gen. nov., sp. nov., isolated from rat caecum. International Journal of Systematic and Evolutionary Microbiology 58(5):1238-40

Minamida K, Tanaka M, Abe A, Sone T, Tomita F, Hara H, Asano K (2006) Production of equol from daidzein by gram-positive rod-shaped bacterium isolated from rat intestine. Journal of Bioscience and Bioengineering 102(3):247-50

Mitsuda M, Iwasaki M (2006) Improvement in the expression of CYP2B6 by co-expression with molecular chaperones GroES/EL in *Escherichia coli*.

Protein Expression and Purification 46(2):401-5

Molitor C, Mauracher SG, Rompel A (2016) Aurone synthase is a catechol oxidase with hydroxylase activity and provides insights into the mechanism of plant polyphenol oxidases. Proceedings of the National Academy of Sciences 113(13):E1806-E1815

Muthyala RS, Ju YH, Sheng S, Williams LD, Doerge DR, Katzenellenbogen BS, Helferich WG, Katzenellenbogen JA (2004) Equol, a natural estrogenic metabolite from soy isoflavones. Bioorganic & Medicinal Chemistry 12(6):1559-67

Nakayama T, Sato T, Fukui Y, Yonekura-Sakakibara K, Hayashi H, Tanaka Y, Kusumi T, Nishino T (2001) Specificity analysis and mechanism of aurone synthesis catalyzed by aureusidin synthase, a polyphenol oxidase homolog responsible for flower coloration. FEBS Letters 499(1-2):107-11

Nash GB, Meiselman HJ (1983) Effects of dextran and polyvinylpyrrolidone on red cell geometry and membrane elasticity. Annals of the New York Academy of Sciences 416(1):255-62

Nazir KNH, Ichinose H, Wariishi H (2011) Construction and application of a functional library of cytochrome P450 monooxygenases from the filamentous fungus *Aspergillus oryzae*. Applied and Environmental Microbiology 77(9):3147-50

Nishihara K, Kanemori M, Kitagawa M, Yanagi H, Yura T (1998) Chaperone coexpression plasmids: Differential and synergistic roles of DnaK-DnaJ-GrpE and GroEL-GroES in assisting folding of an allergen of Japanese cedar

pollen, Cryj2, in *Escherichia coli*. Applied and Environmental Microbiology 64(5):1694-9

Okino S, Noburyu R, Suda M, Jojima T, Inui M, Yukawa H (2008) An efficient succinic acid production process in a metabolically engineered *Corynebacterium glutamicum* strain. Applied Microbiology and Biotechnology 81(3):459-64

Oyama A, Ueno T, Uchiyama S, Aihara T, Miyake A, Kondo S, Matsunaga K (2012) The effects of natural *S*-equol supplementation on skin aging in postmenopausal women: a pilot randomized placebo-controlled trial. Menopause 19(2):202-10

Padan E, Zilberstein D, Rottenberg H (1976) The proton electrochemical gradient in *Escherichia coli* cells. European Journal of Biochemistry 63(2):533-41

Pandey BP, Lee N, Choi K-Y, Jung E, Jeong D-h, Kim B-G (2011) Screening of bacterial cytochrome P450s responsible for regiospecific hydroxylation of (iso) flavonoids. Enzyme and Microbial Technology 48(4-5):386-92

Pandey BP, Lee N, Choi K-Y, Kim J-N, Kim E-J, Kim B-G (2014) Identification of the specific electron transfer proteins, ferredoxin, and ferredoxin reductase, for CYP105D7 in *Streptomyces avermitilis* MA4680. Applied Microbiology and Biotechnology 98(11):5009-17

Pandey BP, Roh C, Choi KY, Lee N, Kim EJ, Ko S, Kim T, Yun H, Kim BG (2010) Regioselective hydroxylation of daidzein using P450 (CYP105D7) from *Streptomyces avermitilis* MA4680. Biotechnology and Bioengineering 105(4):697-704

Park H-Y, Kim M, Han J (2011) Stereospecific microbial production of isoflavanones from isoflavones and isoflavone glucosides. Applied Microbiology and Biotechnology 91(4):1173-81

Park J-S, Kim DH, Lee JK, Lee JY, Kim DH, Kim HK, Lee H-J, Kim HC (2010) Natural *ortho*-dihydroxyisoflavone derivatives from aged Korean fermented soybean paste as potent tyrosinase and melanin formation inhibitors. Bioorganic & Medicinal Chemistry Letters 20(3):1162-4

Park J-S, Park HY, Kim DH, Kim DH, Kim HK (2008) *ortho*-Dihydroxyisoflavone derivatives from aged Doenjang (Korean fermented soypaste) and its radical scavenging activity. Bioorganic & Medicinal Chemistry Letters 18(18):5006-9

Pettersen EF, Goddard TD, Huang CC, Couch GS, Greenblatt DM, Meng EC, Ferrin TE (2004) UCSF Chimera—a visualization system for exploratory research and analysis. Journal of Computational Chemistry 25(13):1605-12

Plesiat P, Nikaido H (1992) Outer membranes of Gram-negative bacteria are permeable to steroid probes. Molecular Microbiology 6(10):1323-33

Qian Z, Fields CJ, Lutz S (2007) Investigating the structural and functional consequences of circular permutation on lipase B from *Candida antarctica*. ChemBioChem 8(16):1989-96

Qian Z, Lutz S (2005) Improving the catalytic activity of *Candida antarctica* lipase B by circular permutation. Journal of the American Chemical Society 127(39):13466-7

Roh C, Choi K-Y, Pandey BP, Kim B-G (2009a) Hydroxylation of daidzein by

CYP107H1 from *Bacillus subtilis* 168. Journal of Molecular Catalysis B: Enzymatic 59(4):248-53

Roh C, Seo S-H, Choi K-Y, Cha M, Pandey BP, Kim J-H, Park J-S, Kim DH, Chang IS, Kim B-G (2009b) Regioselective hydroxylation of isoflavones by *Streptomyces avermitilis* MA-4680. Journal of Bioscience and Bioengineering 108(1):41-6

Rohman A, van Oosterwijk N, Thunnissen A-MW, Dijkstra BW (2013) Crystal structure and site-directed mutagenesis of 3-ketosteroid Δ1-dehydrogenase from *Rhodococcus erythropolis* SQ1 explain its catalytic mechanism. Journal of Biological Chemistry 288(49):35559-68

Rufer CE, Glatt H, Kulling SE (2006) Structural elucidation of hydroxylated metabolites of the isoflavan equol by gas chromatography-mass spectrometry and high-performance liquid chromatography-mass spectrometry. Drug Metabolism and Disposition 34(1):51-60

Salmond CV, Kroll RG, Booth IR (1984) The effect of food preservatives on pH homeostasis in *Escherichia coli*. Journal of General Microbiology 130(11):2845-50

Schroder C, Matthies A, Engst W, Blaut M, Braune A (2013) Identification and expression of genes involved in the conversion of daidzein and genistein by the equol-forming bacterium *Slackia isoflavoniconvertens*. Applied and Environmental Microbiology 79(11):3494-502

Schwarzhans J-P, Luttermann T, Geier M, Kalinowski J, Friehs K (2017) Towards systems metabolic engineering in *Pichia pastoris*. Biotechnology Advances

35(6):681-710

Sendovski M, Kanteev M, Ben-Yosef VS, Adir N, Fishman A (2011) First structures of an active bacterial tyrosinase reveal copper plasticity. Journal of Molecular Biology 405(1):227-37

Seo M-H, Kim B-N, Kim K-R, Lee KW, Lee C-H, Oh D-K (2013a) Production of 8-hydroxydaidzein from soybean extract by *Aspergillus oryzae* KACC 40247. Bioscience, Biotechnology, and Biochemistry 77(6):1245-50

Seo SG, Yang H, Shin SH, Min S, Kim YA, Yu JG, Lee DE, Chung MY, Heo YS, Kwon JY (2013b) A metabolite of daidzein, 6, 7, 4′-trihydroxyisoflavone, suppresses adipogenesis in 3T3-L1 preadipocytes via ATP-competitive inhibition of PI3K. Molecular Nutrition & Food Research 57(8):1446-55

Setchell K (1998) Phytoestrogens: the biochemistry, physiology, and implications for human health of soy isoflavones. The American Journal of Clinical Nutrition 68(6):1333S-46S

Setchell KD (2001) Soy isoflavones—benefits and risks from nature's selective estrogen receptor modulators (SERMs). Journal of the American College of Nutrition 20(sup5):354S-62S

Setchell KD, Brown NM, Lydeking-Olsen E (2002) The clinical importance of the metabolite equol—a clue to the effectiveness of soy and its isoflavones. The Journal of Nutrition 132(12):3577-84

Setchell KD, Clerici C, Lephart ED, Cole SJ, Heenan C, Castellani D, Wolfe BE, Nechemias-Zimmer L, Brown NM, Lund TD (2005) *S*-equol, a potent ligand for estrogen receptor β, is the exclusive enantiomeric form of the soy

isoflavone metabolite produced by human intestinal bacterial flora. The American Journal of Clinical Nutrition 81(5):1072-9

Setchell KDR, Cole SJ (2015) Compositions and products containing *S*-equol, and methods for their making. US9018247B2

Shimada Y, Takahashi M, Miyazawa N, Abiru Y, Uchiyama S, Hishigaki H (2012) Identification of a novel dihydrodaidzein racemase essential for biosynthesis of equol from daidzein in *Lactococcus* sp. strain 20-92. Applied and Environmental Microbiology 78(14):4902-7

Shimada Y, Takahashi M, Miyazawa N, Ohtani T, Abiru Y, Uchiyama S, Hishigaki H (2011) Identification of two novel reductases involved in equol biosynthesis in *Lactococcus* strain 20-92. Journal of Molecular Microbiology and Biotechnology 21(3-4):160-72

Shimada Y, Yasuda S, Takahashi M, Hayashi T, Miyazawa N, Sato I, Abiru Y, Uchiyama S, Hishigaki H (2010) Cloning and expression of a novel NADP(H)-dependent daidzein reductase, an enzyme involved in the metabolism of daidzein, from equol-producing *Lactococcus* strain 20-92. Applied and Environmental Microbiology 76(17):5892-901

Shuster V, Fishman A (2009) Isolation, cloning and characterization of a tyrosinase with improved activity in organic solvents from *Bacillus megaterium*. Journal of Molecular Microbiology and Biotechnology 17(4):188-200

Simons AL, Renouf M, Hendrich S, Murphy PA (2005) Metabolism of glycitein (7, 4'-dihydroxy-6-methoxy-isoflavone) by human gut microflora. Journal of Agricultural and Food Chemistry 53(22):8519-25

Slade D, Ferreira D, Marais JP (2005) Circular dichroism, a powerful tool for the assessment of absolute configuration of flavonoids. Phytochemistry 66(18):2177-215

Slonczewski JL, Rosen BP, Alger JR, Macnab RM (1981) pH homeostasis in *Escherichia coli*: measurement by 31P nuclear magnetic resonance of methylphosphonate and phosphate. Proceedings of the National Academy of Sciences 78(10):6271-5

Solomon EI, Sundaram UM, Machonkin TE (1996) Multicopper oxidases and oxygenases. Chemical Rviews 96(7):2563-606

Sonnenborn U, Schulze J (2009) The non-pathogenic *Escherichia coli* strain Nissle 1917–features of a versatile probiotic. Microbial Ecology in Health and Disease 21(3-4):122-58

Tamura M, Hori S, Nakagawa H (2014) Intestinal bacterium TM-30: an *S*-equol-producing bacterium isolated from human feces is involved in estrogen metabolism *in vitro*. Food Science and Technology Research 20(2):309-16

Tepper AW, Bubacco L, Canters GW (2005) Interaction between the type-3 copper protein tyrosinase and the substrate analogue p-nitrophenol studied by NMR. Journal of the American Chemical Society 127(2):567-75

Tousen Y, Ezaki J, Fujii Y, Ueno T, Nishimuta M, Ishimi Y (2011) Natural *S*-equol decreases bone resorption in postmenopausal, non-equol-producing Japanese women: a pilot randomized, placebo-controlled trial. Menopause 18(5):563-74

Trott O, Olson AJ (2010) AutoDock Vina: improving the speed and accuracy of

docking with a new scoring function, efficient optimization, and multithreading. Journal of Cmputational Cemistry 31(2):455-61

Tsangalis D, Ashton J, McGill A, Shah N (2002) Enzymic Transformation of Isoflavone Phytoestrogens in Soymilk by β-Glucosidase-Producing *Bifidobacteria*. Journal of Food Science 67(8):3104-13

Tsangalis D, Wilcox G, Shah NP, Stojanovska L (2005) Bioavailability of isoflavone phytoestrogens in postmenopausal women consuming soya milk fermented with probiotic bifidobacteria. British Journal of Nutrition 93(6):867-77

Tsuji H, Moriyama K, Nomoto K, Akaza H (2012) Identification of an enzyme system for daidzein-to-equol conversion in *Slackia* sp. strain NATTS. Applied and Environmental Microbiology 78(4):1228-36

Tsuji H, Moriyama K, Nomoto K, Miyanaga N, Akaza H (2010) Isolation and characterization of the equol-producing bacterium *Slackia* sp. strain NATTS. Archives of Microbiology 192(4):279-87

Tsuji H, Nomoto K, Moriyama K, Akaza H (2013) Equol-producing bacterium and use thereof. US8420073B2

Uchiyama S, Ueno T, Suzuki T (2006) Composition containing lactic acid bacterium producing equol. US20060148045A1

Uchiyama S, Ueno T, Suzuki T (2007) Identification of a newly isolated equal-producing lactic acid bacterium from the human feces. Journal of Intestinal Microbiology 21(3):217-20

Uchiyama S, Ueno T, Suzuki T (2013) Equol-producing lactic acid bacteria-containing composition. US8765445B2

Uesugi T, Fukui Y, Yamori Y (2002) Beneficial effects of soybean isoflavone supplementation on bone metabolism and serum lipids in postmenopausal Japanese women: a four-week study. Journal of the American College of Nutrition 21(2):97-102

Umezawa H, Tobe H, Shibamoto N, Nakamura F, Nakamura K, Matsuzaki M, Takeuchi T (1975) Isolation of isoflavones inhibiting DOPA decarboxylase from fungi and streptomyces. The Journal of Antibiotics 28(12):947-52

Urlacher VB, Girhard M (2012) Cytochrome P450 monooxygenases: an update on perspectives for synthetic application. Trends in Biotechnology 30(1):26-36

Veitch NC (2007) Isoflavonoids of the Leguminosae. Natural Product Reports 24(2):417-64

Veitch NC (2013) Isoflavonoids of the Leguminosae. Natural Product Reports 30(7):988-1027

Wähälä K, Koskimies JK, Mesilaakso M, Salakka AK, Leino TK, Adlercreutz H (1997) The synthesis, structure, and anticancer activity of *cis*-and *trans*-4', 7-dihydroxyisoflavan-4-ols. The Journal of Organic Chemistry 62(22):7690-3

Wang H-j, Murphy PA (1994) Isoflavone content in commercial soybean foods. Journal of Agricultural and Food Chemistry 42(8):1666-73

Wang T-Y, Tsai Y-H, Yu I-Z, Chang T-S (2016) Improving 3'-hydroxygenistein production in recombinant *Pichia pastoris* using periodic hydrogen peroxide-shocking strategy. Journal of Microbiology and Biotechnology 26(3):498-502

Wang X-L, Hur H-G, Lee JH, Kim KT, Kim S-I (2005a) Enantioselective synthesis of *S*-equol from dihydrodaidzein by a newly isolated anaerobic human intestinal bacterium. Applied and Environmental Microbiology 71(1):214-9

Wang X-L, Kim H-J, Kang S-I, Kim S-I, Hur H-G (2007) Production of phytoestrogen *S*-equol from daidzein in mixed culture of two anaerobic bacteria. Archives of Microbiology 187(2):155-60

Wang X-L, Shin K-H, Hur H-G, Kim S-I (2005b) Enhanced biosynthesis of dihydrodaidzein and dihydrogenistein by a newly isolated bovine rumen anaerobic bacterium. Journal of Biotechnology 115(3):261-9

Webb B, Sali A (2014) Protein structure modeling with MODELLER. Protein Structure Prediction. Springer, pp 1-15

Wei P, Liu M, Chen Y, Chen D-C (2012) Systematic review of soy isoflavone supplements on osteoporosis in women. Asian Pacific Journal of Tropical Medicine 5(3):243-8

Wells J (1992) Analysis and interpretation of binding at equilibrium. Receptor-Ligand Interactions A Practical Approach:289-395

Wilks JC, Slonczewski JL (2007) pH of the Cytoplasm and periplasm of *Escherichia coli*: rapid measurement by green fluorescent protein fluorimetry. Journal of Bacteriology 189(15):5601-7

Williamson-Hughes PS, Flickinger BD, Messina MJ, Empie MW (2006) Isoflavone supplements containing predominantly genistein reduce hot flash symptoms: a critical review of published studies. Menopause 13(5):831-9

Wu S-C, Chang C-W (2016) Production of 8-hydroxygenistein through

biotransformation by using *Aspergillus oryzae*. Chemical Engineering Communications 203(8):1125-30

Wu S-C, Chang C-W, Lin C-W, Hsu Y-C (2015) Production of 8-hydroxydaidzein polyphenol using biotransformation by *Aspergillus oryzae*. Food Science and Technology Research 21(4):557-62

Xie Y, Liu Z, Gao Y, Wang X, Hao Q, Yu X (2015) Bioconversion of genistein to (-) 5-hydroxyequol by a newly isolated cock intestinal anaerobic bacterium. Journal of Chinese Pharmceutical Sciences 24:442-8

Xu P, Gu Q, Wang W, Wong L, Bower AG, Collins CH, Koffas MA (2013) Modular optimization of multi-gene pathways for fatty acids production in *E. coli*. Nature Communications 4:1409

Yang S, Zhu S-F, Zhang C-M, Song S, Yu Y-B, Li S, Zhou Q-L (2012) Enantioselective iridium-catalyzed hydrogenation of α-arylcinnamic acids and synthesis of (*S*)-equol. Tetrahedron 68(26):5172-8

Yao LH, Jiang Y, Shi J, Tomas-Barberan F, Datta N, Singanusong R, Chen S (2004) Flavonoids in food and their health benefits. Plant Foods for Human Nutrition 59(3):113-22

Yokoyama S-i, Suzuki T (2008) Isolation and characterization of a novel equol-producing bacterium from human feces. Bioscience, Biotechnology, and Biochemistry 72(10):2660-6

Yu Y, Petrik ID, Chacón KN, Hosseinzadeh P, Chen H, Blackburn NJ, Lu Y (2017) Effect of circular permutation on the structure and function of type 1 blue copper center in azurin. Protein Science 26(2):218-26

Yu Z-T, Yao W, Zhu W-Y (2008) Isolation and identification of equol-producing bacterial strains from cultures of pig faeces. FEMS Microbiology Letters 282(1):73-80

Yun H, Choi HL, Fadnavis NW, Kim BG (2005) Stereospecific synthesis of (*R*)-2-hydroxy carboxylic acids using recombinant *E. coli* BL21 overexpressing YiaE from *Escherichia coli* K12 and glucose dehydrogenase from *Bacillus subtilis*. Biotechnology Progress 21(2):366-71

Yun H, Yang Y-H, Cho B-K, Hwang B-Y, Kim B-G (2003) Simultaneous synthesis of enantiomerically pure (*R*)-1-phenylethanol and (*R*)-α-methylbenzylamine from racemic α-methylbenzylamine using ω-transaminase/alcohol dehydrogenase/glucose dehydrogenase coupling reaction. Biotechnology Letters 25(10):809-14

Zhang C, Wang X (2014) Effects of (–)-5-hydroxy-equol on the lifespan and stress resistance of *Caenorhabditis elegans*. Journal of Chinese Pharmaceutical Sciences 23(6):378-84

Zhang P, Schachman H (1996) *In vivo* formation of allosteric aspartate transcarbamoylase containing circularly permuted catalytic polypeptide chains: implications for protein folding and assembly. Protein Science 5(7):1290-300

Zhao H, Wang XL, Zhang HL, Li CD, Wang SY (2011) Production of dihydrodaidzein and dihydrogenistein by a novel oxygen-tolerant bovine rumen bacterium in the presence of atmospheric oxygen. Applied Microbiology and Biotechnology 92(4):803-13

Zheng L (2004) An efficient one-step site-directed and site-saturation mutagenesis protocol. Nucleic Acids Research 32(14):e115

Zilberstein D, Agmon V, Schuldiner S, Padan E (1984) *Escherichia coli* intracellular pH, membrane potential, and cell growth. Journal of Bacteriology 158(1):246-52

Zondlo NJ (2012) Aromatic-proline interactions: Electronically tunable CH/π interactions. Accounts of Chemical Research 46(4):1039-49

국문 초록

이소플라본은 주로 대두에서 자연적으로 관찰되는 식물 이차대사산물로서, 다양한 미생물의 산화환원 대사 경로를 통해 기능성 유도체로 생변환된다. 이러한 기능적 유도체에는 대표적으로 에쿠올, 오르토-수산화 이소플라본 (ODI) 등이 있으며, 이들은 대두 발효 식품 및 사람의 장내 환경에서 발견된 이후로 다양한 건강 기능성으로 인해 큰 주목을 받아 왔다. 최근에는 식품 공학, 영양학, 미생물학에 종사하는 많은 과학자들이 이들의 정확한 생합성 경로와 영양학적 가치를 이해하기 위한 노력을 하고 있으며, 미생물 발효과 효소/전세포 기반 생전환 기술을 이용해 고기능성 이소플라본 유도체를 생산하는 연구를 시도하고 있다. 또한, 생성물의 생산효율과 위치선택성을 향상시키기 위해 미생물 촉매의 재설계 및 산화환원효소의 단백질 공학 등의 연구들이 진행 되어 왔다.

본 연구에서는 이소플라본의 환원 대사산물인 에쿠올과 산화 대사산물인 ODI 를 생산 목표 물질로 선정하여 이들의 효율적인 생합성 전략을 소개하였다. 주요하게는 에쿠올 생산 능력을 보유하는 재조합 대장균을 설계 및 제작하여 에쿠올 및 그 유도체의 합성에 이용하였다. 에쿠올 환원 경로는 니코틴아마이드 아데닌 다이뉴클레오타이드 인산을 대표로 하는 세포 내 환원 전위에 의존하고 있기 때문에 전세포 기반

생전환 시스템을 고효율 저비용 생물 공정 전략으로 채택하였다. 반면, 위치선택적 ODI 생산을 위해서는 공학적으로 재설계된 티로시나아제를 이용하였다. ODI 촉매 반응에서는 티로시나아제의 모노옥시게나아제 활성만을 선택적으로 이용해야하기 때문에 다이페놀레아제 활성을 즉각적으로 억제하는 전략을 이용하였다.

구체적으로, 에쿠올 생산 경로를 구성하는 4 개의 핵심적인 효소인 다이드제인 환원효소 (DZNR), 다이하이드로다이드제인 라세미화 효소 (DDRC), 다이하이드로다이드제인 환원효소 (DHDR), 테트라하이드로다이드제인 환원효소 (THDR)를 포함하는 재조합 대장균을 이용하여 전세포 미생물 반응계에서 에쿠올의 생산을 수행하였다. 저농도 및 고농도 기질 조건에서의 속도결정단계 효소를 각각 동정하였으며, 수용성 고분자 첨가, 반응 구획화 및 컴퓨터 계산 기반 단백질 공학을 이용하여 g/L 수준의 에쿠올 유도체 생산을 할 수 있었다. 결과적으로, 1.9 g/L 의 에쿠올과 1.3 g/L 의 5-하이드록시-에쿠올을 높은 생산성으로 생산하였으며, 이 반응계는 산업적 이용이 용이한 호기성 조작이 가능하다는 점에서 추후 응용 가치가 높은 기술이라고 할 수 있다.

반면, ODI 의 대량생산을 위해서는 미생물 유래 티로시나아제의 모노옥시게나아제 활성을 선택적으로 이용하는 전략을 이용하였다. 야생형 티로시나아제는 이소플라본 수산화 반응에 대해 낮은

위치선택성과 낮은 효소 활성을 보였기 때문에, 티로시나아제에 대한 원순열 단백질 공학과 부위 지정 돌연변이 유발을 수행하였다. 결과적으로 폴리페놀에 높은 활성을 보이는 원순열 돌연변이를 이용하여 1.5 g/L 의 3'-하이드록시-제니스테인을 합성할 수 있었으며, 부위 지정 티로시나아제 돌연변이들로는 6 또는 8-하이드록시-포모노네틴을 위치선택적으로 합성할 수 있었다.

결론적으로, 본 연구는 공학적으로 재설계한 효소 및 미생물 생촉매를 이용하여 기능적 이소플라본 유도체인 에쿠올과 ODI 를 효율적으로 생산하는 방법에 대해서 탐색하였다. 본 연구의 성과는 다양한 생리활성 이소플라본 유도체 생산을 위한 유용한 학문적 기반을 제공한다는 점에서 의의가 있다.

주요어: 에쿠올, 오르토-수산화이소플라본, 전세포 생전환, 단백질 공학, 수용성 고분자, 티로시나아제

학번: 2013-20986